Wiesław Kordalski
Tomasz Stefański
Damian Trofimowicz

TIME- AND FREQUENCY-DOMAIN QUASI-2D SMALL-SIGNAL MOSFET MODELS

Gdańsk 2019

GDAŃSK UNIVERSITY OF TECHNOLOGY PUBLISHING HOUSE
CHAIRMAN OF EDITORIAL BOARD
Janusz T. Cieśliński

EDITOR OF SCIENTIFIC PUBLICATIONS
Michał Szydłowski

REVIEWERS
Ryszard Jan Barczyński
Andrzej Napieralski

LAYOUT, COVER DESIGN
Wioleta Lipska-Kamińska

Published under the permission
of the Rector of Gdańsk University of Technology

Gdańsk University of Technology publications may be purchased at
http://www.pg.edu.pl/wydawnictwo/katalog
orders should be sent to wydaw@pg.edu.pl

ISBN 978-83-7348-773-4

CONTENTS

SELECTED LIST OF SYMBOLS AND ACRONYMS

Symbols

Certain symbols which are used only locally within a section, or whose meaning is clear from the context, are not included in this list.

C_{bd} – body-drain capacitance
C_{bs} – body-source capacitance
C_{bc} – quasi-static body-to-channel capacitance, Sec. 3.7.3
C_{ds} – drain-source capacitance
C_{gb} – gate-body capacitance
C_{gc} – quasi-static gate-to-channel capacitance, Sec. 3.7.2
C_{gd} – gate-drain capacitance
C_{gs} – gate-source capacitance
D_C – dynamic coupling factor of the channel, Sec. 3.3.1
D_p – diffusivity of holes
D_V – dynamic channel-to-current coupling factor, Sec. 3.3.1
D_S – dynamic channel deformation factor, Sec. 3.3.1
d_l – longitudinal dynamic carrier-to-channel coupling factor
$\mathbf{E}$ – electric field vector
E – total longitudinal electric field in the channel
E_0 – steady-state longitudinal electric field in the channel
E_1 – small-signal longitudinal electric field component in the channel
E_{CB} – total transverse electric field on the bottom channel surface, see Fig. 3.3
E_{CB0} – steady-state transverse electric field on the bottom channel surface, see Fig. 3.3
E_{cb} – small-signal transverse electric field component on the bottom channel surface, see Fig. 3.3
E_{CG} – total transverse electric field on the top channel surface, see Fig. 3.3
E_{CG0} – steady-state transverse electric field on the top channel surface, see Fig. 3.3
E_{cg} – small-signal transverse electric field component on the top channel surface, see Fig. 3.3
g_{ds} – quasi-static small-signal drain-source conductance
g_{dsD} – DIBL part of g_{ds}
g_{dso} – ohmic part of g_{ds}
g_m – quasi-static gate small-signal transconductance
g_{mb} – quasi-static body small-signal transconductance

I_{ch} – channel current
i_b – small-signal body-terminal current
i_d – small-signal drain-terminal current
i_g – small-signal gate-terminal current
i_s – small-signal source-terminal current
$\mathbf{J}$ – current density vector field
J – total conduction current density, see (3.60)
J_0 – steady-state conduction current density
J_1 – small-signal conduction current density
J_t – total current density, see (3.59)
J_{t1} – total small-signal current density, see (3.67)
J_{dis} – displacement current density
J_{dis1} – small-signal displacement current density = displacement current density J_{dis}
L – channel length
L_G – gate length
k_D – dimensionless factor, $k_D = g_{dsD} / g_{ds}$
N_d – concentration of ionized donors
p – total concentration of holes at Q-point, see (3.4)
p_0 – steady-state concentration of holes at Q-point
p_1 – small-signal concentration of holes at Q-point
Q_B – total body charge per unit area at Q-point, see (3.13)
Q_{B0} – steady-state body charge per unit area at Q-point
Q_b – small-signal body charge per unit area at Q-point
Q_G – total gate charge per unit area at Q-point, see (3.12)
Q_{G0} – steady-state gate charge per unit area at Q-point
Q_g – small-signal gate charge per unit area at Q-point
q – magnitude of the elementary charge
q_b – overall excess depletion region charge, see (3.143)
q_g – overall excess gate charge, see (3.142)
S – dimensionless parameter, see (4.2)
t_{ox} – oxide thickness
V_{BC} – dc body-channel voltage, see Fig. 3.5
V_{BS} – dc body-source voltage
V_{CS} – dc voltage drop across the channel, see Fig. 3.5
V_{DS} – dc drain-source voltage
V_{GC} – dc gate-channel voltage, see Fig. 3.5
V_{GS} – dc gate-source voltage
V_T – threshold voltage
v_{bs} – small-signal body-source voltage
v_{ds} – small-signal drain-source voltage
v_{gs} – small-signal gate-source voltage
X – total thickness of the channel at Q-point, see (3.6)
X_0 – steady-state thickness of the channel at Q-point

X_1 – small-signal thickness of the channel at Q-point
X_{ch} – average channel thickness, see (4.16)
X_D – channel thickness at the drain
X_d – total thickness of the depletion region at Q-point, see (3.11)
X_{d0} – steady-state thickness of the depletion region at Q-point
X_{d1} – small-signal thickness of the depletion region at Q-point
X_S – channel thickness at the source
y_{bs} – small-signal body-source admittance, see (4.107)
y_{Db} – small-signal body-to-source transadmittance, determined by DIBL see (4.123)
y_{Dg} – small-signal gate-to-source transadmittance determined by DIBL, see (4.122)
y_{ds} – small-signal drain-source admittance, see (4.121)
y_{gs} – small-signal gate-source admittance, see (4.95)
y_m – gate small-signal transadmittance, see (4.94)
y_{mb} – body small-signal transadmittance, see (4.106)
W – width of transistor
ε_0 – permittivity of free space
ε_s – relative permittivity of solicon
η – dimensionless factor, $\eta = g_{mb} / g_m$
ξ – distance (from the source) along the channel
$\mu(\xi, t)$ – total bias-dependent mobility of holes at Q-point, see (3.5)
$\mu_1(\xi, t)$ – differential of μ_q at Q-point, see (3.70) and (4.8)
μ_d – differential mobility at Q-point, see (4.10)
$\mu_q, \mu_q(\xi)$ – mobility of holes at Q-point
τ – relaxation time
τ_{tr} – transit time of carriers across the channel
υ – velocity of carriers
ω – angular frequency

Acronyms

2D – Two-Dimensional
AC, ac – Alternating Current
ACP – Air Coplanar Probe
BSIM – Berkeley Short-channel IGFET Model
CLE – Channel-Lengthening Effect
CSE – Channel-Shortening Effect
CTME – Channel Thickness Modulation Effect
DC, dc – Direct Current
DCTME – Dynamic Channel Thickness Modulation Effect
DIBL – Drain-Induced Barrier Lowering
GCA – Gradual Channel Approximation
GCDE – Gradual Channel Detachment Effect
HSDMAGFET – Horizontally-Split-Drain Magnetic Field-Effect Transistor

MOS – Metal Oxide Semiconductor
MOSFET – Metal Oxide Semiconductor Field-Effect Transistor
NQS – Non-Quasi-Static
NQSCCPR – Non-Quasi-Static Channel Charge Partition Rule
Q-point – Quiescent Point
QS – Quasi-Static
QSCCPR – Quasi-Static Channel Charge Partition Rule
RF – Radio Frequency
VNA – Vector Network Analyzer

Chapter 1

INTRODUCTION

Wiesław Kordalski

This monagraph deals with modeling the small-signal operation of the MOS transistor, and presents original, not yet fully published, results of our research on time- and frequency-domain physics-based small-signal MOSFET models.

To design reliably circuits for communications in the range of radio or microwave frequencies, an adequate non-quasi-static (NQS) MOSFET model is indispensable. Quasi-static (QS) approaches do not accurately describe the operation of the MOSFET at high frequencies or under fast transients. This stems from the fact that the QS approximations assume the movable carriers in the channel of the transistor to respond instantaneously to the perturbations induced by a time-varying external bias, thereby neglecting the delay, dynamic properties of the channel and the coupling between the perturbed carrier beam and the transistor structure (the gate and the body).

Passing over the narrow-channel effects, the MOS transistor is inherently a two-dimensional (2D) device. Thus, to derive an NQS four-terminal small-signal MOSFET model valid in time and frequency domains, one should solve a closed set of partial differential equations, namely: continuity, transport and Poisson's equations. The set of equations cannot be exactly solved in the analytical form in 2D space, which implies the necessity for researchers to decompose the 2D problem into simplified ones.

An adequate model of the channel, especially its shape, is one of the most important issues in the derivation of a small-signal model of the transistor.

In models whose derivation is based, either explicitly or implicitly, on the gradual channel approximation (GCA), presented in e.g. [1–8], the shape of the channel is unrealistic, because its thickness decreases as the distance from the source of the transistor increases, see, e.g. [2–4]. The GCA is one of the assumptions which are most commonly put forward in analytical and semi-analytical approaches to the calculation of the value of the charge induced in the channel. The GCA amounts to the assumption that the surface density of the total uncompensated semiconductor charge, and thus of the channel, is determined only by the transversal electric field acting on the semiconductor surface. For this reason, apparent physical contradictions can appear if the approximation is used, which was pointed out, for instance, in [9–12]. It is the GCA that leads in consequence to such non-realistic phenomena

as the channel pinch-off or the channel-shortening effect (CSE). Therefore, a more comprehensive analysis on the channel shape is an obvious need.

In so-called charge-based or surface-potential-based models, e.g. [13–16], the channel is assumed to be a charge sheet of negligible thickness; however it is difficult to find physical reasons justifying this shape of the channel.

Some attempts were undertaken in order to overcome limitations imposed by the GCA. For example, the question of how changes of the longitudinal electric field component in the drain-to-source region affect the channel charge were considered in several works, e.g. [9–12], however, in each of them there were made some restrictive assumptions dealing with the shape of the depletion region. Namely, in all the works the depletion region and the channel were assumed to be rectangular, which is an unrealistic assumption.

In derivation of quasi-2D dc MOSFET models, which are briefly presented in [17–21], the MOSFET is considered as a 2D object in which the channel has also a 2D nature. The GCA is abandoned in this approach (non-GCA models). In description of these models, there are no such unrealistic terms as pinch-off and channel-shortening effect. According to these models, the channel has the shape of a curvilinear tetragon, and its thickness increases as the distance from the source of the transistor increases. This shape of the channel results from the qualitative and quantitative analysis carried out in detail in the next chapter. {It is worth mentioning that the key features of these quasi-2D dc MOSFET models are the main assumptions of the concept of a new horizontally-split-drain magnetic field-effect transistor (HSDMAGFET) described in works [22–26]}

Other few problems emerge when the exact knowledge of the small-signal behavior of the MOSFET and an adequate small-signal model of the device for radio and microwave frequencies are needed [27]. In addition to an appropriate channel model of the transistor, an adequate small-signal MOSFET model should take into account: the velocity saturation effect of carriers in the channel of the transistor; the field-dependent mobility; the electrical coupling between the perturbed charge in the channel and the gate and the body; local variations in the channel thickness; and the drain-induced barrier lowering (DIBL) effect.

Known small-signal MOSFET models used in designing integrated circuits in the radio frequency (RF) range can be split into two groups: quasi-static (QS) and non-quasi-static (NQS) models. The QS approaches do not aptly describe operation of the MOSFET at high frequencies or under fast transients. This stems from the fact that the QS approximations assume the movable carriers in the channel of the transistor to respond instantaneously to the perturbations induced by a time-varying external voltage, thereby neglecting the delay, dynamic properties of the channel, and the coupling between the perturbed carrier beam and the structure (the gate and the body). As a result, serious inconsistencies arise when the QS approach is used to modeling an RF MOS transistor. For instance, according to the model presented in [28], magnitudes of transadmittances of voltage-controlled current sources tend to infinity as frequency increases, which is an apparent contradiction.

To overcome the limitations, various models have been proposed in [29–36]. However, there are also weak points in those models. For instance, one can infer from the results presented in [32–35] that the magnitude of the gate transadmittance (y_m) does not decrease as the angular frequency ω tends to infinity. The widely used NQS BSIM3 model [36] is

a charge-based model developed on the channel charge relaxation time approach. Moreover, the channel of the MOSFET is modeled in work [36] as an RC distributed transmission line, which is not an adequate model of the transistor because any line of this type is not unilateral (i.e., the two-port admittance parameter $y_{12} \neq 0$). The intrinsic MOSFET (without parasitic elements) has to be unilateral ($y_{12} = 0$) for the reason that the charge carriers (electrons or holes) are injected only through the source-channel potential barrier. Besides, the transport equation for current carriers injected into the channel differs substantially from that for the current in the resistive layer of an RCline (ohmic transport mechanism). This is the fundamental reason for which any RC-line-based small-signal model of the intrinsic MOSFET is not adequate.

A phenomenon that is not included in known small-signal models is the dynamic channel thickness modulation effect (DCTME), see, e.g. [29–31].

The DIBL effect is also not included in the vast majority of known small-signal models, see, e.g. [28–36], and if it is considered, the applicability of these models is limited to a low-frequency range. For example, this phenomenon is included in the model presented in [37], but the model is quasi-static and its validity is restricted to a quasi-static frequency range.

To surmount the above-mentioned weak points of existing models, an attempt has been made to derive from first principles a new DIBL-included physics-based quasi-2D NQS frequency-domain small-signal model of the four-terminal MOSFET operating at an arbitrarily located quiescent point (Q-point). The model is briefly reported in [27, 38–42]. The new model is valid from zero Hz to well above the cut-off frequency f_T and takes into account: the velocity saturation effect of carriers in the channel; the dependence of the mobility on electric field; the electrical coupling between the perturbed charge in the channel and the gate and the body; local variations in the channel thickness; and the DIBL effect. According to the author's knowledge, there is no small-signal model in the literature that takes into account all these effects together. Moreover, there are no non-reciprocal capacitances in the new model, and the GCA is abandoned.

The purpose of this monograph is to present a detailed derivation and results of experimental verification of the new time- and frequency-domain quasi-2D NQS four-terminal small-signal MOSFET models which take into account the DIBL effect.

The monograph is arranged as follows.

The purpose of Chapter 2 is to give a physical background to the new time- and frequency-domain small-signal models. Theoretical discussion and results of numerical analysis in 2D space are given in order to introduce the following three phenomena: gradual channel detachment effect (GCDE), channel thickness modulation effect (CTME), and channel-lengthening effect (CLE). Based on these phenomena, a quasi-2D dc channel representation and a quasi-2D dc representation of the MOSFET are defined.

In Chapter 3, a novel quasi-2D NQS four-terminal time-domain small-signal MOSFET model is presented. A set of partial differential equations for the new physics-based small-signal model is derived. The set consists of a quasi-2D small-signal continuity equation, a quasi-2D small-signal Poisson's equation, and a quasi-2D small-signal transport equation. All the equations give a mathematical description of the behavior of the carriers

in the channel and charges in the gate and the body. A set of supplementary equations for coupling and non-capacitive displacement currents in the MOSFET under dynamic operation is also derived. Based on the quasi-2D dc MOSFET representation, a useful formula for the gate-to-body capacitance C_{gb} is derived, and some rules dealing with channel-to-gate and channel-to-body coupling currents are established. Reciprocal capacitances occurring in this model are defined. The model we propose in this chapter provides the background to a novel frequency-domain small-signal MOSFET model.

In Chapter 4, a novel DIBL-included quasi-2D NQS four-terminal frequency-domain small-signal MOSFET model is proposed. The model takes into account: the velocity saturation effect of carriers in the channel; the dependence of the mobility on electric field; the electrical coupling between the perturbed charge in the channel and the gate and the body; local variations in the channel thickness; and the DIBL effect. Unlike other models, this one is composed only of reciprocal capacitances. A closed set of partial differential equations defining the model in the time domain is formulated and solved in the frequency domain. The solution indicates that two types of waves can propagate from the source to the drain, viz., a longitudinal wave of a disturbance in the carrier density and a transverse wave of a disturbance in the channel thickness. A closed set of equations for frequency-domain non-capacitive terminal currents in the MOSFET under dynamic operation is also derived.

In Chapter 5, the results of experimental verification of the new DIBL-included quasi-2D NQS four-terminal frequency-domain small-signal MOSFET model are presented. For the purpose of the verification, test transistors and dummy structures were designed and fabricated in 0.35-μm technology. The de-embedding procedure is based on the open-short method, optimized for RF measurement up to 30 GHz of scattering parameters of the transistors in the common source configuration with the use of air coplanar probes (ACPs).

The last part includes a summary.

References

[1] Watts J., McAndrew C. C., Enz C., Galup-Montoro C., Gildenblat G., Hu C., Langevelde R., Miura-Mattausch M., Rios R., and Sah C. T., "Advanced compact models for MOSFETs," NSTI-Nanotech 2005, available: http://www.nsti.org.

[2] Tsividis Y. P. and McAndrew C., *The MOS transistor*, Int. 3rd ed., Oxford University Press, New York, Oxford, 2012.

[3] Sze C. M. and Ng K. K., *Physics of semiconductor devices*, 3rd ed., Wiley and Sons, 2007.

[4] Shockley W., "A unipolar "field-effect" transistor," *Proc. of the I.R.E.,* vol. 40, pp. 1365–1376, 1952.

[5] Hauser J. R., "A new and improved physics-based model for MOS transistors," *IEEE Trans. on* Electron *Devices,* vol. 52, No. 12, pp. 2640–2647, 2005.

[6] Chauhan Y. S., Venugopalan S., Chalkiadaki M.-A., Karim M. A. U.,Agarwal H., Khandelwal S., Paydavosi N., Duarte J. P., Enz C. C., Niknejad A. M., and Hu C.,

"BSIM6: analog and RF compact model for Bulk MOSFET," *IEEE Trans. on Electron Devices*, vol. 61, pp. 234–244, 2014.

[7] Cheng Y., Jeng M.-C., Liu Z., Huang J., Chan M., Chen K., Ko P. K., and Hu C., "A physical and scalable *I–V* model in BSIM3v3 for analog/digital circuit simulation," *IEEE Trans. on Electron Devices*, vol. 44, pp. 277–287, 1997.

[8] Enz C., "An MOS transistor model for RF IC design valid in all regions of operation," *IEEE Trans. on Electron Devices*, vol. 50, pp. 342–359, 2002.

[9] Zhang Q. Z. and Schroder D. K., "A new long-channel MOSFET model," *Solid-State* Electronics, vol. 30, pp. 859–888, 1987.

[10] Conti M. and Turcheti C., "On the short-channel theory for MOS transistor," *IEEE Trans. on* Electron *Devices*, vol. 38, pp. 2657–2661, 1991.

[11] Fujishima M. and Asada K., "A nonpinchoff gradual channel model for deep-submicron MOSFET's," *IEEE Trans. on Electron Devices*, vol. 40, pp. 1883–1885, 1993.

[12] Jang S.-L., Hu M.-C., and Chen Y.-S., "Current-voltage model of short-channel MOSFET's operated in the linear region," *Solid-State Electronics*, vol. 38, pp. 1239–1245, 1995.

[13] Brews J. R., "A charge sheet model for the MOSFET," *Solid-State Electronics*, vol. 21, pp. 345–355, 1978.

[14] Cunha A. I. A., Schneider M. C., and Galup-Montoro C., "An explicit physical model for the long-channel MOS transistor including small-signal parameters," *Solid-State Electronics*, vol. 38, pp. 1945–1952, 1995.

[15] Sallese J.-M., Bucher M., Krummenacher F., and Fazan P., "Inversion charge linearization in MOSFET modeling and rigorous derivation of the EKV compact model," *Solid-State Electronics*, vol. 47, pp. 677–683, 2003.

[16] Basu D. and Dutta A. K., "An explicit surface-potential-based MOSFET model incorporating the quantum mechanical effects," *Solid-State Electronics*, vol. 50, pp. 1299–1309, 2006.

[17] Kordalski W., "Unified model of the enhancement-mode MOS transistor," *20th European Solid* State *Device Research Conference*, (ESSDERC'90), pp. 603–606, September 10–13, 1990, Nottingham, United Kingdom.

[18] Kordalski W., "Two-dimensional effects in the MOSFET," *Proc. of the 19th National* Conference *on Circuit Theory and Electronic Circuits*, pp. 239–244, October 23–26, 1996, Krakow-Krynica, Poland.

[19] Kordalski W., Koziel S., and Wilamowski B. M., "An analytical DC model of the enhancement-mode, non-uniformly doped MOS transistor," *Proc. of the 1997 European Conference on Circuit Theory and Design, ECCTD'97*, vol. 2, pp. 743–748, 30th August – 3rd September, 1997, Budapest, Hungary.

[20] Koziel S., Kordalski W., and Wilamowski B. M., "A scalable I-V MOSFET model for analog/digital circuit simulation," *Proc. of the 22nd National Conference on Circuit Theory and Electronic Circuits*, pp. 247–252, October 20–23, 1999, Warszawa-Stare Jablonki, Poland.

[21] Kordalski W. and Stefanski T., "Compatible DC and small-signal MOSFET models for *radio* and microwave frequency simulation," in *Proc. of the 12th International Conf.:*

Mixed Design of Integrated Circuits and systems – MIXDES'2005, pp. 315–320, June 22–25, 2005, Krakow, Poland.

[22] Kordalski W., Boratyński B., Panek M., Ściana B., Zborowska-Lindert I., and Tłaczała M.: "Magnetic Field Microsensor based on GaAs MESFET," *Proc. of the International Conference on Applied Physics of Condensed Matter*, *APCOM 2007*, pp. 36–39, June 27–29, 2007, Bystra, Slovak Republic.

[23] Kordalski W., Polowczyk M., and Panek M., "Horizontally-split-drain MAGFET – a highly sensitive magnetic field sensor," *Bull. Pol. Ac.: Tech.*, vol. 55, No. 3, pp. 325–329, 2007.

[24] Boratyński B., Kordalski W., Ściana B., Panek M., and Zborowska-Lindert I., "A new drain insulation design in GaAs SD-MAGFET," *Materials Science-Poland*, vol. 26, no. 1, pp. 27–32, 2008.

[25] Kordalski W., Boratyński B., and Panek M., "Properties and estimated parameters of a submicrometer HSDMAGFET," *Materials Science-Poland*, vol. 26, no. 1, pp. 33–43, 2008.

[26] Kordalski W., Boratyński B., Zborowska-Lindert I., Panek M., Ściana B., and Tłaczała M., *Magnetic field sensor type MagFET*, Polish Patent PL210965(B1) (2012-03-30); Int. Cl G01R 33/02 (2006.01).

[27] Kordalski W. and Stefanski T., "A non-quasi-static small-signal MOSFET model for radio and microwave frequencies including spreading gate resistances and capacitances," in *Proc. IEEE Radio Frequency Integrated Circuits* (*RFIC*) *Symposium*, pp. 365–368, June 8–10, 2003, Philadelphia, Pennsylvania, USA.

[28] Enz C. C. and Cheng Y., "MOS transistor modeling for RF IC design," *IEEE Trans. on Solid-State Circuits,* vol. 35, no. 2, pp. 186–201, 2000.

[29] Sallese J. M. and Porret A. S., "A novel approach to charge-based non-quasi-static model of the MOS transistor valid in all modes of operation," *Solid-State Electronics,* vol. 44, pp. 887–894, 2000.

[30] Roy A. S., Enz C. C., and Sallese J.-M., "Compact modeling of anomalous high-frequency behavior of MOSFET's small-signal NQS parameters in presence of velocity saturation," *IEEE Trans. on Electron Devices,* vol. 53, no. 9, pp. 2044–2050, 2006.

[31] Aarts A. C. T., Smit G. D., Scholten A. J., and Klaassen D. B. M., "A PSP-based small-signal MOSFET model for both quasi-static and nonquasi-static operation," *IEEE Trans. on Electron Devices,* vol. 55, no. 6, pp. 1424–1432, 2008.

[32] Materka A. and Kacprzak T., "Computer calculation of large-signal GaAs FET amplifier characteristics," *IEEE Trans. on Microwave Theory and Techniques,* vol. 33, no. 2, pp. 129–135, 1985.

[33] Lee S., Kim C. S., and Yu H. K., "A small-signal RF model and its parameter extraction for substrate effects in RF MOSFETs," *IEEE Trans. on Electron Devices,* vol. 48, no. 7, pp. 1374–1379, 2001.

[34] Manku T., "Microwave CMOS-device physics and design," *IEEE J. of Solid-State Circuits,* vol. 34, no. 3, pp. 277–285, 1999.

[35] Sung R., Bendix P., and Das M. B., "Extraction of high-frequency equivalent circuit parameters of submicron gate-length MOSFET's," *IEEE Trans. on Electron Devices,* vol. 45, no. 8, pp. 1769–1775, 1998.

[36] Chan M., Hui K. Y., Hu C., and Ko P. K., "A robust and physical BSIM3 non-quasi-static transient and ac small-signal model for circuit simulation," *IEEE Trans. on Electron Devices*, vol. 45, no. 4, pp. 834–841, 1998.

[37] Liu S. and Nagel L. W., "Small-signal MOSFET models for analog circuit design," *IEEE J. of Solid-State Circuits,* vol. 17, no. 6, pp. 983–998, 1982.

[38] Kordalski W., "A quasi-2D small-signal MOSFET model – main results", *Electronics*, no. 9/2014, pp. 48–51, [in Polish]. DOI: 10.15199/ELE-2014-131.

[39] Stefański T., Kordalski W., and Hauer H., "An experimental verification of a new non-quasi-static small-signal MOSFET model for radio and microwave frequencies," *[CD-ROOM] Proceedings ICCSC 2004. The 2nd IEEE International Conference on Circuits and Systems for Communications*, June 30-July 2, 2004 Moscow, Russia.

[40] Kordalski W.J. and Stefański T.: "A Non-Quasi-Static Small-Signal Model of the Four-Terminal MOSFET for Radio and Microwave Frequencies," *Proc. IEEE Int. Conf. Circuits Syst. for Communications, ICCSC'2002*, pp. 313–319, June 26–28, 2002, St. Petersburg, Russia.

[41] Kordalski W.: "An Injection Non-Quasi-Static Small-Signal MOSFET Model," *Proc. of the* International *Conference on Signals and Electronic Systems, ICSES'2000*, pp. 307–312, October 17–20, 2000, Ustroń, Poland.

[42] Kordalski W., Stefański T., and Blakiewicz G.: "A Non-Quasi-Static Small-Signal MOSFET Model for RF and Microwave Circuits," *Proc. of the International Conference on Signals and Electronic Systems, ICSES'2000*, pp. 313–318, October 17–20, 2000, Ustroń, Poland.

Chapter 2

QUASI-2D REPRESENTATION OF THE MOSFET

Wiesław Kordalski

2.1. Introduction

In this chapter, theoretical considerations and the results of a numerical analysis in 2D space are given in order to introduce the following three phenomena: gradual channel detachment effect (GCDE), channel thickness modulation effect (CTME), and channel-lengthening effect (CLE). These phenomena are physical foundations for defining a quasi-2D dc representation of the channel and subsequently for transforming a 2D dc representation of the MOSFET into a quasi-2D dc representation of the device.

We assume in our analysis that no generation-recombination processes occur, and the tunneling and leakage currents are negligibly small.

2.2. 2D–into–quasi-2D transformation of the MOSFET

In this section, we define a quasi-2D representation of the channel, then a modified 2D dc MOSFET representation, and in the end a quasi-2D dc MOSFET representation.

2.2.1. Quasi-2D representation of the channel

In the MOSFET modeling, concepts such as the actual channel length (also referred to as the effective or electrical channel length), the magnitude and distribution of movable charges carrying the current in the channel, or velocity of carriers are of key importance. In this section, we define these and other concepts referring to a quasi-2D representation of the MOSFET channel, basing on the results of two-dimensional numerical analyses.

Two-dimensional phenomena

Let us consider a four-terminal *p*-type channel MOSFET carrying the source-to-drain current in a stationary electric field, which is depicted in Fig. 2.1, where the shaded p^+-type regions are electrically neutral parts of the source-body and drain-body junctions. The picture corresponds to the transistor that operates in the saturation regime.

Holes are injected into the channel through the source-channel potential barrier, and the current is controlled by the gate-source voltage V_{GS}, the body-source voltage V_{BS}, or by both of them. Note that the drain is a collecting electrode, which stems from the bias conditions.

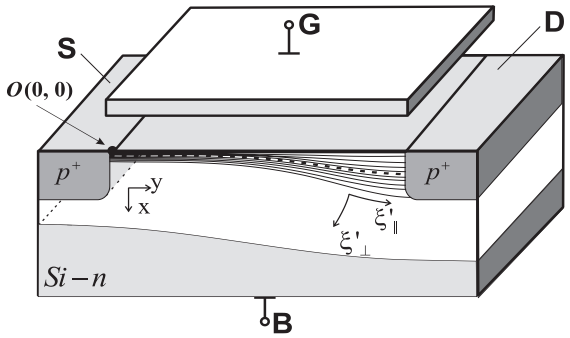

Fig. 2.1. Layers of current in a *p*-channel MOSFET under consideration. $O(0, 0)$ is the origin of both Cartesian coordinates and curvilinear ones. The metallurgical junctions are not shown.

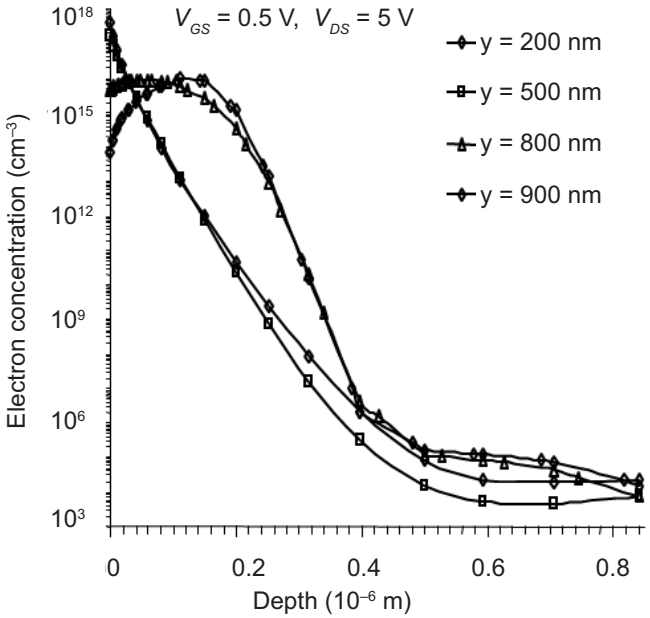

Fig. 2.2. Simulated electron concentration profiles for various cross-sections of the transistor channel of an *n*-MOSFET with the channel length L = 1 μm, unpublished [4]; effective gate-source voltage $V_{GS} - V_T$ = 0.5V, V_{DS} = 5V, and y is the distance from the transistor source.

The two-dimensional nature of kinetic processes in the transistor manifests itself particularly when the magnitude of drain-source voltage $|V_{DS}|$ is greater than $|V_{GS}|$. Under this condition, the direction of the transverse component of the electric field acting on the semiconductor surface in the vicinity of the drain is opposite to that in the vicinity of the source. This leads to repelling the positively charged holes from the semiconductor surface. As a result, trajectories of movable channel carriers are deflected downwards. Therefore, this

phenomenon can be called the gradual channel detachment effect (GCDE). The concept of the GCDE was originally introduced in [1].

In turn, due to the GCDE and diffusion of the non-uniformly distributed carriers, the channel of the transistor spreads out, leading to the channel thickness modulation effect (CTME). Numerical simulations confirm the two phenomena illustrated in Figs. 2.1 and 2.2; see also, e.g., Fig. 7 in [2] and Fig. 1 in [3].

Including these two effects into consideration enables us to gain a deeper insight into the principle of operation of the MOS transistor.

Layers of current and their description

An orthogonal curvilinear system of coordinates $\xi'_{\perp}$ and $\xi'_{\parallel}$ can be introduced if we note that a vector field, denoted by $\mathbf{J}(P)$, is constituted by the current density vector $\mathbf{J}$ at each point P in the channel. Due to stationary conditions, the vector field is solenoidal if generation-recombination processes are neglected at all points of the channel [5]. It means that the divergence of the vector $\mathbf{J}(P)$ is equal to zero, i.e.:

$$\nabla \cdot \mathbf{J}(P) = 0 \tag{2.1}$$

where ∇ is the nabla operator. Since all vector lines of a given solenoidal field $\mathbf{J}(P)$ do not intersect, one can associate with them a set of longitudinal $\xi'_{\parallel}$-coordinates; see Fig. 2.1.

Moreover, if we assume that the vector field is irrotational, i.e.:

$$\nabla \times \mathbf{J}(P) = 0 \tag{2.2}$$

then there exists a function $u(P)$ whose gradient equals $\mathbf{J}(P)$,

$$\mathbf{J}(P) = \nabla u(P) \tag{2.3}$$

The function $u(P)$ is called the potential or the potential function of a vector field $\mathbf{J}(P)$. Equating the function $u(P)$ with a constant, $u(P)$ = const, we obtain an equipotential line (a surface in 3Dspace) that is perpendicular to all the vector lines of agiven field $\mathbf{J}(P)$. Its shape depends on the distance from the source and biasing voltages. It is the equipotential line that is a $\xi'_{\perp}$-coordinate. The other $\xi'_{\perp}$-coordinate lines can be constructed by equating $u(P)$ with various constants. Thus, one can obtain an orthogonal curvilinear system of coordinates $\xi'_{\perp}$ and $\xi'_{\parallel}$ in this way, a so-called system of natural coordinates; see Fig. 2.1.

Taking into account the properties of the vector field $\mathbf{J}(P)$, the total current of the hole beam injected into the channel can be divided into infinitesimally thin layers of the current (i.e., infinitesimally thin channels or elementary channels); see Fig. 2.1. The width of the layers, W, is equal to the width of the transistor. Obviously, the $\xi'_{\parallel}$-coordinate lines of the orthogonal curvilinear system coincide with the trajectories of carriers moving from the source to the drain. The origin $O(0,\ 0)$ of both the curvilinear and Cartesian coordinate systems is placed on the semiconductor surface at the point where the transition between the source and the space charge region of the body-source pn junction occurs; see Fig. 2.1. For clarity, the source and the drain are the regions of the transistor in which the condition of electrical

neutrality is fulfilled; they are reservoirs of carriers. No electric field is assumed to be in the source and the drain.

For a point located on an arbitrarily chosen layer, let say, on the *k*th layer denoted by $(\xi'_{\perp k}, \xi'_{\parallel})$, we can exactly specify the distance of the point from the source, $\xi'_{\parallel}$, and the velocity of carriers at the point, $v'_{\parallel}$. It is worth emphasizing that the velocity of carriers at the point is a tangent vector to the vector line. In this way, a field of carrier velocities in the channel is introduced.

The following boundary condition is satisfied for each of the layers:

$$-\int_{source}^{drain} E'_{\parallel}(\xi'_{\perp k}, \xi'_{\parallel})\, d\xi'_{\parallel} = V_{DS} \tag{2.4}$$

where $E'_{\parallel}(\xi'_{\perp k}, \xi'_{\parallel})$ is the longitudinal component of the electric field in a given (*k*th) layer of current.

The current continuity equation and Gauss's law are fulfilled within each layer of current (see Figs. 2.3 and 2.4), i.e.:

$$p'(\xi'_{\perp 1}, \xi'_{\parallel 1})\, \upsilon'_{\parallel 1}(\xi'_{\perp 1}, \xi'_{\parallel 1})\, dA_1 = p'(\xi'_{\perp 1}, \xi'_{\parallel 2})\, \upsilon'_{\parallel 2}(\xi'_{\perp 1}, \xi'_{\parallel 2})\, dA_2 \tag{2.5}$$

$$\varepsilon_0\, \varepsilon_s \oint_A \mathbf{E} \cdot d\mathbf{A} = q \int_{\Delta\Omega} [N_d + p'(\xi'_{\perp}, \xi'_{\parallel})]\, d\Omega \tag{2.6}$$

where $\Delta\Omega$ is an element of volume bounded by surfaces $\xi'_{\parallel} = \xi'_{\parallel 1}$, $\xi'_{\parallel} = \xi'_{\parallel 2}$, $\xi'_{\perp} = \xi'_{\perp 1}$ and $\xi'_{\perp} = \xi'_{\perp 1} + \Delta\xi'_{\perp}$; A is the closed surface bounding the volume $\Delta\Omega$; $p'(\cdot)$ and N_d are, respectively, spatial charge density distributions of holes and ionized donors; ε_0 and ε_s are, respectively, the permittivity of free space and the relative permittivity of semiconductor substrate, **E** is the electric field vector, and q is the magnitude of the elementary charge.

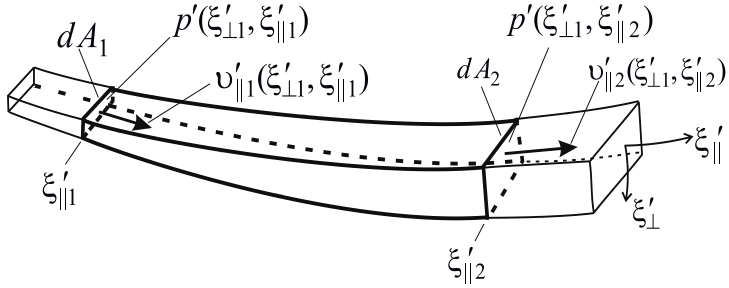

Fig. 2.3. A scheme illustrating the current continuity equation for a separated *p*-type layer of current.

Looking at the *p*-type layers of current shown in Figs. 2.4 and 2.5, an essential difference between the one- and two-dimensional approaches to determining the distribution of carriers along the channel can be noticed. First, let us consider the 2D case.

In Fig. 2.5, directions of transverse components of the electric field $E'_{\perp}(\cdot)$ acting on the surfaces enclosing the parts of space marked as $\Delta\Omega_1$ and $\Delta\Omega_2$ are opposite but it does not

mean that the resultant fluxes of these transverse components through the upper and lower surfaces of $\Delta\Omega_1$ and $\Delta\Omega_2$ are also opposite. On the contrary, the resultant fluxes of these transverse components of the electric field can have the same algebraic signs. What is more, we are sure that the signs of both these fluxes are the same, because the current continuity equation must be satisfied in an arbitrarily chosen cross-section of the layer of current. Thus, applying Gauss's theorem to $\Delta\Omega_1$ and $\Delta\Omega_2$, and taking into account the results of two-dimensional numerical 2D simulations of the MOSFET, we can write the following inequalities:

$$\varepsilon_0 \varepsilon_s \oint_{A_1} \mathbf{E} \cdot d\mathbf{A} = q \int_{\Delta\Omega_1} [N_d + p'(\xi'_\perp, \xi'_{||})]\, d\Omega > 0 \tag{2.7}$$

$$\varepsilon_0 \varepsilon_s \oint_{A_2} \mathbf{E} \cdot d\mathbf{A} = q \int_{\Delta\Omega_2} [N_d + p'(\xi'_\perp, \xi'_{||})]\, d\Omega > 0 \tag{2.8}$$

where A_1 and A_2 are the surfaces enclosing $\Delta\Omega_1$ and $\Delta\Omega_2$, respectively. Depending on the bias conditions and concentration of dopants in the substrate, the integral (2.7) can be greater, lesser, or equal to the integral (2.8), but there still exist conditions for the current flowing through the channel. However, the problem is formulated in a totally different way when the GCA is applied to calculate the distribution of carriers along the channel.

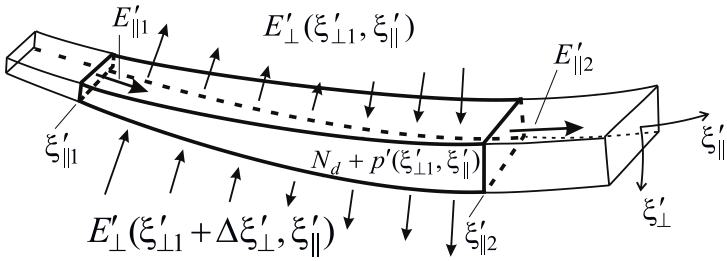

Fig. 2.4. A scheme illustrating of Gauss's law for a separated *p*-type layer of current; only transverse components of the electric field are shown. The transistor operates in the saturation regime.

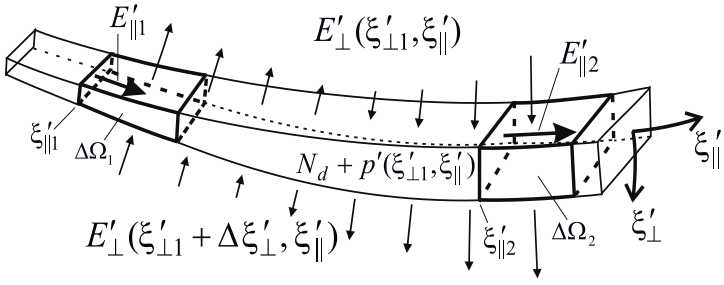

Fig. 2.5. A layer of current with two distinguished volume elements $\Delta\Omega_1$ and $\Delta\Omega_2$; only transverse components of the electric field are shown. The transistor operates in the saturation regime.

According to the GCA (the one-dimensional case), total charges which are inside the given volumes $\Delta\Omega_1$ and $\Delta\Omega_2$ (see Fig. 2.5) should have different signs because transverse electric fields acting on the surfaces enclosing $\Delta\Omega_1$ and $\Delta\Omega_2$ are oppositely directed. Consequently, it implies that only the positively charged holes can appear in the volume $\Delta\Omega_1$ because the GCA imposes only a negative charge in the volume $\Delta\Omega_2$. Therefore, we can say that the GCA "makes it impossible" for the MOSFET to operate when the magnitude of the drain-source voltage V_{DS} is greater than the gate-source voltage V_{GS} (it corresponds to the saturation range of the output voltage–current characteristics), which is an obvious contradiction.

The channel, channel line, channel length, arc-thickness of channel, channel charge and channel-lengthening effect

In general, the channel is the region of the transistor where a non-zero current flows between the source and the drain. Neglecting the narrow-channel effects, it can be considered as a two-dimensional object that is bounded by four surfaces displayed in Fig. 2.6: an injecting wall, a collecting wall, a top channel surface (*t. ch. s.*), and a bottom channel surface (*b. ch. s.*). The injecting wall, through which carriers are injected into the channel, separates the space charge region lying under the semiconductor surface from the electrically neutral source region. The collecting wall separates the space charge region lying under the semiconductor surface from the electrically neutral drain region that collects carriers. The top and bottom channel surfaces are the outer surfaces bounding, respectively, the top and bottom layers of current. Positions and shapes of the four surfaces depend on voltages biasing the transistor. If the drain-source voltage is small, $V_{DS} \approx 0$, the top and bottom channel surfaces as well as the current lines run almost parallel to the semiconductor surface and the system of natural coordinates $\xi'_{\perp}$ and $\xi'_{||}$ tends to the Cartesian one. However, if V_{DS} is increasing, the GCDE and CTME are intensified and subsequently the shape of the channel is becoming more irregular, as seen in Fig. 2.6.

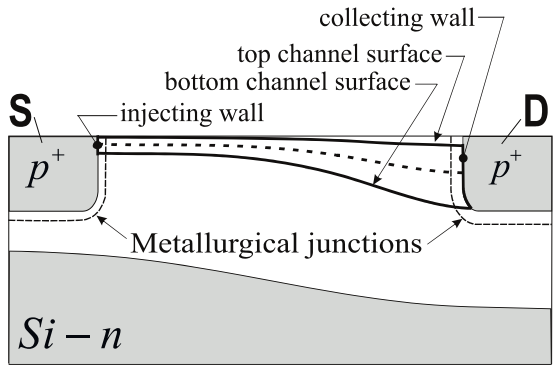

Fig. 2.6. The MOSFET channel and its characteristic bounding surfaces.

Referring to Fig. 2.1, one can see that the length of, let say, the kth layer L_k, being the length of the kth subchannel, is different from the length of the other layers. The length of

the shortest subchannel, L_{min}, is the smallest distance between the electrically neutral regions of the source and the drain or, in other words, between reservoirs of carriers in the source and the drain. Obviously, any average length of the channel, L_{av}, is greater than L_{min}. Similarly, any effective channel length, L_{eff}, is expected to be greater than L_{min}. Thus, after [6–7], the metallurgical channel length, L_{met}, can be defined as the distance between the points at which the metallurgical junctions of the source and drain intersect the silicon surface. We can state that L_{min}, L_{av}, and L_{eff} should be greater than L_{met}. This statement is confirmed by the results presented in Fig. 11 in [6] and in Fig. 3 in [7]. What is more, the considerations and results of two-dimensional numerical computations show that the GCDE intensifies as the drain-source voltage V_{DS} is increasing [2–4], which means that elementary channels are getting longer and subsequently L_{min}, L_{av}, and L_{eff} become greater. We can thus say that a channel-lengthening effect (CLE) occurs, which is the opposite to the channel-shortening effect. The CLE is produced by the GCDE and CTME.

A measure of the length of the channel in the quasi-2D approach to the MOSFET operating under dc conditions is closely related to an average trajectory of movable channel carriers, in other words, to an average channel current line, or simply to a channel line. Strictly speaking, the channel line is a line in the cross-sectional view of the transistor, but in reality it represents a cylindrical surface in a three-dimensional space. The channel line, denoted by l_{ch}, is illustrated by a dashed curve in Fig. 2.1, and its length is equal to the channel length L of the MOS transistor in the quasi-2D representation.

The channel line l_{ch} can be obtained as follows. First, we divide equally the channel current, I_{ch}, into k layers of current so that each layer, l_k, is carrying the current equal to I_{ch}/k. Then, we choose a point M ($\xi'_{\perp 1}$, $\xi'_{||M}$) belonging to the first current layer l_1 and equidistant from the injecting and collecting walls; see Figs. 2.6 and 2.7.

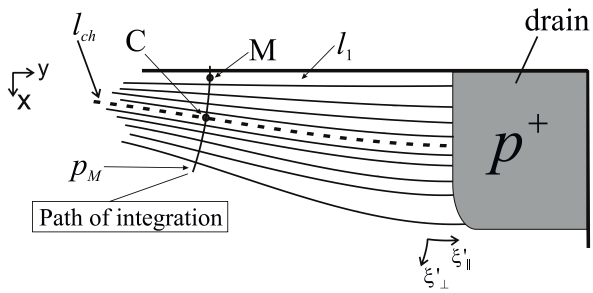

Fig. 2.7. A fragment of the channel; the highlighted elements are necessary to determine the channel line l_{ch}. The transistor operates in the saturation regime. The shaded p^+-region is an electrically neutral part of the drain-body junction; the metallurgical p-n junction is not depicted.

Then, we choose a surface S_M that perpendicularly intersects all the channel current lines and passes through the point M; the surface S_M is represented by a line p_M in Fig. 2.7. The behavior of the longitudinal component of current density as a function of a point over the surface S_M when $\xi'_{\perp}$ is varied and $\xi'_{||} = \xi'_{||M}$ is described by $J'_{||}(\xi'_{\perp}, \xi'_{||M})$. The distribution

of the current density $J'_{\|}(\xi'_{\perp}, \xi'_{\|M})$ versus $\xi'_{\perp}$ (along the line p_M) is just employed to determine the point C $(\xi'_{\perp C}, \xi'_{\|C})$ through which the channel line l_{ch} is passing; see Fig. 2.7.

Namely, the numerical value of the $\xi'_{\perp}$-coordinate of the point C, $\xi'_{\perp C}$, is determined by the $\xi'_{\perp}$-coordinate of the centroid of the current density distribution $J'_{\|}(\xi'_{\perp}, \xi'_{\|M})$, which can be written as follows:

$$\xi'_{\perp C} = \frac{\int_{(t.ch.s)}^{(b.ch.s)} \xi'_{\perp} J'_{\|}(\xi'_{\perp}, \xi'_{\| M})\, d\xi'_{\perp}}{\int_{(t.ch.s)}^{(b.ch.s)} J'_{\|}(\xi'_{\perp}, \xi'_{\| M})\, d\xi'_{\perp}} \tag{2.9}$$

where the integration is made along the line p_M from the top channel surface (*t. ch. s.*) to the bottom channel surface (*b. ch. s.*). In other words, the coordinates $(\xi'_{\perp C}, \xi'_{\| C})$ are a "center of gravity" of the current density distribution along the line p_M. The point C $(\xi'_{\perp C}, \xi'_{\| C})$ belongs to a current line. It is the current line that is the channel line l_{ch} of the MOSFET.

The channel line l_{ch} is very useful and suitable for a mathematical description of various 2D effects and it is the essence of the quasi-2D modeling of the MOS transistor. Therefore, it can be considered as a reference line ξ or, simply, as a coordinate ξ.

As previously stated, the channel length L of the MOS transistor in the quasi-2D dc representation is equal to the length of the channel line l_{ch}, which can be expressed in the natural coordinates as

$$L = \int_{\xi_S}^{\xi_D} d\xi \tag{2.10}$$

where ξ_S and ξ_D are end points of the channel line; see Fig. 2.8.

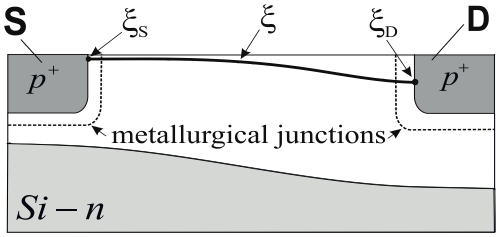

Fig. 2.8. The MOSFET channel line ξ with its end points. The transistor operates in the saturation regime.

Another parameter characterizing geometrically the flow of carriers between the drain and the source is the arc-thickness of the channel, $T_{arc}(\xi)$, understood as the arc-length of the front line of the movable channel charges. In this case, each equipotential line of the vector field $\mathbf{J}(P)$ is the front line. Thus, the arc-thickness $T_{arc}(\xi)$ is a function of the independent variable ξ, and is defined in the natural coordinates as follows:

$$T_{arc}(\xi) = \int_{(t.ch.s)}^{(b.ch.s)} d\xi'_{\perp} \tag{2.11}$$

where the integration is made along the $\xi'_{\perp}$-coordinate that intersects the channel line l_{ch} at ξ and the limits of the integral are the points of intersection of the path of integration with the top channel surface (*t. ch. s.*) and with the bottom channel surface (*b. ch. s.*); see Figs. 2.1, 2.6, and 2.7.

Of high importance for modeling electrical MOSFET characteristics is an integral measure of the movable-charge density, measured in C/m^2, in the channel. It is defined in a similar way as in [8]:

$$Q'_C(\xi) = q \int_{(t.ch.s)}^{(b.ch.s)} p'(\xi'_{\perp}, \xi)\, d\xi'_{\perp} \tag{2.12}$$

where the integration is made in the same way as described in the comment on (2.11) and $p'(\xi'_{\perp}, \xi)$ is the hole density distribution over the path (contour) of integration.

Integral form of the dc continuity equation

Assuming that the MOSFET operates under dc condition and neglecting the generation-recombination phenomena, the channel current I_{ch} must satisfy the continuity equation in the integral form that can be written in the Cartesian coordinates as

$$I_{ch} = \int_A \mathbf{J}(x, y) \cdot d\mathbf{A} \tag{2.13}$$

where the surface integral is taken over an arbitrary surface A intersecting the channel, and $\mathbf{J}(x, y)$ is the current density vector in the channel. The magnitude of the integral is independent of the choice of the integration surface A. In particular, we can write a simpler equivalent formula for the channel current in the natural coordinates $(\xi'_{\perp}, \xi)$, viz.:

$$I_{ch} = W \int_{(b.ch.s)}^{(t.ch.s)} J'_{\parallel}(\xi'_{\perp}, \xi)\, d\xi'_{\perp} \tag{2.14}$$

where the integration is made in the same way as described in the comment on (2.11).

Other quantities of the quasi-2D dc representation of the channel

As already stated, it is impossible to mathematically describe in an analytical form with absolute precision in 2D-space the kinetic phenomena occurring in the MOS transistor. Therefore, we need to simplify the problem, while accounting for the essential aspects of the two-dimensional nature of the transistor.

For the purposes of the quasi-2D analysis, we introduce a rectilinear system of coordinates $\xi_{\perp}$ and ξ in which ξ-coordinate coincides with the channel line l_{ch}, and $\xi_{\perp}$-coordinate is an auxiliary axis that is used for describing quantities and phenomena versus the coordinate perpendicular to the channel line.

A quasi-2D dc representation of the channel presented here is defined by the channel length L, carrier concentration (holes in this case) $p(\xi)$, longitudinal electric field $E(\xi)$, velocity of carriers $v(\xi)$, current density $J(\xi)$, and effective channel thickness $X(\xi)$.

Since the channel line l_{ch} is the reference line in our considerations, it is reasonable to assume that functional dependences on ξ-coordinate of $p(\xi)$, $E(\xi)$, and $\upsilon(\xi)$ are the same as those of, respectively, the carrier concentration, longitudinal electric field, and carrier velocity over the channel line ξ in 2D-space; see Fig. 2.8 and also Figs. 2.1, 2.6, 2.7. This assumption enables us to preserve the well-known form of the current density equation:

$$J(\xi) = q\, p(\xi)\, \upsilon(\xi) \tag{2.15}$$

If we assume further that the channel current I_{ch} is known, an effective channel thickness $X(\xi)$ is defined as follows:

$$X(\xi) = \frac{I_{ch}}{q\, p(\xi)\, \upsilon(\xi)\, W} \tag{2.16}$$

Denoted by $Q_C(\xi)$, the channel charge per unit area in the quasi-2D representation, cf. (2.12), is given by

$$Q_C(\xi) = q\, p(\xi)\, X(\xi) \tag{2.17}$$

The continuity equation for the quasi-2D representation of the channel has the form:

$$I_{ch} = J(\xi)\, X(\xi)\, W \tag{2.18}$$

where the channel current I_{ch} is independent of ξ.

The longitudinal electric field $E(\xi)$ in the channel is related to the distribution of potential along the channel, $V(\xi)$, through the following formula:

$$E(\xi) = -\frac{dV(\xi)}{d\xi} \tag{2.19}$$

and satisfies the boundary condition, cf. (2.4),

$$-\int_{source}^{drain} E(\xi)\, d\xi = V_{DS} \tag{2.20}$$

Obviously, parameter values of the quasi-2D dc channel representation can also be determined by best fitting the experimental characteristics with the theoretical ones.

Finally, based on the results of two-dimensional numerical dc MOSFET analyses and the discussion carried out in this section, we can derive the quasi-2D dc MOSFET channel representation which is illustrated in Fig. 2.9.

The quasi-2D dc channel representation is characterized by the channel line ξ, channel length L, channel width W, effective channel thickness $X(\xi)$, hole concentration $p(\xi)$, carrier velocity $\upsilon(\xi)$, longitudinal electric field $E(\xi)$, and current density $J(\xi)$.

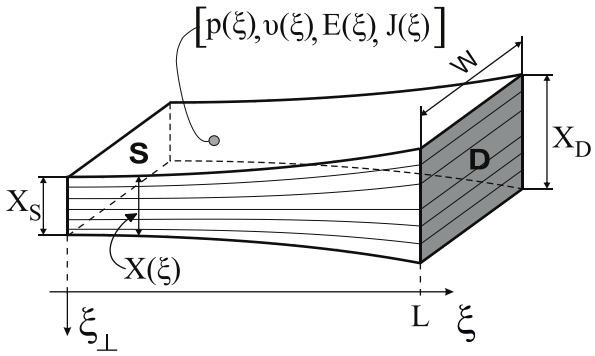

Fig. 2.9. The quasi-2D representation of a *p*-type channel of the MOSFET.

2.2.2. Modified 2D dc MOSFET representation

Basing on the quasi-2D representation of the channel and using some rules, a modified 2D dc representation of the MOSFET is defined in this section.

"Domain" and "image" of a 2D–into–quasi-2D transformation

As stated in Sec. 2.2.1, with increasing $|V_{DS}|$, the transistor channel extends. To take into account the CLE, we must transform a part of the 2D transistor representation into an appropriate part of a modified 2D transistor representation. The general concept of the transformation is shown in Fig. 2.10.

The following symbols of Fig. 2.10a: $N_d^*(x, y)$, $N_a^*(x, y)$, $p^*(x, y)$, and $n^*(x, y)$ represent the density of, respectively, positively ionized donors, negatively ionized acceptors, electrons, and holes, whereas their counterparts of Fig. 2.10b are denoted by $N_d(\xi_\perp, \xi)$, $N_a(\xi_\perp, \xi)$, $p(\xi_\perp, \xi)$, and $n(\xi_\perp, \xi)$, respectively; L_{DS} is the smallest distance between the electrically neutral regions of the source and the drain. The electrically neutral part of the *n*-type substrate is separated from the depletion region of the transistor by a surface represented by $X_d^*(y)$ in Fig. 2.10a, and by $X_d(\xi)$ in Fig. 2.10b.

The "domain" of the transformation, denoted by R_{2D}, is the region defined as follows (see Fig. 2.10a):

$$R_{2D} = \{(x, y) : -t_g^* \le x \le t_b^*,\ 0 \le y \le L_{DS}\} \tag{2.21}$$

and the "image" of the transformation is the region denoted by R_{q2D} and defined as (see Fig. 2.10b):

$$R_{q2D} = \{(\xi_\perp, \xi) : -t_g \le \xi_\perp \le t_b,\ 0 \le \xi \le L\} \tag{2.22}$$

The transformation is defined as follows:

$$\xi_\perp = x, \quad \xi = \lambda y, \quad \lambda = L / L_{DS} \ge 1 \tag{2.23}$$

Relationships (2.21)–(2.23) enable us to determine quantities of the modified 2D representation of the transistor.

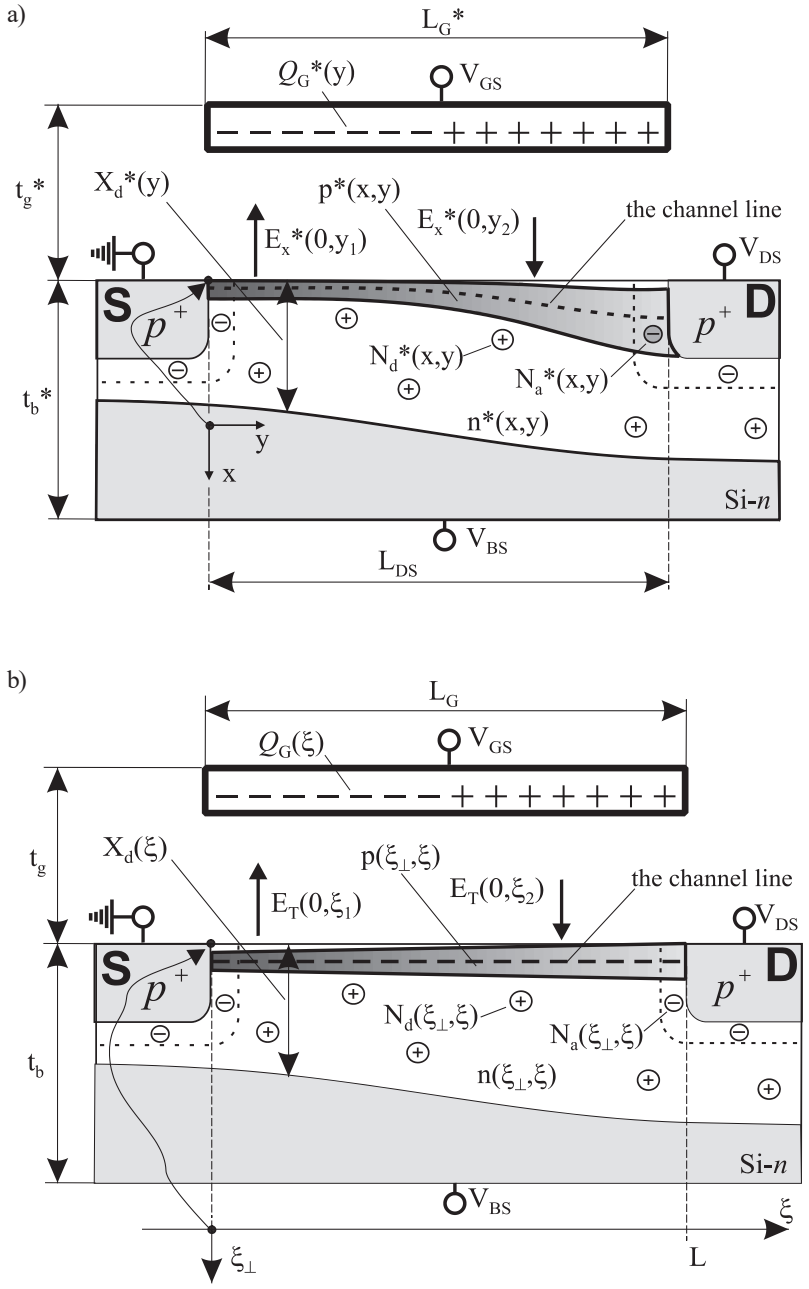

Fig. 2.10. Transformation of the 2D MOSFET representation into a modified 2D MOSFET representation. (a) Two-dimensional picture of a real *p*-channel MOSFET. (b) Modified 2D representation of the *p*-channel MOSFET.

Obvious transformation of some quantities

According to (2.23), we have the following relationships:

$$L = \lambda\, L_{DS}\,, \qquad \lambda \geq 1 \tag{2.24}$$

$$L_G = \lambda\, L_G^* \tag{2.25}$$

$$X_d(\xi) = X_d^*(\xi/\lambda) \tag{2.26}$$

$$\psi_s(0,\xi) = \psi_s^*\left(0, \frac{\xi}{\lambda}\right) \tag{2.27}$$

$$t_{ox} = t_{ox}^*, \quad t_g = t_g^*, \quad t_b = t_b^* \tag{2.28}$$

Transformation of the other quantities

In the modified 2D MOSFET representation presented here, the transformation of $N_A^*(x, y)$, $N_D^*(x, y)$ $N_a^*(x, y)$, $N_d^*(x, y)$, $n^*(x, y)$, and $p^*(x, y)$, determined in the region

$$S_{2D} = \{(x,y):\, 0 \leq x \leq t_b^*,\, 0 \leq y \leq L_{DS}\} \tag{2.29}$$

into their equivalents $N_A(\xi_\perp, \xi)$, $N_D(\xi_\perp, \xi)$, $N_a(\xi_\perp, \xi)$, $N_d(\xi_\perp, \xi)$, $n(\xi_\perp, \xi)$, and $p(\xi_\perp, \xi)$, determined in the region

$$S_{q2D} = \{(\xi_\perp, \xi):\, 0 \leq \xi_\perp \leq t_b,\, 0 \leq \xi \leq L\} \tag{2.30}$$

is governed by a principle that the numbers of dopants, ionized dopants, and carriers in their respective regions (S_{2D} and S_{q2D}) are equal; $N_A^*(x, y)$ and $N_A(\xi_\perp, \xi)$ as well as $N_D^*(x, y)$ and $N_D(\xi_\perp, \xi)$ stand for density of acceptors and donors, respectively.

Applying this principle, for instance, to donors, we have:

$$\int_{S_{2D}} N_D^*(x,y)\, dx\, dy = \int_{S_{q2D}} N_D(\xi_\perp, \xi)\, d\xi_\perp d\xi \tag{2.31}$$

Reducing double integrals in (2.31) to iterated ones, we get:

$$\int_0^{L_{DS}} dy \int_0^{t_b^*} N_D^*(x,y)\, dx = \int_0^{L} d\xi \int_0^{t_b} N_D(\xi_\perp, \xi)\, d\xi_\perp \tag{2.32}$$

Changing variables in the integral of the left-hand side of (2.32) according to the transformation (2.23), we can write:

$$\int_0^{L_{DS}} dy \int_0^{t_b^*} N_D^*(x,y)\, dx = \int_0^{L} d\xi \int_0^{t_b} N_D^*\left(\xi_\perp, \frac{\xi}{\lambda}\right) \left|\frac{\partial(x,y)}{\partial(\xi_\perp, \xi)}\right| d\xi_\perp \tag{2.33}$$

where

$$\left|\frac{\partial(x,y)}{\partial(\xi_\perp,\xi)}\right| = \begin{vmatrix} \frac{\partial x}{\partial \xi_\perp} & \frac{\partial x}{\partial \xi} \\ \frac{\partial y}{\partial \xi_\perp} & \frac{\partial y}{\partial \xi} \end{vmatrix}, \qquad \text{here}: \left|\frac{\partial(x,y)}{\partial(\xi_\perp,\xi)}\right| = \frac{1}{\lambda} \tag{2.34}$$

is the Jacobian of (2.23).

If we replace the Jacobian in (2.33) by its value, $1/\lambda$, then:

$$\int_0^{L_{DS}} dy \int_0^{t_b^*} N_D^*(x,y)\, dx = \int_0^{L} d\xi \int_0^{t_b} \frac{1}{\lambda} N_D^*\left(\xi_\perp, \frac{\xi}{\lambda}\right) d\xi_\perp \tag{2.35}$$

When comparing (2.32) with (2.35), we obtain the following formula for the transformation of $N_D^*(x, y)$ to $N_D(\xi_\perp, \xi)$:

$$N_D(\xi_\perp, \xi) = \frac{1}{\lambda} N_D^*\left(\xi_\perp, \frac{\xi}{\lambda}\right) \tag{2.36}$$

Then, it can be shown by an argument analogous to the one that leads to (2.36) that

$$N_A(\xi_\perp, \xi) = \frac{1}{\lambda} N_A^*\left(\xi_\perp, \frac{\xi}{\lambda}\right) \tag{2.37}$$

$$N_a(\xi_\perp, \xi) = \frac{1}{\lambda} N_a^*\left(\xi_\perp, \frac{\xi}{\lambda}\right) \tag{2.38}$$

$$N_d(\xi_\perp, \xi) = \frac{1}{\lambda} N_d^*\left(\xi_\perp, \frac{\xi}{\lambda}\right) \tag{2.39}$$

$$n(\xi_\perp, \xi) = \frac{1}{\lambda} n^*\left(\xi_\perp, \frac{\xi}{\lambda}\right) \tag{2.40}$$

$$p(\xi_\perp, \xi) = \frac{1}{\lambda} p^*\left(\xi_\perp, \frac{\xi}{\lambda}\right) \tag{2.41}$$

Transformation of x-component of the electric field vector on the semiconductor surface, $E_x^*(0, y)$, into its analog, $E_T(0, \xi)$, is depicted in Fig. 2.11.

It is worth noticing that if L_{DS} is many times greater than thickness of the gate oxide t_{ox} then a good approximation for $E_x^*(0, y)$ is as follows, see, e.g., [8, p. 302], [9], [10, p. 133],

$$E_x^*(0,y) = \frac{V_G - \psi_s^*(0,y)}{t_{ox}} \tag{2.42}$$

where V_G denotes the electrostatic potential at the gate, and $\psi_s^*(0, y)$ is the electrostatic potential at the semiconductor-oxide interface.

The transformation $E_x^*(0, y) \to E_T(0, \xi)$ is based on the assumption that total amounts of charges in the region D_{2D} (see the curvilinear trapezoid in Fig. 2.11a),

$$D_{2D} = \{(x,y):\ 0 \le x \le X_d^*(y),\ 0 \le y \le L_{DS}\} \tag{2.43}$$

and in the region D_{q2D} (see the curvilinear trapezoid in Fig. 2.11b),

$$D_{q2D} = \{(\xi_\perp, \xi) : 0 \le \xi_\perp \le X_d(\xi),\ 0 \le \xi \le L\} \tag{2.44}$$

are equal.

Thus, making use of the assumption, referring to Fig. 2.11, and applying Gauss's law to the transistor of a unit width, we can write:

$$\begin{aligned} &-\varepsilon_0\varepsilon_{ox}\int_0^{L_{DS}} E_x^*(0,y)\,dy + \varepsilon_0\varepsilon_s\int_0^{X_d^*(L_{DS})} E_y^*(x,L_{DS})\,dx - \varepsilon_0\varepsilon_s\int_0^{X_d^*(0)} E_y^*(x,0)\,dx \\ &= -\varepsilon_0\varepsilon_{ox}\int_0^{L} E_T(0,\xi)\,d\xi + \varepsilon_0\varepsilon_s\int_0^{X_d(L)} E_L(\xi_\perp, L)\,d\xi_\perp - \varepsilon_0\varepsilon_s\int_0^{X_d(0)} E_L(\xi_\perp, 0)\,d\xi_\perp \end{aligned} \tag{2.45}$$

If we assume that fluxes of the electric displacement through the corresponding surfaces (see Fig. 2.11) are equal, i.e.:

$$\int_0^{X_d^*(L_{DS})} \varepsilon_0\varepsilon_s\, E_y^*(x,L_{DS})\,dx = \int_0^{X_d(L)} \varepsilon_0\varepsilon_s\, E_L(\xi_\perp, L)\,d\xi_\perp \tag{2.46}$$

$$-\int_0^{X_d^*(0)} \varepsilon_0\varepsilon_s\, E_y^*(x,0)\,dx = -\int_0^{X_d(0)} \varepsilon_0\varepsilon_s\, E_L(\xi_\perp, 0)\,d\xi_\perp \tag{2.47}$$

then (2.45) can be reduced to:

$$\int_0^{L_{DS}} E_x^*(0,y)\,dy = \int_0^{L} E_T(0,\xi)\,d\xi \tag{2.48}$$

Changing the variable in the integral of the left-hand side of (2.48) according to (2.23), we get:

$$\int_0^{L} \frac{1}{\lambda} E_x^*\left(0, \frac{\xi}{\lambda}\right) d\xi = \int_0^{L} E_T(0,\xi)\,d\xi \tag{2.49}$$

and hence

$$E_T(0,\xi) = \frac{1}{\lambda} E_x^*\left(0, \frac{\xi}{\lambda}\right) \tag{2.50}$$

Transformation of the charge per unit area on the inner gate surface, $Q_G^*(y)$, into its counterpart, $Q_G(\xi)$, is based on the assumption that the charge induced on the gate surface by $E_x^*(0, y)$ is equal to that which is induced by $E_T(0, \xi)$; see Fig. 2.11. Relying on this assumption, we can write:

$$\int_0^{L_{DS}} Q_G^*(y)\,dy = \int_0^{L} Q_G(\xi)\,d\xi \tag{2.51}$$

Changing the variable in the integral of the left-hand side of (2.51) according to (2,23), we have:

$$\int_0^{L} \frac{1}{\lambda} Q_G^*\left(\frac{\xi}{\lambda}\right) d\xi = \int_0^{L} Q_G(\xi)\,d\xi \tag{2.52}$$

and this in turn results in:

$$Q_G(\xi) = \frac{1}{\lambda} Q_G^*\left(\frac{\xi}{\lambda}\right) \tag{2.53}$$

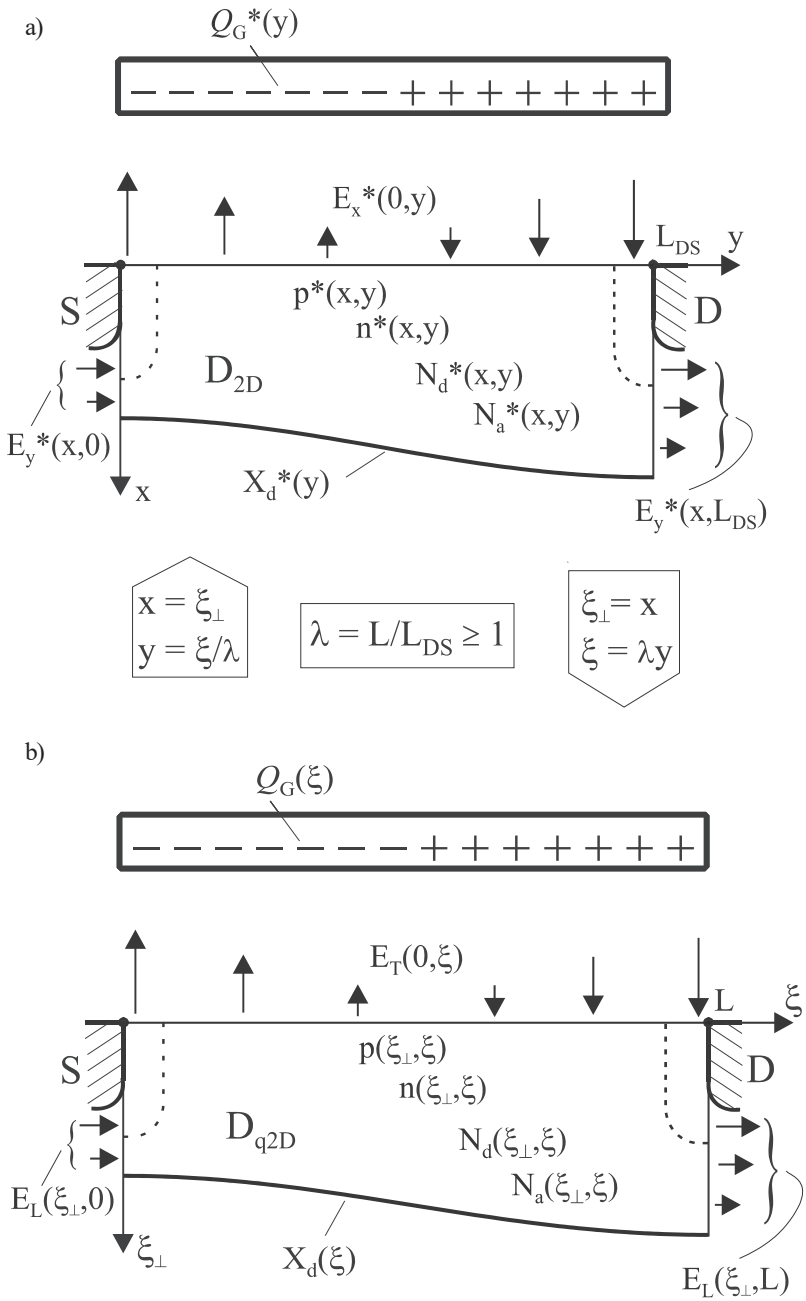

Fig. 2.11. Transformation of $\{E_x^*(0, y), Q_G^*(y)\}$ into $\{E_T(0, \xi), Q_G(\xi)\}$; only transverse components of the electric field are shown.

2.2.3. Quasi-2D dc MOSFET representation

Under dc conditions, almost all quantities of the quasi-2D MOSFET representation depend on bias voltages, and are functions of the spatial variable ξ.

Geometrical parameters as well as physical quantities characterizing the quasi-2D dc representation of the channel are defined and comprehensively discussed in Sec. 2.2.1.

Based on the modified 2D representation of the device, some useful quantities of the quasi-2D MOSFET representation, such as $X_d(\xi)$, $\psi_s(0,\xi)$, $E_T(0,\xi)$, and $Q_G(\xi)$, have already been defined in Sec. 2.2.2.

Now, we proceed to define the other quantities of the quasi-2D representation of the transistor.

Effective spatial densities of donors, acceptors, ionized donors, and ionized acceptors in the depletion region (region D_{q2D} in Fig. 2.11b), denoted, respectively, by $N_D(\xi)$, $N_A(\xi)$, $N_d(\xi)$, and $N_a(\xi)$, are determined as follows:

$$N_D(\xi)=\frac{\int_0^{X_d(\xi)} N_D(\xi_\perp,\xi)\,d\xi_\perp}{X_d(\xi)} \tag{2.54}$$

$$N_A(\xi)=\frac{\int_0^{X_d(\xi)} N_A(\xi_\perp,\xi)\,d\xi_\perp}{X_d(\xi)} \tag{2.55}$$

$$N_d(\xi)=\frac{\int_0^{X_d(\xi)} N_d(\xi_\perp,\xi)\,d\xi_\perp}{X_d(\xi)} \tag{2.56}$$

$$N_a(\xi)=\frac{\int_0^{X_d(\xi)} N_a(\xi_\perp,\xi)\,d\xi_\perp}{X_d(\xi)} \tag{2.57}$$

Denoted by $N(\xi)$, the net effective spatial density of positively ionized donors and negatively ionized acceptors in the region D_{q2D} (see Fig. 2.11b) are given by

$$N(\xi)=N_d(\xi)-N_a(\xi) \tag{2.58}$$

As in [2, 7], the surface charge densities (C/cm^2) of uncompensated ionized dopants, $Q_B(\xi)$, holes, $Q_p(\xi)$, and electrons, $Q_n(\xi)$, in the depletion region D_{q2D} are defined as follows:

$$Q_B(\xi)=q\,N(\xi)\,X_d(\xi) \tag{2.59}$$

$$Q_p(\xi)=q\int_0^{X_d(\xi)} p(\xi_\perp,\xi)\,d\xi_\perp \tag{2.60}$$

$$Q_n(\xi)=-q\int_0^{X_d(\xi)} n(\xi_\perp,\xi)\,d\xi_\perp \tag{2.61}$$

The charges denoted by $Q(\xi)$ with proper subscripts are interpreted as charges per unit area that are seen in $\xi_\perp$ direction across an infinitesimal element of area of the plane $\xi_\perp = 0$. They are commonly found in theory of the MOSFET.

It is worth emphasizing that functions $Q_p(\xi)$ and $Q_C(\xi)$ are slightly different from each other, but the following formula holds:

$$\int_0^L Q_p(\xi)\,d\xi = \int_0^L Q_C(\xi)\,d\xi \tag{2.62}$$

For the purposes of further quasi-2D analysis, we propose a quasi-2D representation of the device, which is shown in Fig. 2.12.

The symbols $E_{CB}(\xi)$ and $E_{CG}(\xi)$ denote, respectively, the vertical electric field on the bottom channel surface and the vertical electric field on the top channel surface. We present the vector $E_{CB}(\xi)$ as an arrow "attached" to a point belonging to the bottom channel surface, and the vector $E_{CG}(\xi)$ as an arrow "attached" to a point belonging to the top channel surface.

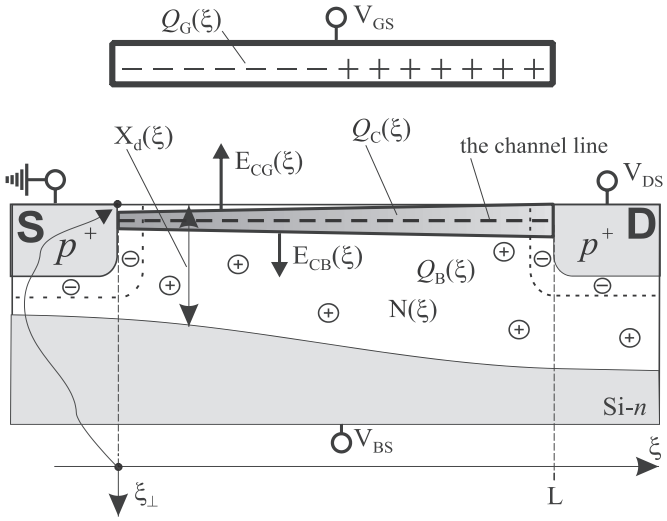

Fig. 2.12. The quasi-2D dc MOSFET representation.

2.3. Conclusion

A quasi-2D dc MOSFET representation has been proposed in this chapter. The representation is a result of a 2D–into–quasi-2D transformation that is governed by some principles we have established, and takes into account three newly introduced phenomena: the gradual channel detachment effect (GCDE), the channel thickness modulation effect (CTME), a and the channel-lengthening effect (CLE).

The quasi-2D representation of the MOS transistor lays the foundations for new quasi-2D non-quasi-static four-terminal small-signal MOSFET models that are developed in Chapters 3 and 4.

References

[1] Kordalski W., "Unified model of the enhancement-mode MOS transistor," *20th European Solid* State *Device Research Conference*, (ESSDERC'90), pp. 603–606, September 10–13, 1990, Nottingham, United Kingdom.

[2] Selberherr S., Schutz A., and Potzl H. W., "MINIMOS – a two-dimensional MOS transistor analyzer", *IEEE J. of Solid-State Circuits,* vol. SC-15, no. 4, pp. 605–615, 1980.

[3] Yamaguchi K., "Fiel-d-dependent mobility model for two-dimensional numerical analysis of MOSFETs", *IEEE Trans. on Electron Devices*, vol. ED-26, no. 7, pp. 1068–1074, Jul. 1979.

[4] Tomaszewski D. and Kordalski W., "Simulation with the use of ATLAS (Silvaco Int., 1998)", unpublished.

[5] Stratton J. A., *Electromagnetic theory*, Wiley-Interscience, 2007.

[6] Taur Y., "MOSFET channel length: extraction and interpretation", *IEEE Trans. on Electron Devices*, vol. ED-47, no. 1, pp. 160–170, Jan. 2000.

[7] Meer H., Henson K., Lyu J.-H., Rosmeulen M., Kubicek S., Collaret N., and De Meyer K., "Limitations of shift-and-ratio based L_{eff} extraction techniques for MOS transistor with halo or pockets implants", *IEEE Electron Device Letters*, vol. EDL-21, no. 3, pp. 133–136, Mar. 2000.

[8] Sze C. M. and Ng K. K., *Physics of semiconductor devices*, 3rd ed., Wiley and Sons, 2007.

[9] Tsividis Y. P. and McAndrew C., *The MOS transistor*, Int. 3rd ed., Oxford University Press, New York, 2012.

[10] Selberherr S., *Analysis and Simulation of Semiconductor Devices.* Wien, Springer-Verlag, 1984.

Chapter 3
TIME-DOMAIN MODEL

Wiesław Kordalski

3.1. Introduction

Basing on the quasi-2D MOSFET representation proposed in Chapter 2, derivation of a novel quasi-2D NQS four-terminal time-domain small-signal MOSFET model is presented in this chapter.

In Section 3.2, physics of the transistor under small signal excitation is described. In Sections 3.3, 3.4, and 3.5, respectively, a quasi-2D continuity equation, a quasi-2D Poisson's equation, and a transport equation are derived from first principles. Capacitive and non-capacitive terminal currents are analyzed in Section 3.6. A formula for the gate-to-body capacitance C_{gb} is derived in Section 3.7. Supplementary equations and useful rules are established in Section 3.8. Section 3.9 provides main conclusions.

In this chapter, we assume that the gate, drain, source, and electrically neutral part of the substrate are perfect conductors, no generation-recombination processes occur, and the tunneling and leakage currents are negligibly small.

3.2. MOSFET under small excitation

In the dc state, neither the channel-gate nor the channel-body displacement current occurs—no dynamic electrical coupling exists. However, if terminal voltages change with time, then perturbations in carrier distribution, velocity of carriers, electric field, and channel thickness occur. A transverse coupling appears between the channel and the structure. The coupling is produced by the transverse electric field, and hence displacement currents flow between the channel, the gate and the body. Furthermore, a regrouping of carriers in the channel in the perpendicular direction occurs, which causes the current lines to deflect in the transistor. As a result, the channel thickness $X(\xi)$, conduction current density $J(\xi)$, electric field, and the other parameters that uniquely determine the quasi-2D dc representation of the MOSFET change.

Let us consider a p-channel MOSFET operating in the saturation region of its output characteristics under the dc and small-signal conditions, which is shown in Fig. 3.1.

When the MOS transistor is biased with constant terminal voltages, all quantities of the quasi-2D model of the transistor related to the channel, gate, and body depend only on the spatial variable ξ, as shown in Fig. 3.1a. Under the steady-state conditions, the displacement current occurs neither at the gate nor in the body, because electric charges on the gate and in the body do not vary.

If we add in series small time-varying voltage sources $\upsilon_{gs}(t)$, $\upsilon_{ds}(t)$, and $\upsilon_{bs}(t)$ to their respective biasing voltages V_{GS}, V_{DS}, and V_{BS} (see Fig. 3.1b) then the total magnitudes of, respectively, the gate-source voltage $\upsilon_{GS}(t)$, drain-source voltage $\upsilon_{DS}(t)$, and body-source voltage $\upsilon_{BS}(t)$ can be written as follows:

$$\upsilon_{GS}(t) = V_{GS} + \upsilon_{gs}(t) \tag{3.1}$$

$$\upsilon_{DS}(t) = V_{DS} + \upsilon_{ds}(t) \tag{3.2}$$

$$\upsilon_{BS}(t) = V_{BS} + \upsilon_{bs}(t) \tag{3.3}$$

The time-varying terminal voltages cause perturbations in: concentration and velocity of holes in the channel, electric field distribution in the transistor structure, thickness of the channel, as well as in the gate and body charges. A transverse electrical coupling appears between the channel and the transistor structure, which produces coupling currents in the gate and the body.

For the purposes of further analysis, we introduce the following symbols: $p(\xi, t)$, $\mu(\xi, t)$, $X(\xi, t)$, $E(\xi, t)$, $E_{CB}(\xi, t)$, $E_{CG}(\xi, t)$, $J(\xi, t)$, $X_d(\xi, t)$, $Q_G(\xi, t)$, and $Q_B(\xi, t)$, for denoting the total quantities of, respectively, the hole density, effective bias-dependent mobility of holes, thickness of the channel (see Fig. 3.2), longitudinal electric field in the channel (see Fig. 3.3), transverse electric field on the bottom channel surface (see Fig. 3.3), transverse electric field on the top channel surface (see Fig. 3.3), conduction current density of holes, thickness of the depletion region, gate charge per unit area, and body charge per unit area. Small departures $p_1(\xi, t)$, $\mu_1(\xi, t)$, $X_1(\xi, t)$, $E_1(\xi, t)$, $E_{cb}(\xi, t)$, $E_{cg}(\xi, t)$, $J_1(\xi, t)$, $X_{d1}(\xi, t)$, $Q_g(\xi, t)$, and $Q_b(\xi, t)$ of the total quantities from their dc values at the Q-point (quiescent point) , respectively, $p_0(\xi)$, $\mu_q(\xi)$, $X_0(\xi)$, $E_0(\xi)$, $E_{CB0}(\xi)$, $E_{CG0}(\xi)$, $J_0(\xi)$, $X_{d0}(\xi)$, $Q_{G0}(\xi)$, and $Q_{B0}(\xi)$ can be written as follows:

$$p_1(\xi,t) = p(\xi,t) - p_0(\xi) \tag{3.4}$$

$$\mu_1(\xi,t) = \mu(\xi,t) - \mu_q(\xi) \tag{3.5}$$

$$X_1(\xi,t) = X(\xi,t) - X_0(\xi) \tag{3.6}$$

$$E_1(\xi,t) = E(\xi,t) - E_0(\xi) \tag{3.7}$$

$$E_{cb}(\xi,t) = E_{CB}(\xi,t) - E_{CB0}(\xi) \tag{3.8}$$

$$E_{cg}(\xi,t) = E_{CG}(\xi,t) - E_{CG0}(\xi) \tag{3.9}$$

$$J_1(\xi,t) = J(\xi,t) - J_0(\xi) \tag{3.10}$$

$$X_{d1}(\xi,t) = X_d(\xi,t) - X_{d0}(\xi) \tag{3.11}$$

$$Q_g(\xi,t) = Q_G(\xi,t) - Q_{G0}(\xi) \tag{3.12}$$

$$Q_b(\xi,t) = Q_B(\xi,t) - Q_{B0}(\xi) \tag{3.13}$$

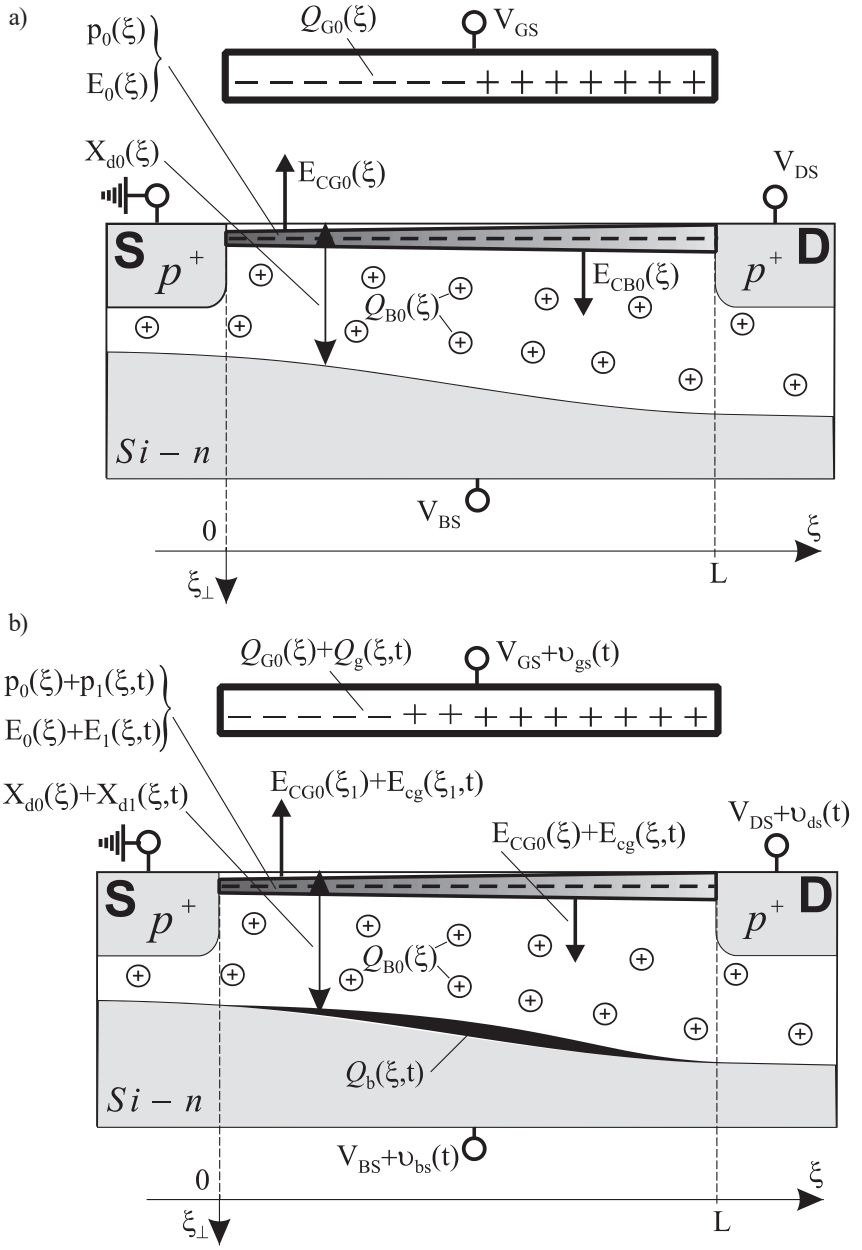

Fig. 3.1. The quasi-2D representation of a *p*-channel MOSFET operating in saturation region of its output characteristics ($|V_{DS}| > |V_{GS}|$). (a) dc conditions. (b) dc and small-signal conditions.

To give a mathematical description of the dynamic behavior of carriers in the channel as well as to calculate terminal and coupling currents, we need to use a quasi-2D continuity equation for carriers in the channel, Poisson's equation for the quasi-2D representation of the transistor, and current transport equation. These equations are derived in Secs. 3.3–3.5.

3.3. Quasi-2D continuity equation

In this section, we derive quasi-2D continuity equations for current carriers in the channel under dc and small-signal conditions, and propose some simplifications of the continuity equation for small-signal conditions. The derivation is based on the quasi-2D representation of the MOSFET channel, which is presented in Sec. 2.2.

3.3.1. Basic equations

Let us consider a sector of the quasi-2D representation of a *p*-type channel that is cut out by planes perpendicular to the channel line ξ, with $\Delta\xi$ being the length of the sector; see Fig. 3.2. The equations describe the flow of carriers in the channel in terms of two independent variables: ξ-coordinate and time denoted by t. As stated, generation-recombination processes in the transistor are neglected in this work.

Let the steady-state concentration of carriers (holes) $p_0(\xi)$ be lightly disturbed in a macroscopic volume $\Delta\Omega_0(\xi, \Delta\xi)$ shown in Fig. 3.2. A small perturbation (departure) in the carrier concentration causes small variations in the channel thickness and conduction current density in the channel. Using (3.4), (3.6), and (3.10), the total quantities $p(\xi, t)$, $X(\xi, t)$, and $J(\xi, t)$ can be written as follows:

$$p(\xi,t) = p_0(\xi) + p_1(\xi,t) \tag{3.14}$$

$$X(\xi,t) = X_0(\xi) + X_1(\xi,t) \tag{3.15}$$

$$J(\xi,t) = J_0(\xi) + J_1(\xi,t) \tag{3.16}$$

According to (3.15), the macroscopic volume element $\Delta\Omega_0(\xi, \Delta\xi)$ highlighted in Fig. 3.2 also changes its volume with time because the top and bottom channel surfaces change their positions. Therefore, by analogy with (3.14)–(3.16), we can write:

$$\Delta\Omega(\xi,\Delta\xi,t) = \Delta\Omega_0(\xi,\Delta\xi) + \Delta\Omega_1(\xi,\Delta\xi,t) \tag{3.17}$$

where $\Delta\Omega_1(\xi, \Delta\xi, t)$ is the time-dependent departure of the total macroscopic volume $\Delta\Omega(\xi, \Delta\xi, t)$ from its dc value.

Since the perturbations are assumed to be small, the following inequalities are true:

$$p_0(\xi) >> p_1(\xi,t) \tag{3.18}$$

$$X_0(\xi) >> X_1(\xi,t) \tag{3.19}$$

$$J_0(\xi) >> J_1(\xi,t) \tag{3.20}$$

For small perturbations, we can assume that relative time-dependent changes of the carrier concentration in the channel are directly proportional to relative time-dependent changes of the channel thickness. Thus, we may introduce a dimensionless ratio of the proportionality $D_C(\xi, t)$, which can be called a dynamic coupling factor of the channel,

$$D_C(\xi,t) = \frac{\dfrac{1}{X_0(\xi)}\dfrac{\partial X_1(\xi,t)}{\partial t}}{\dfrac{1}{p_0(\xi)}\dfrac{\partial p_1(\xi,t)}{\partial t}} \tag{3.21}$$

We proceed to the mathematical formulation of the law of conservation of carriers in the volume $\Delta\Omega(\xi, \Delta\xi, t)$ highlighted in Fig. 3.2. The law states that the number of holes in the volume may increase because of the net flow into the volume.

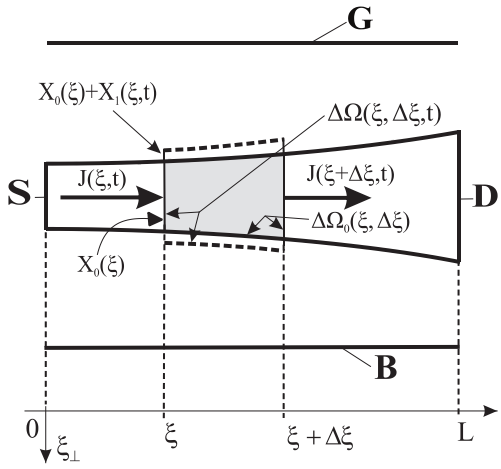

Fig. 3.2. The channel with a time-dependent macroscopic volume element that is subjected to a small perturbation, where $J(\xi, t)$ is the conduction current density.

Denoted by $P_V(t)$, the number of holes contained in the volume $\Delta\Omega(\xi, \Delta\xi, t)$ at a time t is as follows:

$$P_V(t) = \int_{\xi}^{\xi+\Delta\xi} W\, p(\xi,t)\, X(\xi,t)\, d\xi \tag{3.22}$$

An infinitesimal increase of $P_V(t)$, denoted by $dP_V(t)$, corresponding to an infinitesimal time interval, denoted by dt, can be written as

$$dP_V(t) = dt \int_{\xi}^{\xi+\Delta\xi} W \frac{\partial}{\partial t}\left[\, p(\xi,t)\, X(\xi,t)\right] d\xi \tag{3.23}$$

with W being the channel width.

On the other hand, $dP_V(t)$ is equal to the flux of the holes through the surface bounding the volume $\Delta\Omega(\xi, \Delta\xi, t)$ multiplied by dt. Hence, we have:

$$dP_V(t) = dt\left[\frac{W}{q}X(\xi,t)J(\xi,t) - \frac{W}{q}X(\xi+\Delta\xi,t)J(\xi+\Delta\xi,t)\right] \tag{3.24}$$

Equating the two expressions for $dP_V(t)$, canceling out dt, and then dividing the result by $\Delta\xi\, W/q$, we obtain:

$$\begin{aligned} q\frac{1}{\Delta\xi}\int_{\xi}^{\xi+\Delta\xi}\frac{\partial}{\partial t}\big[\,p(\xi,t)\,X(\xi,t)\big]\,d\xi \\ = \frac{1}{\Delta\xi}\big[\,X(\xi,t)\,J(\xi,t) - X(\xi+\Delta\xi,t)\,J(\xi+\Delta\xi,t)\big] \end{aligned} \tag{3.25}$$

Assuming that all the functions appearing in (3.25) are differentiable, passing to the limit with $\Delta\xi \to 0$, performing the necessary calculations (details are given in Appendix A), referring to (A12) and (A13), and omitting the mixed terms $X_1(\xi, t)\cdot[\partial J_1(\xi, t)/\partial\xi]$ and $J_1(\xi, t)\cdot[\partial X_1(\xi, t)/\partial\xi]$ in (A13), we may write the quasi-2D continuity equation for a small departure of hole concentration:

$$\begin{aligned} q\big[1+D_C(\xi,t)\big]\frac{\partial p_1(\xi,t)}{\partial t} = &-\frac{\partial J_1(\xi,t)}{\partial\xi} - \frac{J_1(\xi,t)}{X_0(\xi)}\frac{dX_0(\xi)}{d\xi} \\ &- \frac{X_1(\xi,t)}{X_0(\xi)}\frac{dJ_0(\xi)}{d\xi} - \frac{J_0(\xi)}{X_0(\xi)}\frac{\partial X_1(\xi,t)}{\partial\xi} \end{aligned} \tag{3.26}$$

and for dc conditions

$$\frac{dJ_0(\xi)}{d\xi} + \frac{J_0(\xi)}{X_0(\xi)}\frac{dX_0(\xi)}{d\xi} = 0 \tag{3.27}$$

Similarly, it can be shown that for the n-channel MOSFET of which the source, drain, and ξ-coordinate have the same orientation as in Fig. 3.2, the quasi-2D continuity equation for a small departure of electron concentration $n_1(\xi, t)$ is as follows:

$$\begin{aligned} q\big[1+D_C(\xi,t)\big]\frac{\partial n_1(\xi,t)}{\partial t} = &\frac{\partial J_1(\xi,t)}{\partial\xi} + \frac{J_1(\xi,t)}{X_0(\xi)}\frac{dX_0(\xi)}{d\xi} \\ &+ \frac{X_1(\xi,t)}{X_0(\xi)}\frac{dJ_0(\xi)}{d\xi} + \frac{J_0(\xi)}{X_0(\xi)}\frac{\partial X_1(\xi,t)}{\partial\xi} \end{aligned} \tag{3.28}$$

and (3.27) is still held for dc conditions.

Based on (3.26) and (3.28), one can see that the rate of changes in the excess carrier concentration depends on: the dc channel thickness, as well as its gradients of the dc and

small-signal values. Moreover, it depends on the dc conduction current density, as well as its gradients of the dc and small-signal values, and the dynamic coupling factor of the channel.

The right-hand sides of (3.26) and (3.28) can be written in terms of $J_1(\xi, t)$, $X_0(\xi)$, and $dX_0(\xi)/d\xi$ if we introduce two factors $D_V(\xi, t)$ and $D_S(\xi, t)$ which interrelate variations in the shape and thickness of the channel with the perturbations in the conduction current density.

Let the dynamic channel-to-current coupling factor $D_V(\xi, t)$ be defined by

$$D_V(\xi,t) = -\frac{X_1(\xi,t)}{X_0(\xi)} \Big/ \frac{J_1(\xi,t)}{J_0(\xi)} \tag{3.29}$$

and the dynamic channel deformation factor $D_S(\xi, t)$ by

$$D_S(\xi,t) = \frac{\dfrac{1}{X_0(\xi)}\dfrac{\partial X_1(\xi,t)}{\partial \xi}}{\dfrac{1}{J_0(\xi)}\dfrac{\partial J_1(\xi,t)}{\partial \xi}} \tag{3.30}$$

Then, using (3.27) and inserting (3.29) and (3.30) into (3.26) and (3.28), the quasi-2D continuity equations for the small excess carrier concentrations may be rewritten in the form:

$$q\big[1+D_C(\xi,t)\big]\frac{\partial p_1(\xi,t)}{\partial t} = -\big[1+D_S(\xi,t)\big]\frac{\partial J_1(\xi,t)}{\partial \xi} - \frac{1+D_V(\xi,t)}{X_0(\xi)}\frac{dX_0(\xi)}{d\xi}J_1(\xi,t) \tag{3.31}$$

for the *p*-channel transistor, and

$$q\big[1+D_C(\xi,t)\big]\frac{\partial n_1(\xi,t)}{\partial t} = \big[1+D_S(\xi,t)\big]\frac{\partial J_1(\xi,t)}{\partial \xi} + \frac{1+D_V(\xi,t)}{X_0(\xi)}\frac{dX_0(\xi)}{d\xi}J_1(\xi,t) \tag{3.32}$$

for the *n*-channel transistor.

As in the case of $D_C(\xi, t)$, the coupling factors $D_V(\xi, t)$ and $D_S(\xi, t)$ are functions of ξ and t, however, the behavior of $D_V(\xi, t)$ and $D_S(\xi, t)$ versus ξ and t is an open question and the definitive answer to the problem requires an additional (numerical) analysis.

3.3.2. Some simplifications

Under some assumptions, simplifications of (3.26) and (3.28) are possible.

Channel-shape-conserved approximation

Differentiating (3.15) with respect to ξ yields:

$$\frac{\partial X(\xi,t)}{\partial \xi} = \frac{dX_0(\xi)}{d\xi} + \frac{\partial X_1(\xi,t)}{\partial \xi} \tag{3.33}$$

If we assume that the shape of the channel is conserved during perturbations, as shown in Fig. 3.2, i.e.:

$$\frac{\partial X(\xi,t)}{\partial \xi} = \frac{d X_0(\xi)}{d\xi} \tag{3.34}$$

then taking account of (3.33) leads to $\partial X_1(\xi, t)/\partial\xi = 0$. As a result, (3.26) and (3.28) take their respective forms:

$$q\left[1 + D_C(\xi,t)\right]\frac{\partial p_1(\xi,t)}{\partial t} = -\frac{\partial J_1(\xi,t)}{\partial \xi} - \frac{J_1(\xi,t)}{X_0(\xi)}\frac{d X_0(\xi)}{d\xi} - \frac{X_1(\xi,t)}{X_0(\xi)}\frac{d J_0(\xi)}{d\xi} \tag{3.35}$$

and

$$q\left[1 + D_C(\xi,t)\right]\frac{\partial n_1(\xi,t)}{\partial t} = \frac{\partial J_1(\xi,t)}{\partial \xi} + \frac{J_1(\xi,t)}{X_0(\xi)}\frac{d X_0(\xi)}{d\xi} + \frac{X_1(\xi,t)}{X_0(\xi)}\frac{d J_0(\xi)}{d\xi} \tag{3.36}$$

Gradually-thickened-channel approximation

Equation (3.27) can be rewritten as

$$\frac{d J_0(\xi)}{d\xi} = -\frac{J_0(\xi)}{X_0(\xi)}\frac{d X_0(\xi)}{d\xi} \tag{3.37}$$

If we assume in (3.37) that the CTME can be neglected, $d X_0(\xi) / d\xi = 0$, the channel is thick enough, and the conduction current density $J_0(\xi)$ is small, then the term $dJ_0(\xi)/d\xi$ can be ignored. Therefore, the second and third term in (3.26) and (3.28) can be ignored, and as a consequence the equations take their respective forms:

$$q\left[1 + D_C(\xi,t)\right]\frac{\partial p_1(\xi,t)}{\partial t} = -\frac{\partial J_1(\xi,t)}{\partial \xi} - \frac{J_0(\xi)}{X_0(\xi)}\frac{\partial X_1(\xi,t)}{\partial \xi} \tag{3.38}$$

and

$$q\left[1 + D_C(\xi,t)\right]\frac{\partial n_1(\xi,t)}{\partial t} = \frac{\partial J_1(\xi,t)}{\partial \xi} + \frac{J_0(\xi)}{X_0(\xi)}\frac{\partial X_1(\xi,t)}{\partial \xi} \tag{3.39}$$

Gradually-thickened-and-slightly-deformed-channel approximation

We can considerably simplify (3.26) and (3.28) if we simultaneously apply both of the above-introduced approximations, i.e., if we assume that the channel is thick enough, $\partial X_1(\xi, t)/\partial\xi = 0$, and $d X_0(\xi) / d\xi = 0$. Then, (3.26) and (3.28) become, respectively,

$$q\left[1 + D_C(\xi,t)\right]\frac{\partial p_1(\xi,t)}{\partial t} = -\frac{\partial J_1(\xi,t)}{\partial \xi} \tag{3.40}$$

and

$$q\left[1+D_C(\xi,t)\right]\frac{\partial n_1(\xi,t)}{\partial t}=\frac{\partial J_1(\xi,t)}{\partial \xi} \tag{3.41}$$

It is worth noticing that (3.31) and (3.32) are becoming identical to (3.40) and (3.41), respectively, if the factors $D_V(\xi, t)$ and $D_S(\xi, t)$ tend to zero and $dX_0(\xi) / d\xi \approx 0$.

Gradually-thickened-and-strongly-deformed-channel approximation

If the channel thickness changes gradually, $dX_0(\xi) / d\xi \approx 0$, the dynamic channel-to-current coupling factor $D_V(\xi, t)$ is sufficiently small, and the dynamic channel deformation factor $D_S(\xi, t)$ cannot be neglected, then (3.31) and (3.32) are as follows:

$$q\left[1+D_C(\xi,t)\right]\frac{\partial p_1(\xi,t)}{\partial t}=-\left[1+D_S(\xi,t)\right]\frac{\partial J_1(\xi,t)}{\partial \xi} \tag{3.42}$$

and

$$q\left[1+D_C(\xi,t)\right]\frac{\partial n_1(\xi,t)}{\partial t}=\left[1+D_S(\xi,t)\right]\frac{\partial J_1(\xi,t)}{\partial \xi} \tag{3.43}$$

Slightly-deformed-channel approximation

If the dynamic channel-to-current coupling factor $D_V(\xi, t)$ is large enough and the dynamic channel deformation factor $D_S(\xi, t)$ can be neglected, then (3.31) and (3.32) can be reduced to, respectively,

$$q\left[1+D_C(\xi,t)\right]\frac{\partial p_1(\xi,t)}{\partial t}=-\frac{\partial J_1(\xi,t)}{\partial \xi}-\frac{1+D_V(\xi,t)}{X_0(\xi)}\frac{dX_0(\xi)}{d\xi}J_1(\xi,t) \tag{3.44}$$

and

$$q\left[1+D_C(\xi,t)\right]\frac{\partial n_1(\xi,t)}{\partial t}=\frac{\partial J_1(\xi,t)}{\partial \xi}+\frac{1+D_V(\xi,t)}{X_0(\xi)}\frac{dX_0(\xi)}{d\xi}J_1(\xi,t) \tag{3.45}$$

Slightly-deformed-channel-and-weakly-coupled-channel-to-current approximation

If both the dynamic channel-to-current coupling factor $D_V(\xi, t)$ and the dynamic channel deformation factor $D_S(\xi, t)$ are sufficiently small, then (3.31) and (3.32) simplify to:

$$q\left[1+D_C(\xi,t)\right]\frac{\partial p_1(\xi,t)}{\partial t}=-\frac{\partial J_1(\xi,t)}{\partial \xi}-\frac{1}{X_0(\xi)}\frac{dX_0(\xi)}{d\xi}J_1(\xi,t) \tag{3.46}$$

and

$$q\left[1+D_C(\xi,t)\right]\frac{\partial n_1(\xi,t)}{\partial t}=\frac{\partial J_1(\xi,t)}{\partial \xi}+\frac{1}{X_0(\xi)}\frac{dX_0(\xi)}{d\xi}J_1(\xi,t) \tag{3.47}$$

3.4. Quasi-2D Poisson's equations

In this section, we derive quasi-2D Poisson's equations for dc and small-signal conditions, and propose some simplified versions of these equations.

3.4.1. Equations for steady-state (dc) and small-signal conditions

If voltages at the transistor terminals change with time, one can observe perturbations in carrier concentration, channel thickness, longitudinal and transverse electric field, and the other quantities shown in Fig. 3.1b.

Let us consider a volume $\Delta\Omega(\xi, \Delta\xi, t)$ depicted in Fig. 3.3.

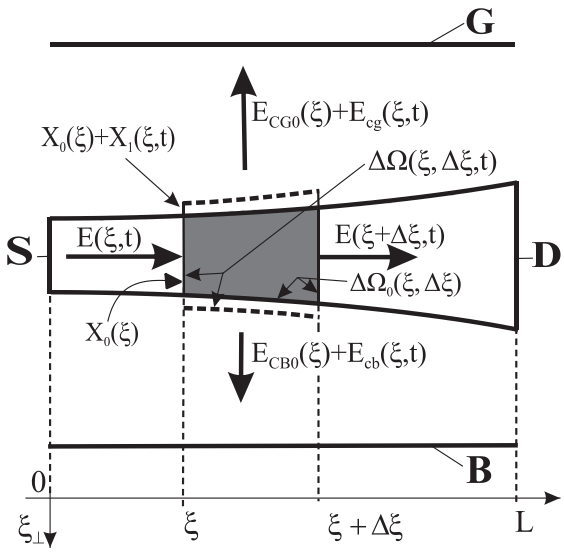

Fig. 3.3. A time-dependent macroscopic volume element of the channel under a small perturbation.

Applying Gauss's theorem to the volume, we can write:

$$\oint_{A} \mathbf{D} \cdot d\mathbf{A} = q \int_{\Delta\Omega\,(\xi,\,\Delta\xi,\,t)} [N(\xi) + p(\xi,t)]\, d\Omega \tag{3.48}$$

where A is the closed surface bounding the volume $\Delta\Omega(\xi, \Delta\xi, t)$, $N(\xi)$ is the effective concentration of ionized impurities in the substrate [see (2.58)], $\mathbf{D}$ is the displacement vector, and q is the magnitude of the electronic charge.

Due to regularity of the domain $\Delta\Omega(\xi, \Delta\xi, t)$, (3.48) can be transformed into:

$$q\int_{\xi}^{\xi+\Delta\xi} X(\xi,t)\,[N(\xi)+p(\xi,t)]\,d\xi = \varepsilon_0\varepsilon_s\int_{\xi}^{\xi+\Delta\xi} E_{CB}(\xi,t)\,d\xi + \varepsilon_0\varepsilon_s\int_{\xi}^{\xi+\Delta\xi} E_{CG}(\xi,t)\,d\xi + \varepsilon_0\varepsilon_s\,[X(\xi+\Delta\xi,t)\,E(\xi+\Delta\xi,t) - X(\xi,t)\,E(\xi,t)] \tag{3.49}$$

with ε_0 and ε_s being, respectively, the permittivity of free space and the relative permittivity of the semiconductor substrate.

Dividing (3.49) by $\Delta\xi$, we have:

$$\frac{q}{\Delta\xi}\int_{\xi}^{\xi+\Delta\xi} X(\xi,t)[N(\xi)+p(\xi,t)]\,d\xi = \frac{\varepsilon_0\varepsilon_s}{\Delta\xi}\int_{\xi}^{\xi+\Delta\xi} E_{CB}(\xi,t)\,d\xi + \frac{\varepsilon_0\varepsilon_s}{\Delta\xi}\int_{\xi}^{\xi+\Delta\xi} E_{CG}(\xi,t)\,d\xi + \frac{\varepsilon_0\varepsilon_s}{\Delta\xi}\left[X(\xi+\Delta\xi,t)\,E(\xi+\Delta\xi,t) - X(\xi,t)\,E(\xi,t)\right] \tag{3.50}$$

Assuming that all the functions appearing in (3.50) are continuously differentiable, passing to the limit with $\Delta\xi \to 0$, performing the necessary calculations (details are given in Appendix B), and omitting the mixed terms—$p_1(\xi, t)\cdot X_1(\xi, t)$, $X_1(\xi, t)\cdot[\partial E_1(\xi, t)/\partial\xi]$, and $E_1(\xi, t)\cdot[\partial X_1(\xi, t)/\partial\xi]$—in the analysis, we obtain a quasi-2D Poisson's equation for dc conditions [refer to (A29)]:

$$q\left[X_0(\xi)\,N(\xi) + X_0(\xi)\,p_0(\xi)\right] = \varepsilon_0\varepsilon_s\left[X_0(\xi)\frac{dE_0(\xi)}{d\xi} + E_0(\xi)\frac{dX_0(\xi)}{d\xi} + E_{CG0}(\xi) + E_{CB0}(\xi)\right] \tag{3.51}$$

and a quasi-2D Poisson's equation for small-signal time-varying conditions [see (A30)]:

$$q\left[X_0(\xi)\,p_1(\xi,t) + N(\xi)\,X_1(\xi,t) + p_0(\xi)\,X_1(\xi,t)\right] = \varepsilon_0\varepsilon_s\left[X_0(\xi)\frac{\partial E_1(\xi,t)}{\partial\xi} + X_1(\xi,t)\frac{dE_0(\xi)}{d\xi} + E_{cg}(\xi,t) + E_{cb}(\xi,t) + E_0(\xi)\frac{\partial X_1(\xi,t)}{\partial\xi} + E_1(\xi,t)\frac{dX_0(\xi)}{d\xi}\right] \tag{3.52}$$

The quasi-2D dc Poisson's equation (3.51) can be written in a more convenient form:

$$q\,p_0(\xi)\,X_0(\xi)\left[1+\frac{N(\xi)}{p_0(\xi)}\right] = \varepsilon_0\varepsilon_s\left[E_{CG0}(\xi)+E_{CB0}(\xi)\right] + \varepsilon_0\varepsilon_s\,X_0(\xi)\left[\frac{dE_0(\xi)}{d\xi}+\frac{E_0(\xi)}{X_0(\xi)}\frac{dX_0(\xi)}{d\xi}\right] \tag{3.53}$$

Likewise, the quasi-2D small-signal Poisson's equation (3.52) can be rearranged as follows:

$$q\,p_1(\xi,t)\,X_0(\xi)\left[1+P_C(\xi,t)\left(1+\frac{N(\xi)}{p_0(\xi)}\right)\right]=\varepsilon_0\varepsilon_s\left[E_{cg}(\xi,t)+E_{cb}(\xi,t)\right]$$
$$+\varepsilon_0\varepsilon_s\,X_0(\xi)\left[\frac{E_0(\xi)}{X_0(\xi)}\frac{\partial X_1(\xi,t)}{\partial\xi}+\frac{E_1(\xi,t)}{X_0(\xi)}\frac{dX_0(\xi)}{d\xi}+\frac{X_1(\xi,t)}{X_0(\xi)}\frac{dE_0(\xi)}{d\xi}+\frac{\partial E_1(\xi,t)}{\partial\xi}\right] \tag{3.54}$$

where $P_C(\xi, t)$ is a dynamic carrier-to-channel coupling factor, defined by

$$P_C(\xi,t)=\frac{X_1(\xi,t)}{X_0(\xi)}\Big/\frac{p_1(\xi,t)}{p_0(\xi)} \tag{3.55}$$

3.4.2. Simplified equations

Useful simplifications of (3.54) are presented in this section.

Thick-channel approximation

If we assume that the transistor channel is thick enough to neglect the last three terms in the square brackets of the right-hand side of (3.54), we have:

$$\begin{aligned}&q\,p_1(\xi,t)\,X_0(\xi)\left[1+P_C(\xi,t)\left(1+\frac{N(\xi)}{p_0(\xi)}\right)\right]\\&=\varepsilon_0\varepsilon_s\left[E_{cg}(\xi,t)+E_{cb}(\xi,t)+X_0(\xi)\frac{\partial E_1(\xi,t)}{\partial\xi}\right]\end{aligned} \tag{3.56}$$

Weakly-coupled-carrier-to-channel approximation

If the dynamic carrier-to-channel coupling factor $P_C(\xi, t)$ is negligibly small, we may reduce (3.54) to:

$$\begin{aligned}q\,p_1(\xi,t)\,X_0(\xi)&=\varepsilon_0\varepsilon_s\left[E_{cg}(\xi,t)+E_{cb}(\xi,t)\right]+\varepsilon_0\varepsilon_s\,X_0(\xi)\left[\frac{\partial E_1(\xi,t)}{\partial\xi}\right.\\&\left.+\frac{E_1(\xi,t)}{X_0(\xi)}\frac{dX_0(\xi)}{d\xi}+\frac{X_1(\xi,t)}{X_0(\xi)}\frac{dE_0(\xi)}{d\xi}+\frac{E_0(\xi)}{X_0(\xi)}\frac{\partial X_1(\xi,t)}{\partial\xi}\right]\end{aligned} \tag{3.57}$$

Thick-channel-and-weakly-coupled-carrier-to-channel approximation

If the dynamic carrier-to-channel coupling factor $P_C(\xi, t)$ is negligibly small and the thickness of the channel sufficiently large, then (3.54) may be reduced to:

$$q\,p_1(\xi,t)\,X_0(\xi) = \varepsilon_0\,\varepsilon_s[E_{cg}(\xi,t) + E_{cb}(\xi,t)] + \varepsilon_0\,\varepsilon_s\,X_0(\xi)\frac{\partial E_1(\xi,t)}{\partial \xi} \tag{3.58}$$

Other simplifications of (3.54) are also possible.

3.5. Transport equation

We assume that electromagnetic radiation effects can be ignored in our analysis because the dimensions of a typical transistor are much smaller than the wavelength corresponding to 1-THz frequency.

In the time domain, the total current density in the transistor channel $J_t(\xi, t)$ consists of two components, namely, the total conduction current density $J(\xi, t)$ and the displacement current density $J_{dis}(\xi, t)$, see, e.g., [1, Ch. 10], [2, Ch. 3]; drift and diffusion are the basic carrier transport mechanisms of the conduction current [1–10]. Thus, we can write:

$$J_t(\xi,t) = J(\xi,t) + J_{dis}(\xi,t) \tag{3.59}$$

$$J(\xi,t) = q\,\mu(\xi,t)\,p(\xi,t)\,E(\xi,t) - q\,D_p(\xi,t)\frac{\partial p(\xi,t)}{\partial \xi} \tag{3.60}$$

$$J_{dis}(\xi,t) = \varepsilon_0\,\varepsilon_s\frac{\partial E(\xi,t)}{\partial t} \tag{3.61}$$

where $D_p(\xi, t)$ is the diffusivity of holes.

Combining (3.59)–(3.61), we may write:

$$J_t(\xi,t) = q\,\mu(\xi,t)\,p(\xi,t)\,E(\xi,t) - q\,D_p(\xi,t)\frac{\partial p(\xi,t)}{\partial \xi} + \varepsilon_0\,\varepsilon_s\frac{\partial E(\xi,t)}{\partial t} \tag{3.62}$$

At a Q-point, we may split the total current density $J_t(\xi, t)$ between the dc conduction current density $J_0(\xi)$ and the total small-signal current density $J_{t1}(\xi, t)$:

$$J_t(\xi,t) = J_0(\xi) + J_{t1}(\xi,t) \tag{3.63}$$

For small perturbations, we can neglect time-varying changes in the diffusivity of holes and subsequently assume that the diffusivity is determined by values of respective quantities referring to the dc operating point:

$$D_p(\xi,t) = D_{p0}(\xi) \tag{3.64}$$

in which $D_{p0}(\xi)$ is the diffusivity of holes at the Q-point.

Using (3.4), (3.5), (3.7), (3.63), and (3.64), we can rewrite (3.62) as follows:

$$J_0(\xi)+J_{t1}(\xi,t) = q\,[\,\mu_q(\xi)+\mu_1(\xi,t)][\,p_0(\xi)+p_1(\xi,t)][E_0(\xi)+E_1(\xi,t)] - q\,D_{p0}(\xi)\frac{\partial[\,p_0(\xi)+p_1(\xi,t)]}{\partial\xi}+\varepsilon_0\,\varepsilon_s\frac{\partial[E_0(\xi)+E_1(\xi,t)]}{\partial t} \tag{3.65}$$

Making some calculations in (3.65), then neglecting higher-order mixed terms, and finally separately grouping the zero-order and first-order terms, we have:

$$J_0(\xi) = q\,\mu_q(\xi)\,p_0(\xi)\,E_0(\xi) - q\,D_{p0}(\xi)\frac{\partial p_0(\xi)}{\partial\xi} \tag{3.66}$$

for dc conditions at the Q-point, and

$$J_{t1}(\xi,t) = J_1(\xi,t)+J_{dis1}(\xi,t) \tag{3.67}$$

for small-signal conditions, where $J_1(\xi, t)$ is the small-signal conduction current density of holes,

$$J_1(\xi,t) = q\,\mu_q(\xi)\,E_0(\xi)\,p_1(\xi,t)+q\,\mu_q(\xi)\,p_0(\xi)\,E_1(\xi,t) + q\,p_0(\xi)\,E_0(\xi)\,\mu_1(\xi,t)-q\,D_{p0}(\xi)\frac{\partial p_1(\xi,t)}{\partial\xi} \tag{3.68}$$

$$J_{dis1}(\xi,t) = \varepsilon_0\,\varepsilon_s\frac{\partial E_1(\xi,t)}{\partial t} \tag{3.69}$$

Obviously, $J_{dis1}(\xi, t)$ in (3.69) equals $J_{dis}(\xi, t)$ in (3.61).

We can see from (3.67) to (3.69) that the total small-signal current density consists of five terms: the first one represents the drift of the excess holes $p_1(\xi, t)$ in the stationary field $E_0(\xi)$, the second is the drift of the holes of the stationary distribution $p_0(\xi)$ in the small-signal field $E_1(\xi, t)$, the third is the drift of the holes of the stationary distribution $p_0(\xi)$ moving in the stationary field $E_0(\xi)$ with the mobility $\mu_1(\xi, t)$, the fourth is the diffusion component of the excess holes $p_1(\xi, t)$, and the fifth is the displacement current.

Referring to (3.5) and assuming isothermal conditions, one can see that, for sufficiently small perturbations around the Q-point, $\mu_1(\xi, t)$ is simply the differential of the mobility $\mu_q(\xi)$ with respect to the following electric fields: $E_0(\xi)$, $E_{CG0}(\xi)$, and $E_{CB0}(\xi)$; see [1–6]. However, the impact of $E_{CB0}(\xi)$ on the mobility can be ignored, because the effect of the body-source voltage V_{BS} on the mobility is negligibly small; refer to, e.g., [3, Sec. 4.10]. Hence, we can write:

$$\mu_1(\xi,t) = \frac{\partial\mu_q(\xi)}{\partial E_0(\xi)}E_1(\xi,t)+\frac{\partial\mu_q(\xi)}{\partial E_{CG0}(\xi)}E_{cg}(\xi,t) \tag{3.70}$$

Thus, (3.67)–(3.70) constitute a set of non-quasi-static time-domain small-signal equations describing propagation of excess carriers in the channel.

3.6. Terminal currents

Small-signal currents in the MOSFET can be split into capacitive and non-capacitive ones, ignoring generation-recombination processes and the leakage and tunneling, currents.

The capacitive currents charge capacitances of the transistor.

We can distinguish three types of the non-capacitive currents: the conduction current described in the previous section, coupling currents induced on the gate and in the body by perturbation in the channel charge (they are analyzed in Sec. 3.8), and the non-capacitive displacement current described in Sec. 3.6.2.

By virtue of the principle of superposition, we separately analyze terminal capacitive currents and terminal non-capacitive ones.

3.6.1. Capacitive currents

To determine the terminal capacitive currents, we suppose that the relaxation time τ [3, 11],

$$\tau = \varepsilon_0 \varepsilon_m / \sigma_m \tag{3.71}$$

of conducting regions of the gate, body, drain, and source is exceedingly small. Consequently, we may assume that these regions are perfect conductors; with ε_m and σ_m being, respectively, the relative permittivity and conductivity of the conducting regions. We can thus regard the gate, body, drain, and source, as a system of four conductors capacitively coupled with each other by six differential (small-signal) reciprocal capacitances C_{gs}, C_{gd}, C_{gb}, C_{bs}, C_{bd}, and C_{ds}, as shown in Fig. 3.4; see also [12].

It should be emphasized that each of these capacitances does not consist of so-called intrinsic, extrinsic, fringing or overlap capacitances. Each of these is simply a reciprocal capacitance. Obviously, small-signal currents charging the capacitances C_{gs}, C_{gd}, C_{gb}, C_{bs}, C_{bd}, and C_{ds} appear if small-signal voltages $\upsilon_{gs}(t)$, $\upsilon_{ds}(t)$, and $\upsilon_{bs}(t)$ are non-zero ones.

Denoting the small-signal charging currents by $i_g^{cap}(t)$, $i_d^{cap}(t)$, $i_b^{cap}(t)$, and $i_s^{cap}(t)$, and applying Kirchhoff"s current law to each electrode, we have:

$$i_g^{cap}(t) = C_{gs}\frac{d\upsilon_{gs}}{dt} + C_{gb}\frac{d\upsilon_{gb}}{dt} + C_{gd}\frac{d\upsilon_{gd}}{dt} \tag{3.72}$$

$$i_d^{cap}(t) = C_{ds}\frac{d\upsilon_{ds}}{dt} + C_{gd}\frac{d\upsilon_{dg}}{dt} + C_{bd}\frac{d\upsilon_{db}}{dt} \tag{3.73}$$

$$i_b^{cap}(t) = C_{bs}\frac{d\upsilon_{bs}}{dt} + C_{gb}\frac{d\upsilon_{bg}}{dt} + C_{bd}\frac{d\upsilon_{bd}}{dt} \tag{3.74}$$

$$i_s^{cap}(t) = -\,C_{gs}\frac{d\upsilon_{gs}}{dt} - C_{ds}\frac{d\upsilon_{ds}}{dt} - C_{bs}\frac{d\upsilon_{bs}}{dt} \tag{3.75}$$

If we transform all the voltages in (3.72)–(3.74) into voltages referenced to the source, as shown in Fig. 3.4, then (3.72)–(3.74) can be rewritten as follows:

$$i_g^{\,cap}(t) = (C_{gs} + C_{gb} + C_{gd})\frac{d\upsilon_{gs}}{dt} - C_{gd}\frac{d\upsilon_{ds}}{dt} - C_{gb}\frac{d\upsilon_{bs}}{dt} \tag{3.76}$$

$$i_d^{\,cap}(t) = -\,C_{gd}\frac{d\upsilon_{gs}}{dt} + (C_{gd} + C_{ds} + C_{bd})\frac{d\upsilon_{ds}}{dt} - C_{bd}\frac{d\upsilon_{bs}}{dt} \tag{3.77}$$

$$i_b^{\,cap}(t) = -\,C_{gb}\frac{d\upsilon_{gs}}{dt} - C_{bd}\frac{d\upsilon_{ds}}{dt} + (C_{bs} + C_{gb} + C_{bd})\frac{d\upsilon_{bs}}{dt} \tag{3.78}$$

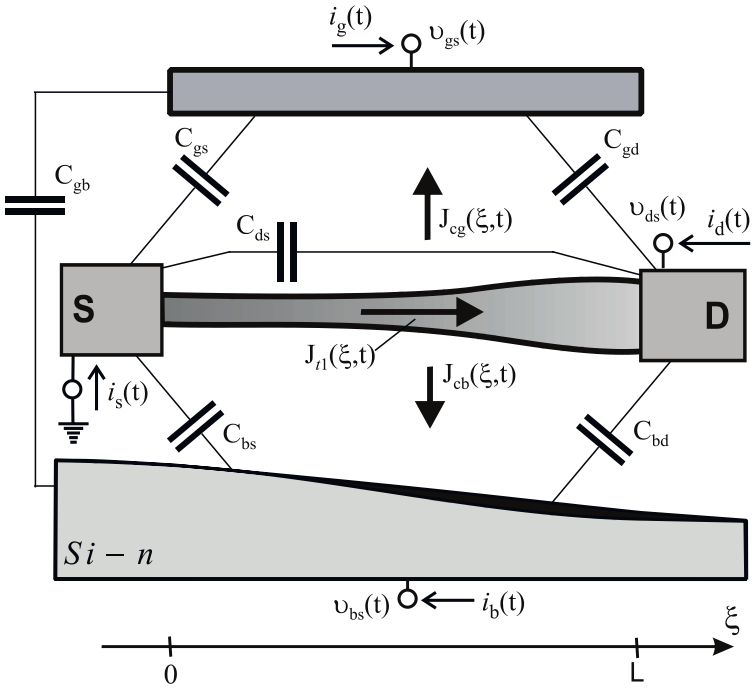

Fig. 3.4. The time-domain small-signal representation of the MOSFET with terminal voltages referenced to the source.

It is important to note that the algebraic sum of the terminal charging currents entering the transistor as a whole is zero [see (3.75)–(3.78)]:

$$i_s^{\,cap}(t) + i_g^{\,cap}(t) + i_d^{\,cap}(t) + i_b^{\,cap}(t) = 0 \tag{3.79}$$

The result is not surprising, because each of the six reciprocal capacitances stores no net charge. This means that the charging currents satisfy Kirchhoff's current law expressed by (3.79).

3.6.2. Drain- and source-terminal non-capacitive currents

By virtue of the principle of superposition, the small-signal terminal currents $i_g(t)$, $i_d(t)$, $i_b(t)$, and $i_s(t)$—see Fig. 3.4—are given by

$$i_g(t) = i_g^{cap}(t) + i_g^{ind}(t) \tag{3.80}$$

$$i_d(t) = i_d^{cap}(t) + i_d^{nc}(t) \tag{3.81}$$

$$i_b(t) = i_b^{cap}(t) + i_b^{ind}(t) \tag{3.82}$$

$$i_s(t) = i_s^{cap}(t) + i_s^{nc}(t) \tag{3.83}$$

where $i_g^{ind}(t)$ and $i_b^{ind}(t)$ are the coupling currents induced on the gate and in the body, respectively, and $i_s^{nc}(t)$ and $i_d^{nc}(t)$ are, accordingly, the source- and drain-terminal non-capacitive currents.

According to Kirchhoff's current law, the algebraic sum of the currents $i_g(t)$, $i_d(t)$, $i_b(t)$, and $i_s(t)$ should be zero,

$$i_s(t) + i_g(t) + i_d(t) + i_b(t) = 0 \tag{3.84}$$

If we add the equations from (3.80) to (3.83) and take account of (3.79) and (3.84), we obtain:

$$i_g^{ind}(t) + i_d^{nc}(t) + i_b^{ind}(t) + i_s^{nc}(t) = 0 \tag{3.85}$$

Equation (3.85) is Kirchhoff's current law for non-capacitive currents in the MOSFET under dynamic operation conditions.

Based on (3.67), the total drain-terminal non-capacitive time-domain small-signal current $i_d^{nc}(t)$ and the total source-terminal non-capacitive time-domain small-signal current $i_s^{nc}(t)$ are defined by

$$i_d^{nc}(t) = i_d^{con}(t) + i_{ddis}^{nc}(t) \tag{3.86}$$

$$i_s^{nc}(t) = i_s^{con}(t) + i_{sdis}^{nc}(t) \tag{3.87}$$

where $i_d^{con}(t)$ and $i_s^{con}(t)$ are, respectively,the drain- and source-terminal time-domain small-signal conduction currents, described by the two equations:

$$i_d^{con}(t) = -W\, X(L,t)\, J_1(L,t) \tag{3.88}$$

$$i_s^{con}(t) = W\, X(0,t)\, J_1(0,t) \tag{3.89}$$

whereas $i_{ddis}^{nc}(t)$ and $i_{sdis}^{nc}(t)$ represent, respectively, the drain- and source-terminal time-domain small-signal non-capacitive displacement currents.

The current $i_d^{con}(t)$ is not equal to $-i_s^{con}(t)$ in general, because moveable charges can be accumulated in or extracted from the channel.

Displacement currents depend on the electric field in the channel including its ends. In general, when carriers are injected into the channel and $v_{ds}(t)$ is not equal to zero, the electric field $E_1(\xi, t)$ acting on carriers in the channel can be written as follows:

$$E_1(\xi,t) = E_{1ext}(\xi,t) + E_{1i}(\xi,t) \tag{3.90}$$

where $E_{1ext}(\xi, t)$ is an external field set up by $v_{ds}(t)$,

$$E_{1ext}(\xi,t) = -\frac{v_{ds}(t)}{L} \tag{3.91}$$

and $E_{1i}(\xi, t)$ is an inner field set up by the small-signal excess charges $p_1(\xi, t)$; see Sec. 4.4.1.

Given (3.69) and (3.90), we have:

$$J_{dis1}(\xi,t) = \varepsilon_0 \varepsilon_s \frac{\partial E_{1ext}(\xi,t)}{\partial t} + \varepsilon_0 \varepsilon_s \frac{\partial E_{1i}(\xi,t)}{\partial t} \tag{3.92}$$

Denoted by $J_{dis}^{cap}(\xi,t)$, the first term on the right-hand side of (3.92),

$$J_{dis}^{cap}(\xi,t) = \varepsilon_0 \varepsilon_s \frac{\partial E_{1ext}(\xi,t)}{\partial t} \tag{3.93}$$

represents a displacement current density induced by the external field $E_{1ext}(\xi, t)$ [see (3.91)], and therefore it is simply a capacitive current density that is associated with the capacitance C_{ds}; see Fig. 3.4. Based on (3.91) and (3.93), one can see that $J_{dis}^{cap}(\xi,t)$ is independent of ξ, which confirms the capacitive character of the current. The displacement current density $J_{dis}^{cap}(\xi,t)$ produces a capacitive current flowing through the capacitance C_{ds}. The capacitive current is separately taken into account in the model (see Fig. 3.4) as well as currents $i_d^{cap}(t)$ and $i_s^{cap}(t)$ in (3.79)–(3.83).

The second term on the right-hand side of (3.92), denoted by

$$J_{dis}^{nc}(\xi,t) = \varepsilon_0 \varepsilon_s \frac{\partial E_{1i}(\xi,t)}{\partial t} \tag{3.94}$$

is a non-capacitive displacement current density in the channel, which is determined by the inner field $E_{1i}(\xi, t)$; see Sec. 4.4.1.

We know from physics of the transistor that the small-signal excess charges $p_1(\xi, t)$ induce surface charges on the gate, body, drain and source; see Secs. 3.2 and 3.4. In a real MOSFET, the distributions of surface charges are nonuniform and the regions of the drain

and the source are bounded by cylindrical surfaces in a three-dimensional space. It means that the distribution of the longitudinal electric field is not confined only to the channel. Therefore, in our quasi-2D approach, we assume that the longitudinal electric field $E_{1i}(\xi, t)$, set up by the small-signal excess charges $p_1(\xi, t)$, is associated with an equivalent parallel-plate capacitor whose capacitance equals C_{ds} and its plates are separated by a distance L (L being the channel length). Thus, denoted by A_{cds}, an effective area of each of the two plates is:

$$A_{cds} = \frac{L C_{ds}}{\varepsilon_0 \varepsilon_s} \tag{3.95}$$

Therefore, based on (3.94), (3.95), and Fig. 3.4, the drain-terminal time-domain small-signal non-capacitive displacement current $i_{ddis}^{nc}(t)$ is:

$$i_{ddis}^{nc}(t) = -L C_{ds} \frac{\partial E_{1i}(L,t)}{\partial t} \tag{3.96}$$

Similarly, the source-terminal time-domain small-signal non-capacitive displacement current $i_{sdis}^{nc}(t)$ is:

$$i_{sdis}^{nc}(t) = L C_{ds} \frac{\partial E_{1i}(0,t)}{\partial t} \tag{3.97}$$

The coupling currents $i_g^{ind}(t)$ and $i_b^{ind}(t)$ are analyzed in Sec. 3.8.

3.7. Gate-to-body capacitance C_{gb}

The quasi-2D dc MOSFET representation enables us to calculate the capacitance C_{gb}. First, we evaluate two circuit elements: a differential (quasi-static) gate-to-channel capacitance C_{gc} and differential (quasi-static) body-to-channel capacitance C_{bc}, which are subsequently used to estimate the differential gate-to-body capacitance C_{gb}.

3.7.1. Preliminary remarks

In the quasi-static small-signal analysis performed in this section, we assume that variations in the terminal voltages V_{GS} and V_{BS} are sufficiently slow, which—after [3]—means that charges per unit area at any time on the gate, in the body, and in the channel are identical to those that would be found if dc voltages were used instead.

In the case of small harmonic signals exciting the transistor, we may say that the assumption of quasi-static operation is justified if the period T of the signals is over one hundred times greater than the transit time τ_{tr} of carriers across the channel:

$$T \geq 100\, \tau_{tr} \tag{3.98}$$

where τ_{tr} is given by

$$\tau_{tr} = \int_0^L \frac{d\xi}{\upsilon(\xi)} \tag{3.99}$$

where $\upsilon(\xi)$ is the velocity of carriers traveling along the channel line; see Figs. 2.8, 2.12, and 3.5. It is worth pointing out that $\upsilon(\xi)$ is determined by biasing voltages at the Q-point.

Let us consider a quasi-2D picture of a *p*-channel MOSFET that operates under dc conditions, which is shown in Fig. 3.5.

If V_{GS} is large enough, a dc drain current I_D flows in the drain-source circuit, which is a function of three biasing voltages, i.e., $I_D = I_D(V_{DS}, V_{GS}, V_{BS})$.

For any point $\xi \in [0, L]$ on the channel line, we can define three voltages: $V_{CS}(\xi)$, $V_{GC}(\xi)$, and $V_{BC}(\xi)$ between the point and, respectively, the source, the gate, and the body, as shown in Fig. 3.5. Due to potentiality of the electric field in the device, the voltages must satisfy Kirchhoff's voltage law, i.e.:

$$V_{GS} = V_{CS}(\xi) + V_{GC}(\xi) \tag{3.100}$$

$$V_{BS} = V_{CS}(\xi) + V_{BC}(\xi) \tag{3.101}$$

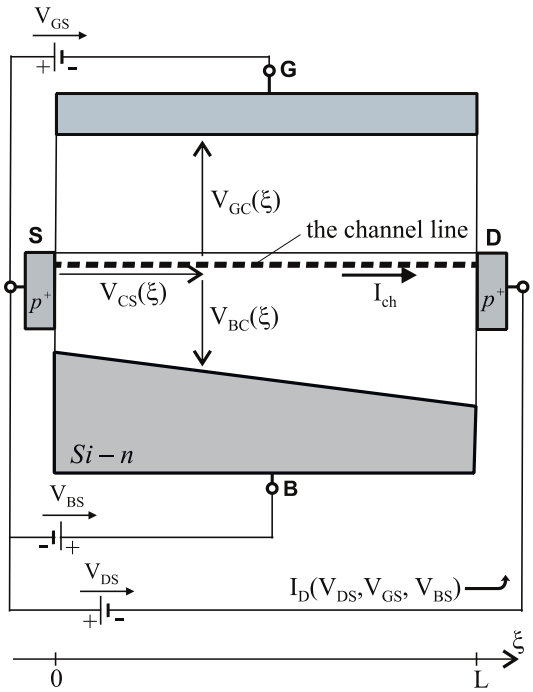

Fig. 3.5. A quasi-2D picture of a *p*-channel MOSFET under dc conditions with terminal voltages referenced to the source.

A system consisting of the gate, depletion region, and the channel should be electrically neutral as a whole. Hence, the overall charge neutrality equation for the quasi-2D MOSFET model can be written as follows:

$$q_G + q_C + q_B = 0 \tag{3.102}$$

where q_G, q_C, and q_B are, respectively, the charge on the gate, the moveable charge in the channel, and the charge being the sum of the uncompensated charge of ionized impurities in the body and the effective charge of the ($Si–SiO_2$)-interface.

The charges occurring in (3.102) are defined by

$$q_G = W \int_0^L Q_G(\xi)\, d\xi \tag{3.103}$$

$$q_C = W \int_0^L Q_C(\xi)\, d\xi \tag{3.104}$$

$$q_B = W \int_0^L Q_B(\xi)\, d\xi + WL\, Q_0 \tag{3.105}$$

with W, $Q_G(\xi)$, $Q_C(\xi)$, $Q_B(\xi)$, and Q_0 being, respectively, the width of the transistor, the surface charge density on the gate, the channel charge per unit area [defined by (2.17)], the surface charge density of ionized impurities in the depletion layer [defined by (2.59)], and the effective ($Si–SiO_2$)-interface charge per unit area [3].

It is worth emphasizing that charges of the six capacitors of Fig. 3.4 do not bring anything to (3.102) because each of these capacitors is electrically neutral as a whole.

3.7.2. Quasi-static gate-to-channel capacitance C_{gc}

If V_{GS} is quasi-statically changed by an infinitesimally small voltage dV_{GS}, as illustrated in Fig. 3.6, then the charges $Q_C(\xi)$ and $Q_G(\xi)$ as well as the drain current I_D and the charges on the capacitances C_{gs} and C_{gd} (see Fig. 3.4) also change. Since dV_{GS} is infinitesimally small and the voltages V_{DS} and V_{BS} are fixed, we can take an assumption that distributions of the voltage $V_{CS}(\xi)$ and the longitudinal electric field over the channel line (see Fig. 3.5) do not change. Taking this into account and differentiating (3.100), we obtain:

$$dV_{GC}(\xi) = dV_{GS} \tag{3.106}$$

As the gate is equipotential, (3.106) implies that the channel line is also an equipotential line for small variations in V_{GS}. Consequently, the system consisting of the gate and the channel may be regarded as a quasi-static capacitance C_{gc}.

Let $I_{D\text{-}gs}$, $q_{G\text{-}gs}$, $q_{C\text{-}gs}$, $q_{B\text{-}gs}$, and $Q_{C\text{-}gs}(\xi)$ denote, respectively, I_D q_G, q_C, q_B, and $Q_C(\xi)$ referred to the circumstances shown in Fig. 3.6.

The body charge q_B does not vary in the circumstances shown in Fig. 3.6. Taking this into account and differentiating (3.102), we obtain:

$$dq_{G-gs} = -\, dq_{C-gs} \tag{3.107}$$

The quasi-static capacitance C_{gc} is defined as follows:

$$C_{gc} \equiv \frac{dq_{G-gs}}{dV_{GS}} = \frac{-dq_{C-gs}}{dV_{GS}} \tag{3.108}$$

Before proceeding further, we state that all the terminal currents in this work are defined as entering the device, as shown in Figs. 3.4–3.8. Therefore, for quasi-static condition, we can write:

$$I_D = -I_{ch} \tag{3.109}$$

and combining (2.16), (2.17), and (3.109), we have:

$$I_D = -W\,\upsilon\,(\xi)\,Q_C(\xi) \tag{3.110}$$

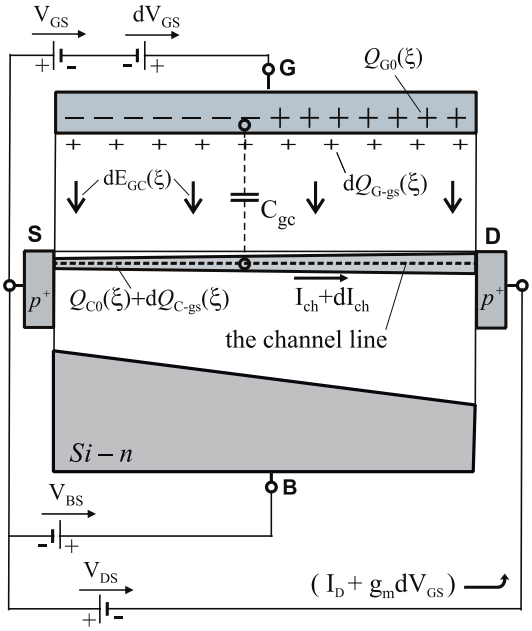

Fig. 3.6. An MOSFET under a small quasi-static excitation dV_{GS}.

As stated previously, the distributions of the voltage $V_{CS}(\xi)$ and longitudinal electric field over the channel line do not change in the situation depicted in Fig. 3.6. Thus, we may assume the distribution of the carrier velocity $\upsilon(\xi)$ in the channel also not to change, which means that the differential $d\upsilon(\xi) = 0$. Taking this into account and differentiating (3.110), we can write the following formula for the differential dI_{Dgs} in the circumstances shown in Fig. 3.6:

$$dI_{D-gs} = -W\upsilon(\xi)\, dQ_{C-gs}(\xi) \tag{3.111}$$

Equation (3.111) is true for every $\xi \in [0, L]$, because the continuity equation should be fulfilled also for infinitesimals under quasi-static conditions.

On the other hand, based on the definition of the gate transconductance g_m, one can write:

$$dI_{D-gs} = g_m\, dV_{GS} \tag{3.112}$$

Comparing (3.111) and (3.112), we obtain:

$$dQ_{C-gs}(\xi) = -\frac{g_m\, dV_{GS}}{W\upsilon(\xi)} \tag{3.113}$$

Integrating (3.113) and taking account of (3.99), we get the following formula for the differential $dq_{C\text{-}gs}$ of the channel charge:

$$\begin{aligned} dq_{C-gs} &= W\int_0^L dQ_{C-gs}(\xi)\, d\xi \\ &= -g_m\, dV_{GS}\int_0^L \frac{d\xi}{\upsilon(\xi)} \\ &= -g_m\,\tau_{tr}\, dV_{GS} \end{aligned} \tag{3.114}$$

Combining (3.108) with (3.114), we get:

$$C_{gc} = g_m\,\tau_{tr} \tag{3.115}$$

The capacitance C_{gc} is nonuniform, because $dQ_{C\text{-}gs}(\xi)$ determined by (3.113) is not a constant function of ξ in general.

3.7.3. Quasi-static body-to-channel capacitance C_{bc}

The method used to derive the formula for C_{gc} can be directly applied to finding a formula for the quasi-static capacitance C_{bc}.

Let us consider a quasi-2D picture of a p-channel MOSFET that operates under an infinitesimally small quasi-static excitation dV_{BS}, as shown in Fig. 3.7.

The small voltage dV_{BS} causes small variations in $Q_C(\xi)$, $Q_B(\xi)$, I_D, and also in the charges on the capacitances C_{bs} and C_{bd} (see Fig. 3.4). Since dV_{BS} is infinitesimally small and the voltages V_{DS} and V_{GS} are fixed, we can take an assumption that the voltage $V_{CS}(\xi)$ and longitudinal electric field over the channel line (see Fig. 3.5) do not change. Taking account of the assumption and differentiating (3.101), we obtain:

$$dV_{BC}(\xi) = dV_{BS} \tag{3.116}$$

As the gate is equipotential, (3.116) implies that the channel line is also an equipotential line for small variations in V_{BS}. Consequently, the system consisting of the gate and the channel may be regarded as a quasi-static capacitance C_{bc}.

Let $I_{D\text{-}bs}$, $q_{G\text{-}bs}$, $q_{C\text{-}bs}$, $q_{B\text{-}bs}$, and $Q_{C\text{-}bs}(\xi)$ denote, respectively, I_D q_G, q_C, q_B, and $Q_C(\xi)$ referred to the circumstances shown in Fig. 3.7.

In the circuit shown in Fig. 3.7, the gate charge q_G does not vary. Taking this into account and differentiating (3.102), we get:

$$dq_{B-bs} = -\,dq_{C-bs} \tag{3.117}$$

The quasi-static capacitance C_{bc} is defined as follows:

$$\begin{aligned} C_{bc} &\equiv \frac{dq_{B-bs}}{dV_{BS}} \\ &= \frac{-\,dq_{C-bs}}{dV_{BS}} \end{aligned} \tag{3.118}$$

As stated previously, the distributions of the voltage $V_{CS}(\xi)$ and longitudinal electric field over the channel line do not change in the situation depicted in Fig. 3.7. We may thus assume the distribution of the carrier velocity $v(\xi)$ in the channel also not to change, which means the differential $dv(\xi) = 0$. Taking this into account and differentiating (3.110), we can write the following formula for the differential $dI_{D\text{-}bs}$ in the circumstances shown in Fig. 3.7:

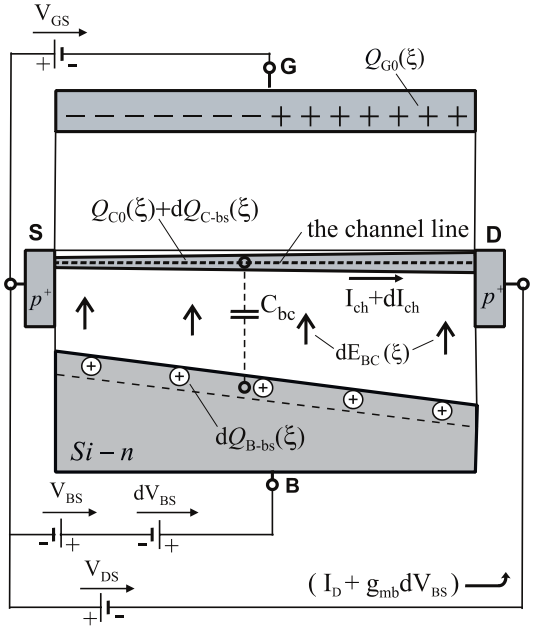

Fig. 3.7. An MOSFET under a small quasi-static excitation dV_{BS}.

$$dI_{D-bs} = -\,W\,\upsilon\,(\xi)\,dQ_{C-bs}(\xi) \tag{3.119}$$

Equation (3.119) is true for every $\xi \in [0, L]$, because the continuity equation should be fulfilled also for infinitesimals under quasi-static conditions.

On the other hand, basing on the definition of the body transconductance g_{mb}, one can write

$$dI_{D-bs} = g_{mb}\ dV_{BS} \tag{3.120}$$

Comparing (3.119) and (3.120), we obtain:

$$dQ_{C-bs}(\xi) = -\,\frac{g_{mb}\ dV_{BS}}{W\,\upsilon\,(\xi)} \tag{3.121}$$

Integrating (3.121) and taking account of (3.99), we get the following formula for the differential $dq_{C\text{-}bs}$ of the channel charge:

$$\begin{aligned} dq_{C-bs} &= W\int_0^L dQ_{C-bs}(\xi)\,d\xi \\ &= -\,g_{mb}\ dV_{BS}\int_0^L \frac{d\xi}{\upsilon\,(\xi)} \\ &= -\,g_{mb}\,\tau_{tr}\,dV_{BS} \end{aligned} \tag{3.122}$$

Combining (3.118) with (3.122), we get:

$$C_{bc} = g_{mb}\ \tau_{tr} \tag{3.123}$$

The capacitance C_{bc} is nonuniform, because the differential $dQ_{C\text{-}bs}(\xi)$ determined by (3.121) is not a constant function of ξ in general.

3.7.4. Gate-to-body capacitance C_{gb}

The capacitance C_{gb} is defined by

$$\begin{aligned} C_{gb} &\equiv \frac{dq_G}{dV_{GB}} \\ &= \frac{-dq_B}{dV_{GB}} \end{aligned} \tag{3.124}$$

provided that

$$dq_G = -\,dq_B \tag{3.125}$$

To derive a formula for the capacitance C_{gb}, let us consider the circuit shown in Fig. 3.8.

The infinitesimally small voltages dV_{GS} and dV_{BS} produce infinitesimally small changes in q_G, q_C, q_B, and I_D whose differentials are dq_G, dq_C, dq_B, and dI_D, respectively.

For the same reasons as in the case of the capacitance C_{gc} or C_{bc}, the channel line in Fig. 3.8 is also an equipotential line for small signals.

The differentials dq_G, dq_C, and dq_B have to satisfy the following equation obtained by differentiating (3.102):

$$dq_G + dq_C + dq_B = 0 \tag{3.126}$$

If V_{DS} = constant (see Fig. 3.8), the differential dI_D is:

$$dI_D = g_m\, dV_{GS} + g_{mb}\, dV_{BS} \tag{3.127}$$

From Fig. 3.5 and Kirchhoff"s voltage law, we have:

$$V_{GB} = V_{GS} - V_{BS} \tag{3.128}$$

Differentiating (3.128), we get:

$$dV_{GB} = dV_{GS} - dV_{BS} \tag{3.129}$$

To use (3.124) to calculate the capacitance C_{gb}, we must prove that the condition (3.125) can be satisfied in the circumstances shown in Fig. 3.8.

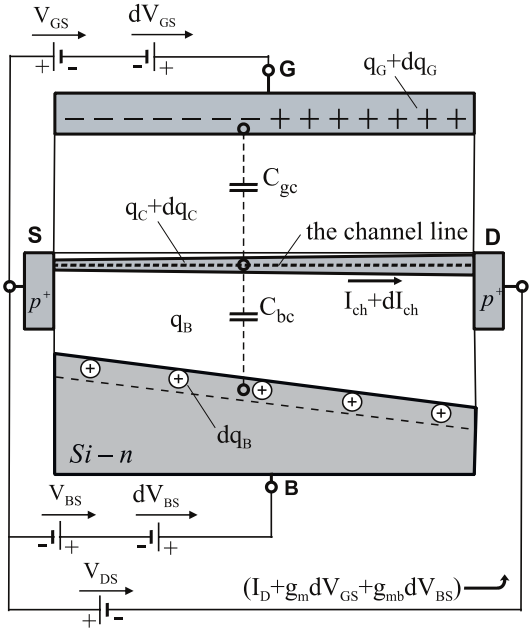

Fig. 3.8. An MOSFET excited by small quasi-static voltages dV_{GS} and dV_{BS}.

Indeed, we infer from (3.125) and (3.126) that dq_C should be zero; this implies that dI_D should also be zero, and—by virtue of (3.127)—we get the following condition:

$$g_m \, dV_{GS} = - \, g_{mb} \, dV_{BS} \tag{3.130}$$

Thus, if (3.130) is satisfied, the condition (3.125) is fulfilled. Hence, we may use (3.124) to calculate C_{gb}.

Taking $1/C_{gb}$ from (3.124) and using (3.129) and (3.125), we obtain:

$$\begin{aligned} \frac{1}{C_{gb}} &= \frac{dV_{GS}}{dq_G} - \frac{dV_{BS}}{dq_G} \\ &= \frac{dV_{GS}}{dq_G} + \frac{dV_{BS}}{dq_B} \end{aligned} \tag{3.131}$$

Using (3.108) and (3.118), the previous equation takes the form:

$$\frac{1}{C_{gb}} = \frac{1}{C_{gc}} + \frac{1}{C_{bc}} \tag{3.132}$$

We see that C_{gb} is the equivalent capacitance of two capacitors C_{gc} and C_{bc} connected in series, which is illustrated in Fig. 3.8.

Combining (3.115) and (3.123) with (3.132), we get:

$$C_{gb} = \frac{g_m \, \eta \, \tau_{tr}}{1+\eta} \tag{3.133}$$

where

$$\eta = g_{mb} / g_m \tag{3.134}$$

Although derivation of the formula for the differential capacitance C_{gb} is based on the differential (quasi-static) capacitances C_{gc} and C_{bc}, the applicability of this formula is not limited only to the quasi-static conditions, since the gate and body regions are assumed to be good conductors.

3.8. Supplementary equations and rules

Based on the results of Secs. 3.4–3.7, additional equations and rules are formulated in this section.

The terminal coupling currents $i_g^{ind}(t)$ and $i_b^{ind}(t)$ are produced by perturbations in carrier concentration in the channel or, equivalently, by time-changing in the transverse electric fields $E_{cg}(\xi, t)$ and $E_{cb}(\xi, t)$; see Fig. 3.3 They are induced between the channel and the gate, and between the channel and the body. The densities of these currents are, respectively, $J_{cg}(\xi, t)$ and $J_{cb}(\xi, t)$, as illustrated in Fig. 3.4. However, in our approach, we derive a rule that establishes a relationship between the coupling currents $i_g^{ind}(t)$ and $i_b^{ind}(t)$. This approach guarantees that Kirchhoff's current law for the terminal non-capacitive displacement currents is satisfied.

Analyzing the situation shown in Fig. 3.8 and applying the superposition principle, we can write the following equation for the surface charge density $dQ_C(\xi)$ induced by the voltages dV_{GS} and dV_{BS} that are changed quasi-statically:

$$dQ_C(\xi) = dQ_{C-gs}(\xi) + dQ_{C-bs}(\xi) \tag{3.135}$$

To find a relationship between $dQ_{C\text{-}gs}(\xi)$ and $dQ_{C\text{-}bs}(\xi)$, we divide (3.113) by (3.121), which leads to the following:

$$\frac{dQ_{C-gs}(\xi)}{dQ_{C-bs}(\xi)} = \frac{g_m\, dV_{GS}}{g_{mb}\, dV_{BS}} \tag{3.136}$$

Taking assumption that $dV_{GS} = dV_{BS}$ in (3.136), we can formulate a quasi-static channel charge partition rule (QSCCPR) as follows: the surface density $dQ_C(\xi)$ of the infinitesimal channel charge induced by the voltages dV_{GS} and dV_{BS} is divided between $dQ_{C\text{-}gs}(\xi)$ and $dQ_{C\text{-}bs}(\xi)$ in direct proportion to respective transconductances g_m / g_{mb}. The reverse is also true; that is, if a quasi-static increase in the surface density $dQ_C(\xi)$ of the infinitesimal channel charge produces surface charge densities $dQ_{C\text{-}gs}(\xi)$ and $dQ_{C\text{-}bs}(\xi)$, respectively, on the gate and in the body, then the proportion of $dQ_{C\text{-}gs}(\xi)$ to $dQ_{C\text{-}bs}(\xi)$ is g_m to g_{mb}, provided that the infinitesimal increases of V_{GS} and V_{BS} are equal to each other, i.e., $dV_{GS} = dV_{BS}$.

Hence, if $dV_{GS} = dV_{BS}$, then:

$$dQ_{C-bs}(\xi) = \frac{g_{mb}}{g_m} dQ_{C-gs}(\xi) \tag{3.137}$$

Now, we proceed to analyze the dynamic non-quasi-static coupling between the excess channel charge and the transistor structure.

By analogy with (3.12) and (3.13), we can write:

$$Q_c(\xi,t) = Q_C(\xi,t) - Q_C(\xi) \tag{3.138}$$

where $Q_c(\xi, t)$ is the small excess channel charge (linear approximation) per unit area, $Q_C(\xi, t)$ is the total channel charge per unit area, and $Q_C(\xi)$ is the channel charge per unit area at dc condition (at the Q-point).

Based on Gauss's law, we may divide the excess channel charge per unit area, $Q_c(\xi, t)$, into two parts:

$$Q_c(\xi,t) = Q_{c\perp}(\xi,t) + Q_{c-l}(\xi,t) \tag{3.139}$$

where $Q_{c\perp}(\xi, t)$ and $Q_{c\text{-}l}(\xi, t)$ are excess channel charges per unit area associated with, respectively, the perpendicular and longitudinal component of electric field in the channel.

Then, we divide the charge $Q_{c\perp}(\xi, t)$ into two parts as follows:

$$Q_{c\perp}(\xi,t) = Q_{cb}(\xi,t) + Q_{cg}(\xi,t) \tag{3.140}$$

where $Q_{cb}(\xi, t)$ and $Q_{cg}(\xi, t)$ are excess channel charges per unit area associated with the channel-to-body and channel-to-gate coupling, respectively.

Finally, having regard to the results of the quasi-static analysis, we assume that the non-quasi-static partitioning of the charge $Q_{c\perp}(\xi, t)$ is also governed by the QSCCPR, which is expressed by (3.137), i.e.:

$$Q_{cb}(\xi,t) = \frac{g_{mb}}{g_m} Q_{cg}(\xi,t) \tag{3.141}$$

[Obviously, the charges $Q_{cb}(\xi, t)$ and $Q_{cg}(\xi, t)$ have the same algebraic sign.]

Thus, (3.141) reflects the mathematical meaning of the non-quasi-static channel charge partition rule (NQSCCPR).

Denoted by $q_g(t)$ and $q_b(t)$, overall excess charges induced, respectively, on the gate and in the body by the excess channel charge can be expressed as

$$q_g(t) = -W\int_0^L Q_{cg}(\xi,t)\,d\xi \tag{3.142}$$

$$q_b(t) = -W\int_0^L Q_{cb}(\xi,t)\,d\xi \tag{3.143}$$

By definition, the terminal coupling currents, $i_g^{ind}(t)$ and $i_b^{ind}(t)$, are:

$$i_g^{ind}(t) = \frac{d}{dt}\left[\, q_g(t)\right] \tag{3.144}$$

$$i_b^{ind}(t) = \frac{d}{dt}\left[\, q_b(t)\right] \tag{3.145}$$

Dividing (3.145) by (3.144) and subsequently taking account of (3.142), (3.143), and (3.141) in the resultant equation, we get a useful rule for the coupling currents:

$$\frac{i_b^{ind}(t)}{i_g^{ind}(t)} = \frac{g_{mb}}{g_m} \tag{3.146}$$

To sum up, in order to fulfill Kirchhoff's current law, we need to calculate values of the coupling and non-capacitive displacement currents [$i_g^{ind}(t)$, $i_b^{ind}(t)$, $i_d^{nc}(t)$, and $i_s^{nc}(t)$] from (3.85)–(3.87) and (3.146).

3.9. Conclusion

A novel quasi-2D non-quasi-static four-terminal time-domain small-signal MOSFET model has been established in this chapter.

A set of partial differential equations for the new physics-based quasi-2D time-domain small-signal MOSFET model is derived. The set consists of a quasi-2D small-signal continuity equation, a quasi-2D small-signal Poisson's equation, and a quasi-2D small-signal trans-

port equation. All the equations give—in the time domain—a mathematical description of the behavior of the carrier concentration in the channel, charges in the gate and body, carrier transport in the channel, as well as terminal and coupling currents. A set of supplementary equations for coupling and non-capacitive displacement currents in the MOSFET under dynamic operation is also derived.

Based on the quasi-2D dc MOSFET representation, a useful formula for the gate-to-body capacitance C_{gb} is derived, and some rules dealing with channel-to-gate and channel-to-body coupling currents are established.

The model presented in this chapter lays the foundations for a novel quasi-2D frequency-domain small-signal MOSFET model that is developed in Chapter 4.

References

[1] Sze C. M. and Ng K. K., *Physics of semiconductor devices*, 3rd ed., Wiley and Sons, 2007.
[2] ATLAS *User's Manual*, SILVACO International, Santa Clara, CA, vol. 1, 1998.
[3] Tsividis Y. P. and McAndrew C., *The MOS transistor*, Int. 3rd ed., Oxford University Press, New York, 2012.
[4] Selberherr S., *Analysis and Simulation of Semiconductor Devices.* Wien, Springer-Verlag, 1984.
[5] Hansch W., *The drift diffusion equation and its applications in MOSFET modeling*, Springer-Verlag, Wien, 1991.
[6] Muller R. S. and Kamins T. I., *Device electronics for integrated circuits*, Wiley and Sons, New York, 1986.
[7] Jacoboni C., Canali C., Ottaviani G., and Quaranta A. A., "A review of some charge transport properties of silicon", *Solid-State Electronics*, vol. 20, p. 77, 1977.
[8] Lundstrom M., *Fundamentals of Carrier Transport*, Cambridge, U.K.: Cambridge Univ. Press, 2000.
[9] Datta S., *Quantum Transport: Atom to Transistor*, Cambridge, U.K.: Cambridge Univ. Press, 2005.
[10] Sverdlov V., Ungersboeck E., Kosina H., and Selberherr S., "Current transport models for nanoscale semiconductor devices", Materials Science and Engineering R, vol. 58, pp. 228–270, 2008.
[11] Stratton J. A., *Electromagnetic theory*, Wiley-Interscience, 2007.
[12] Smythe W. R., *Static and dynamic electricity*, 3rd ed., McGraw-Hill Book Company, 1968.

Chapter 4

FREQUENCY-DOMAIN MODEL

Wiesław Kordalski

4.1. Introduction

The purpose of this chapter is to present derivation of a novel DIBL-included quasi-2D NQS four-terminal frequency-domain small-signal model for the MOSFET with a linearly thickened channel. The GCA is abandoned in this derivation.

Some final results of a simplified version (without the DIBL effect) of the new model are briefly reported in [1, 2].

This chapter is organized as follows. In Section 4.2, a set of equations defining the model in the time-domain is formulated. A frequency-domain analysis is performed in Section 4.3. A DIBL-included model and a four-terminal small-signal equivalent circuit for the MOSFET are derived in Section 4.4. A four-terminal small-signal equivalent circuit for the long-channel MOSFET is presented in Section 4.5. Section 4.6 contains the main conclusions.

In this chapter, we assume that no generation-recombination processes occur, and the tunneling and leakage currents are negligibly small.

A general note: the analysis presented here is carried out for a *p*-channel MOS transistor, and the symbols for small-signal voltages (υ_{gs}, υ_{ds}, υ_{bs}) and currents (i_1, i_d, i_s, i_b, i_g, i_b^{ind}, i_g^{ind}, i_d^{ch}, i_s^{ch}) occurring in this chapter are consistent with those used in Chapter 3 and have the meaning of phasors.

4.2. Formulation of time-domain equations

In this model, the thickness of the channel at the Qpoint, denoted by $X_0(\xi)$, is assumed to be a linear function of ξ described by

$$X_0(\xi) = X_S[1+(S-1)\,\xi/L\,] \tag{4.1}$$

$$S = X_D/X_S\,, \qquad S \geq 1 \tag{4.2}$$

where X_S and X_D are thicknesses of the channel at the source and the drain, respectively, and L denotes the channel length of the quasi-2D dc representation of the channel; see Fig. 4.1 and Sec. 2.2.

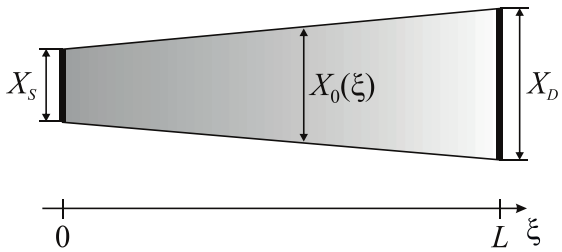

Fig. 4.1. A linearly thickened channel of the PMOSFET under consideration.

Basic equations and their simplifications that govern kinetics of carriers in the channel under small-signal perturbation for the quasi-2D NQS time-domain model of the MOSFET are derived in Chap. 3.

The symbols occurring in this section are exactly the same as those in Secs. 3.2–3.5 unless otherwise stated.

4.2.1. Continuity equation

We use the gradually-thickened-and-slightly-deformed-channel approximation of the continuity equation [see (3.40)], in which the dynamic coupling factor of the channel D_C, defined by (3.21), is assumed to be a constant at the Q-point, i.e.:

$$q\,(1+D_C)\frac{\partial p_1(\xi,t)}{\partial t} = -\frac{\partial J_1(\xi,t)}{\partial \xi} \tag{4.3}$$

where $J_1(\xi, t)$ is the small-signal conduction current density of holes; cf. for instance [3], [4, p. 503], [5, eq. (1)], [6, eq. (6)].

4.2.2. Transport equation

We make assumptions that the effective bias-dependent mobility at the Q-point, $\mu_q(\xi)$, and the dc component of the longitudinal electric field along the channel line, $E_0(\xi)$, are constant functions of ξ, and are equal to μ_q and E_0, respectively. Relying on these assumptions and taking (3.67)–(3.69) into account, the total small-signal current density $J_{t1}(\xi, t)$ is:

$$J_{t1}(\xi,t) = J_1(\xi,t) + J_{dis\,1}(\xi,t) \tag{4.4}$$

where the small-signal conduction current density of holes can be written as follows:

$$J_1(\xi,t) = q\,\mu_q\,E_0\,p_1(\xi,t) + q\,\mu_q\,p_0(\xi)\,E_1(\xi,t) + q\,\mu_1(\xi,t)\,E_0\,p_0(\xi) - q\,D_{p\,0}\,\frac{\partial p_1(\xi,t)}{\partial \xi} \tag{4.5}$$

and

$$J_{dis\,1}(\xi,t) = \varepsilon_0 \varepsilon_s \frac{\partial E_1(\xi,t)}{\partial t} \tag{4.6}$$

is the small-signal displacement current density. The dc longitudinal electric field E_0 along the channel is assumed to be:

$$E_0 = -V_{DS} / L \tag{4.7}$$

where V_{DS} is the dc drain-to-source voltage.

The mobility $\mu_1(\xi, t)$ in (4.5) is defined by (3.70). However, we assume that $\mu_1(\xi, t)$ is determined by only the first component of (3.70), whereas the mobility μ_q is only a function of E_0, i.e., $\mu_q = \mu_q (E_0)$. Taking these assumptions into account, we can write:

$$\mu_1(\xi,t) = \frac{d\mu_q}{dE_0} E_1(\xi,t) \tag{4.8}$$

Employing (4.8), we can rewrite (4.5) as follows:

$$J_1(\xi,t) = q\,\mu_q\,E_0\,p_1(\xi,t) - q\,D_{p\,0}\frac{\partial p_1(\xi,t)}{\partial \xi} + q\,p_0(\xi)\left(\mu_q + \frac{d\mu_q}{dE_0}E_0\right)E_1(\xi,t) \tag{4.9}$$

Equation (4.9) can be written in a simpler form if, after [3, p. 514], the definition of differential mobility μ_d at the Q-point is introduced, i.e.:

$$\mu_d = \frac{d\upsilon}{dE_0} \tag{4.10}$$

where υ is the velocity of carriers in the channel,

$$\upsilon = \mu_q E_0 \tag{4.11}$$

Differentiating (4.11) with respect to E_0, we have:

$$\mu_d = \mu_q + \frac{d\mu_q}{dE_0}E_0 \tag{4.12}$$

Given (4.12), we can rewrite (4.9) in the following simpler form:

$$J_1(\xi,t) = q\,\mu_q\,E_0\;p_1(\xi,t) - q\,D_{p\,0}\frac{\partial p_1(\xi,t)}{\partial \xi} + q\,\mu_d\;p_0(\xi)\;E_1(\xi,t) \tag{4.13}$$

The last component of the right-hand side of (4.13) can be expressed through a so-called ohmic part of the quasi-static small-signal drain-source conductance, denoted by g_{ds0}; see (A.39). (Formulas for g_{ds0} and the quasi-static small-signal drain-source conductance g_{ds} are derived in Appendix C.)

Using (A.39) and assuming that Einstein's relationship exists between the mobility μ_q and diffusivity D_{p0} [3, 4],

$$D_{p0} = V_t \, \mu_q \tag{4.14}$$

where $V_t = kT/q$ is thermal voltage (25.9 mV at 300°K) , we can rewrite (4.13) in the form:

$$J_1(\xi,t) = q\,\mu_q \left[E_0 \; p_1(\xi,t) - V_t \, \frac{\partial p_1(\xi,t)}{\partial \xi} \right] + \frac{g_{dso}\, L}{W\, X_0(\xi)} \, E_1(\xi,t) \tag{4.15}$$

We can obtain a useful simplification of (4.15) if we replace $X_0(\xi)$ with an average channel thickness, denoted by X_{ch},

$$X_{ch} = (X_S + X_D)/2 \tag{4.16}$$

$$X_D = S X_S , \qquad S \geq 1 \tag{4.17}$$

see Fig. 4.1. As a consequence, we get the following simplified formula for the small-signal conduction current density:

$$J_1(\xi,t) = q\,\mu_q \left[E_0 \; p_1(\xi,t) - V_t \, \frac{\partial p_1(\xi,t)}{\partial \xi} \right] + \frac{g_{dso}\, L}{W\, X_{ch}} \, E_1(\xi,t) \tag{4.18}$$

4.2.3. Poisson's equation

In the model, we choose a simpler version of the quasi-2D small-signal Poisson's equation [see (3.54)]:

$$\frac{\partial E_1(\xi,t)}{\partial \xi} = \frac{q\, p_1(\xi,t)}{\varepsilon_0 \varepsilon_s} - \frac{E_{cg}(\xi,t)}{X_0(\xi)} - \frac{E_{cb}(\xi,t)}{X_0(\xi)} \tag{4.19}$$

which is a transformed version of the thick-channel-and-weakly-coupled-carrier-to-channel approximation defined by (3.58).

We may rewrite (4.19) in a more convenient form for physical interpretation, i.e.:

$$\varepsilon_0 \varepsilon_s \, \frac{\partial E_1(\xi,t)}{\partial \xi} = q\, p_1(\xi,t) \left[1 - \frac{\varepsilon_0 \varepsilon_s \, E_{cg}(\xi,t)}{q\, p_1(\xi,t)\, X_0(\xi)} - \frac{\varepsilon_0 \varepsilon_s \, E_{cb}(\xi,t)}{q\, p_1(\xi,t)\, X_0(\xi)} \right].$$

A dimensionless quantity inside the square brackets on the right-hand side of (4.20), denoted here by $d_1(\xi, t)$,

$$d_l(\xi,t) = 1 - \frac{\varepsilon_0 \varepsilon_s E_{cg}(\xi,t)}{q\, p_1(\xi,t)\, X_0(\xi)} - \frac{\varepsilon_0 \varepsilon_s E_{cb}(\xi,t)}{q\, p_1(\xi,t)\, X_0(\xi)} \tag{4.21}$$

is a function of ξ and t, and can be termed a longitudinal dynamic carrier-to-channel coupling factor. The quantity $d_l(\xi, t)$ shows us what a fraction of the spatial excess charge density $q \cdot p_1(\xi, t)$ is associated with the longitudinal electric field component $E_1(\xi, t)$.

Furthermore, we introduce two other dimensionless factors, $d_{cg}(\xi, t)$ and $d_{cb}(\xi, t)$:

$$d_{cg}(\xi,t) = \frac{\varepsilon_0 \varepsilon_s E_{cg}(\xi,t)}{q\, p_1(\xi,t)\, X_0(\xi)} \tag{4.22}$$

$$d_{cb}(\xi,t) = \frac{\varepsilon_0 \varepsilon_s E_{cb}(\xi,t)}{q\, p_1(\xi,t)\, X_0(\xi)} \tag{4.23}$$

which can be termed, respectively, a dynamic channel-to-gate coupling factor and a dynamic channel-to-body coupling factor. These factors tell us what fractions of the surface excess charge density, $q{\cdot}p_1(\xi, t) \cdot X_0(\xi)$, produce, respectively, the channel-to-gate and channel-to-body electric field components.

In this approximation of Poisson's equation, the following inequalities hold:

$$0 \le d_l(\xi,t) \le 1 \tag{4.24}$$

$$0 \le d_{cg}(\xi,t) + d_{cb}(\xi,t) \le 1 \tag{4.25}$$

In the model presented here, we assume that these dynamic coupling factors are positive constants, denoted by d_l, d_{cg}, and d_{cb}. Thus, (4.19) takes the form as follows:

$$\frac{\partial E_1(\xi,t)}{\partial \xi} = \frac{q\, d_l\, p_1(\xi,t)}{\varepsilon_0 \varepsilon_s} \tag{4.26}$$

where

$$d_l = 1 - d_{cg} - d_{cb} \tag{4.27}$$

Furthermore, we can apply the non-quasi-static channel charge partition rule (NQSCCPR) established in Sec. 3.8 to find a relationship between the coupling factors d_{cg} and d_{cb}. Namely, dividing (4.23) by (4.22), we get:

$$\frac{d_{cb}}{d_{cg}} = \frac{\varepsilon_0 \varepsilon_s E_{cb}(\xi,t)}{\varepsilon_0 \varepsilon_s E_{cg}(\xi,t)} \tag{4.28}$$

On the other hand, from (3.141), we have:

$$\frac{Q_{cb}(\xi,t)}{Q_{cg}(\xi,t)} = \frac{g_{mb}}{g_m} \tag{4.29}$$

where $Q_{cb}(\xi, t)$ and $Q_{cg}(\xi, t)$ are excess (small-signal) channel charges per unit area associated with the channel-to-body and channel-to-gate couplings, respectively.

In accordance with Fig. 4.5, the charges $Q_{cb}(\xi, t)$ and $Q_{cg}(\xi, t)$ are determined by the following:

$$Q_{cb}(\xi,t) = \varepsilon_0 \varepsilon_s E_{cb}(\xi,t) \tag{4.30}$$

$$Q_{cg}(\xi,t) = \varepsilon_0 \varepsilon_s E_{cg}(\xi,t) \tag{4.31}$$

Thus, combining (4.28)–(4.31), we obtain:

$$\frac{d_{cb}}{d_{cg}} = \frac{g_{mb}}{g_m} \tag{4.32}$$

4.3. Quasi-2D frequency-domain analysis

In this and the next sections, the symbols for small-signal quantities have the meaning of phasors unless otherwise stated.

4.3.1. Frequency-domain equations

A set of partial differential equations consisting of (4.3), (4.18), (4.26), (4.4) and (4.6) defines the model in the time domain. Transforming the equations into the frequency domain, we obtain, respectively:

$$\frac{dJ_1(\xi, j\omega)}{d\xi} = -q(1+D_C)j\omega\, p_1(\xi, j\omega) \tag{4.33}$$

$$J_1(\xi, j\omega) = q\mu_q \left[E_0\, p_1(\xi, j\omega) - V_t \frac{dp_1(\xi, j\omega)}{d\xi} \right] + \frac{g_{dso}\, L}{W X_{ch}} E_1(\xi, j\omega) \tag{4.34}$$

$$\frac{dE_1(\xi, j\omega)}{d\xi} = \frac{q\, d_l\, p_1(\xi, j\omega)}{\varepsilon_0 \varepsilon_s} \tag{4.35}$$

$$J_{t1}(\xi, j\omega) = J_1(\xi, j\omega) + J_{dis\,1}(\xi, j\omega) \tag{4.36}$$

$$J_{dis\,1}(\xi, j\omega) = j\omega \varepsilon_0 \varepsilon_s E_1(\xi, j\omega) \tag{4.37}$$

where j is the imaginary unit ($j \cdot j = -1$), and ω is the angular frequency (in rad/s). The small-signal displacement current density $J_{dis1}(\xi, j\omega)$ is discussed in detail in Sec. 4.4.1.

As a result, we have a system of linear ordinary differential equations for quantities of the model in the time-independent phasor notation.

4.3.2. Solution for $p_1(\xi, j\omega)$

Differentiating (4.34) with respect to ξ, taking account of (4.35), and then putting the resultant equation into (4.33), we obtain:

$$0 = \frac{d^2 p_1(\xi, j\omega)}{d\xi^2} - \frac{E_0}{V_t}\frac{dp_1(\xi, j\omega)}{d\xi} - \left[\frac{d_l g_{dso} L}{\mu_q V_t W X_{ch} \varepsilon_0 \varepsilon_s} + \frac{j\omega(1+D_C)}{\mu_q V_t}\right] p_1(\xi, j\omega) \quad (4.38)$$

The solutions to (4.38) are given in Appendix D. We write them in the form as follows:

$$p_1(\xi, j\omega) = K \exp(\gamma\xi) \quad (4.39)$$

$$p_1^*(\xi, j\omega) = K^* \exp(\gamma^*\xi) \quad (4.40)$$

$$\gamma = \alpha - j\beta \quad (4.41)$$

$$\gamma^* = \alpha^* + j\beta \quad (4.42)$$

where α and α^* are real parts, respectively, of γ and γ^* [refer to (A.43), (A.45), and (A.46)],

$$\alpha = \frac{E_0}{2V_t} - \frac{\sqrt{2}}{4}\sqrt{a + \sqrt{a^2 + b^2}} \quad (4.43)$$

$$\alpha^* = \frac{E_0}{2V_t} + \frac{\sqrt{2}}{4}\sqrt{a + \sqrt{a^2 + b^2}} \quad (4.44)$$

whereas β is defined as fallows [refer to (A.45) and (A.46)]:

$$\beta = \frac{\sqrt{2}}{4}\sqrt{-a + \sqrt{a^2 + b^2}} \quad (4.45)$$

Rewriting (A.47), we complete a description of the quantities a and b occurring in (4.43)–(4.45):

$$a = \frac{E_0^2}{V_t^2} + \frac{4 d_l g_{dso} L}{\mu_q V_t W X_{ch} \varepsilon_0 \varepsilon_s} \quad (4.46)$$

$$b = \frac{4\omega(1+D_C)}{\mu_q V_t} \quad (4.47)$$

Note that β in (4.45) is an increasing function of the angular frequency ω, and $\beta = 0$ if $\omega = 0$.

4.3.3. Wave phenomena in the channel

Using (4.41) and (4.42), we can write (4.39) and (4.40) in the time-dependent phasor notation as follows:

$$p_1(\xi, j\omega t) = K \exp(\alpha\xi) \exp\left[j(\omega t - \beta\xi)\right] \tag{4.48}$$

$$p_1^*(\xi, j\omega t) = K^* \exp(\alpha^* \xi) \exp\left[j(\omega t + \beta\xi)\right] \tag{4.49}$$

Equation (4.48) represents a longitudinal wave of a disturbance in the hole density traveling in the positive ξ-direction, see Fig. 4.2, whereas (4.49) represents a similar wave but traveling in the negative ξ-direction.

Since carriers in the channel of the MOSFET move only from the source to the drain (in the positive direction of ξ-coordinate in Fig. 4.2), the wave $p_1^*(\xi, j\omega t)$, described by (4.49), is ignored in the analysis.

As seen from (4.48), the wave $p_1(\xi, j\omega t)$ is an exponentially damped ($\alpha < 0$ for all ω) sinusoidal one that travels with a phase velocity υ_{ph} in the positive ξ-direction,

$$\upsilon_{ph} = \frac{\omega}{\beta} \tag{4.50}$$

Denoted by λ, the wavelength of $p_1(\xi, j\omega t)$ is:

$$\lambda = \frac{2\pi}{\beta} \tag{4.51}$$

According to Sec. 3.3, small perturbations in carrier density cause small variations in the channel thickness. This means that a transverse wave of a disturbance in the channel thickness $X_1(\xi, j\omega t)$ is associated with the wave $p_1(\xi, j\omega t)$.

Assuming that the dynamic coupling factor of the channel D_C is a positive real number and transforming (3.21) into the frequency domain, we have:

$$X_1(\xi, j\omega t) = \frac{D_C X_0(\xi)}{p_0(\xi)} p_1(\xi, j\omega t) \tag{4.52}$$

or, using (4.48), we can explicitly write:

$$X_1(\xi, j\omega t) = \frac{K D_C X_0(\xi)}{p_0(\xi)} \exp(\alpha\xi) \exp\left[j(\omega t - \beta\xi)\right] \tag{4.53}$$

As seen from (4.48) and (4.53), these waves are in phase if the product $K{\cdot}D_C$ is a positive real number. The waves $X_1(\xi, j\omega t)$ and $p_1(\xi, j\omega t)$ are illustrated in Fig. 4.2.

A comprehensive analysis of the wave phenomena in the MOSFET channel is beyond the scope of this work.

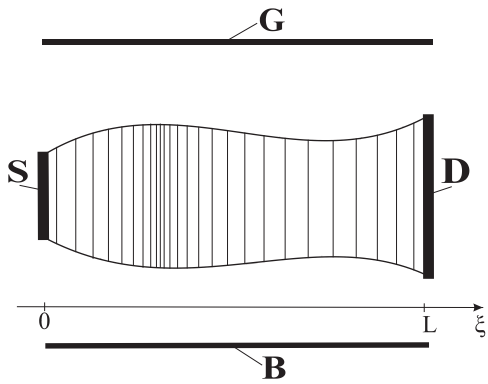

Fig. 4.2. A scheme illustrating waves in the MOSFET channel for the case in which the product $K{\cdot}D_C$ is a positive real number.

4.3.4. The electric field $E_1(\xi, j\omega)$

By solving (4.35), we find the longitudinal small-signal electric field in the channel. Details of the solution are given in Appendix E.

According to (A.50) and (A.52), we have:

$$E_1(\xi, j\omega) = E_1(0, j\omega) + \frac{q\, d_l\, K\left[\exp(\gamma\xi) - 1\right]}{\varepsilon_0 \varepsilon_s \gamma} \tag{4.54}$$

where

$$E_1(0, j\omega) = -\frac{\upsilon_{ds}}{L} - \frac{q\, d_l\, K\left[\exp(\gamma L) - \gamma L - 1\right]}{\varepsilon_0 \varepsilon_s \gamma^2 L} \tag{4.55}$$

4.4. DIBL-included model

To derive the DIBL-included model, we separately analyze non-capacitive currents and then, by virtue of the principle of superposition, add the capacitive terminal currents, which is described in Sec. 3.6. In other words, we first develop a four-terminal equivalent circuit for the non-capacitive currents, and then include the six reciprocal capacitances described in Sec. 3.6.1.

4.4.1. Non-capacitive terminal currents

In order to develop an equivalent circuit of the transistor for non-capacitive small-signal currents, we first calculate the non-capacitive terminal currents as a response to a small-signal control voltage that is turned on in three different configurations. Then, using the principle of superposition, we add the results obtained for each of the three configurations, thus obtaining the equivalent circuit for the non-capacitive terminal currents.

The drain and source non-capacitive currents, generally

Referring to Sec. 3.6.2 and transforming (3.86)–(3.87) into the frequency domain, we obtain the following formulas for phasors of the total drain- and source-terminal non-capacitive currents i_d^{nc} and i_s^{nc}, respectively:

$$i_d^{nc} = i_d^{con} + i_{ddis}^{nc} \tag{4.56}$$

$$i_s^{nc} = i_s^{con} + i_{sdis}^{nc} \tag{4.57}$$

where i_d^{con} and i_s^{con} are phasors of the drain- and source-terminal conduction currents, respectively, whereas i_{ddis}^{nc} and i_{sdis}^{nc} represent phasors of the drain- and source-terminal non-capacitive displacement currents, respectively.

Ignoring variations in the thickness of the channel at the drain and source ends, transforming (3.88)–(3.89) into the frequency domain, and finally taking account of (4.1), we obtain:

$$i_d^{con} = - W S X_S J_1(L, j\omega) \tag{4.58}$$

$$i_s^{con} = W X_S J_1(0, j\omega) \tag{4.59}$$

The currents i_d^{con} and i_s^{con} are different for $\omega > 0$ due to the wave phenomena in the channel; see Sec. 4.3.3. They are equal only for $\omega = 0$.

To improve the accuracy of the analysis, we transform (4.15) into the frequency domain and use the resultant equation in the further analysis. [One can see that (4.15) is more accurate than (4.18).] Hence, we have a more adequate expression to calculate the frequency-domain small-signal conduction current density:

$$J_1(\xi, j\omega) = q \mu_q \left[E_0 \; p_1(\xi, j\omega) - V_t \frac{\partial p_1(\xi, j\omega)}{\partial \xi} \right] + \frac{g_{dso} L}{W X_0(\xi)} E_1(\xi, j\omega) \tag{4.60}$$

Transforming (3.90) into frequency domain and combining (4.54) and (4.55), we get a formula for the electric field $E_1(\xi, j\omega)$ acting on carriers in the channel:

$$E_1(\xi, j\omega) = E_{1ext}(\xi, j\omega) + E_{1i}(\xi, j\omega) \tag{4.61}$$

in which $E_{1ext}(\xi, j\omega)$ is an external field set up by v_{ds},

$$E_{1ext}(\xi, j\omega) = -\frac{v_{ds}}{L} \tag{4.62}$$

and $E_{1i}(\xi, j\omega)$ is an inner field set up by the small-signal excess charges $[p_1(\xi, j\omega) = K \cdot \exp(\gamma\xi)]$,

$$E_{1i}(\xi, j\omega) = \frac{q d_l K \left[\gamma L \exp(\gamma\xi) - \exp(\gamma L) + 1 \right]}{\varepsilon_0 \varepsilon_s \gamma^2 L} \tag{4.63}$$

Substituting (4.39) into (4.60) and taking account of (4.61)–(4.63), we obtain:

$$J_1(\xi, j\omega) = -\frac{g_{dso}\,\upsilon_{ds}}{W\,X_0(\xi)} + q\,K\,\mu_q\,(E_0 - \gamma V_t)\exp(\gamma\xi) + \frac{qK\,d_l\,g_{dso}\left[\gamma L\exp(\gamma\xi) - \exp(\gamma L) + 1\right]}{\varepsilon_0\,\varepsilon_s\,\gamma^2\,W\,X_0(\xi)} \tag{4.64}$$

Setting $\xi = L$ in (4.64) and taking (4.1) into account, we obtain the small-signal conduction current density at the drain end of the channel:

$$J_1(L, j\omega) = -\frac{g_{dso}\,\upsilon_{ds}}{W\,S\,X_S} + q\,K\,\mu_q\,(E_0 - \gamma V_t)\exp(\gamma L) + \frac{qK\,d_l\,g_{dso}\left[\gamma L\exp(\gamma L) - \exp(\gamma L) + 1\right]}{\varepsilon_0\,\varepsilon_s\,\gamma^2\,W\,S\,X_S} \tag{4.65}$$

Similarly, setting $\xi = 0$ in (4.64) and taking (4.1) into account, we obtain the small-signal conduction current density at the source end of the channel:

$$J_1(0, j\omega) = -\frac{g_{dso}\,\upsilon_{ds}}{W\,X_S} + q\,K\,\mu_q\,(E_0 - \gamma V_t) + \frac{qK\,d_l\,g_{dso}\left[\gamma L - \exp(\gamma L) + 1\right]}{\varepsilon_0\,\varepsilon_s\,\gamma^2\,W\,X_S} \tag{4.66}$$

Given (4.37) and (4.61), we have:

$$J_{dis\,1}(\xi, j\omega) = j\omega\,\varepsilon_0\,\varepsilon_s\,E_{1ext}(\xi, j\omega) + j\omega\,\varepsilon_0\,\varepsilon_s\,E_{1i}(\xi, j\omega) \tag{4.67}$$

The first term on the right-hand side of (4.67), denoted by

$$J_{dis}^{cap}(\xi, j\omega) = j\omega\,\varepsilon_0\,\varepsilon_s\,E_{1ext}(\xi, j\omega) \tag{4.68}$$

represents a capacitive displacement current density induced by the external field $[E_{1ext}(\xi, j\omega) = -\upsilon_{ds}/L]$. It is simply a capacitive current density that is associated with the capacitance C_{ds}; see Fig. 4.10 and Sec. 3.6. The current density $J_{dis}^{cap}(\xi, j\omega)$ produces a capacitive current flowing through the capacitance C_{ds}. The capacitive current is separately taken into account in the model; see Fig. 4.10.

The second term on the right-hand side of (4.67), denoted by

$$J_{dis}^{nc}(\xi, j\omega) = j\omega\,\varepsilon_0\,\varepsilon_s\,E_{1i}(\xi, j\omega) \tag{4.69}$$

is a frequency-domain non-capacitive displacement current density in the channel.

Taking account of (4.63), one can rewrite (4.69) as follows:

$$J_{dis}^{nc}(\xi, j\omega) = \frac{j\omega q\,d_l\,K}{\gamma^2 L}\left[\gamma L\exp(\xi L) - \exp(\gamma L) + 1\right] \tag{4.70}$$

Setting $\xi = L$ in (4.70), we obtain the frequency-domain non-capacitive displacement current density at the drain end of the channel:

$$J_{dis}^{nc}(L, j\omega) = \frac{j\omega q d_l K}{\gamma^2 L}\left[\gamma L \exp(\gamma L) - \exp(\gamma L) + 1\right] \tag{4.71}$$

Similarly, setting $\xi = 0$ in (4.70), we obtain the frequency-domain non-capacitive displacement current density at the source end of the channel:

$$J_{dis}^{nc}(0, j\omega) = \frac{j\omega q d_l K\left[\gamma L - \exp(\gamma L) + 1\right]}{\gamma^2 L} \tag{4.72}$$

As in the case of the time-domain small-signal model presented in Sec. 3.6.2, we assume that the longitudinal electric field $E_{1i}(\xi, j\omega)$, set up by the small-signal excess charges $p_1(\xi, j\omega)$, is associated with an equivalent parallel-plate capacitor whose capacitance equals C_{ds} and the parallel plates are separated by a distance L (L is the channel length). Thus, denoted by A_{cds}, an effective area of each of the two plates is:

$$A_{cds} = \frac{L C_{ds}}{\varepsilon_0 \varepsilon_s} \tag{4.73}$$

Therefore, based on (4.71) and (4.73), the drain-terminal frequency-domain non-capacitive displacement current i_{ddis}^{nc} is:

$$i_{ddis}^{nc} = -\frac{j\omega q d_l K C_{ds}\left[\gamma L \exp(\gamma L) - \exp(\gamma L) + 1\right]}{\varepsilon_0 \varepsilon_s \gamma^2} \tag{4.74}$$

Based on (4.72) and (4.73), the source-terminal frequency-domain non-capacitive displacement current i_{sdis}^{nc} is:

$$i_{sdis}^{nc} = \frac{j\omega q d_l K C_{ds}\left[\gamma L - \exp(\gamma L) + 1\right]}{\varepsilon_0 \varepsilon_s \gamma^2} \tag{4.75}$$

Given (4.56), (4.58), (4.65) and (4.74), we have the following formula for the total drain-terminal frequency-domain non-capacitive current i_d^{nc}:

$$i_d^{nc} = -qK W S X_S F_D \exp(\gamma L) + g_{dso} \upsilon_{ds} \tag{4.76}$$

in which

$$F_D = \mu_q\left(E_0 - \gamma V_t\right) + \frac{d_l[\exp(-\gamma L) + \gamma L - 1]}{\varepsilon_0 \varepsilon_s \gamma^2 W S X_S}\left(g_{dso} + j\omega C_{ds}\right) \tag{4.77}$$

Similarly, given (4.57), (4.59), (4.66) and (4.75), we have the following formula for the total source-terminal frequency-domain non-capacitive current i_s^{nc}:

$$i_s^{nc} = qK\,W\,X_S\,F_S - g_{dso}\,\upsilon_{ds} \tag{4.78}$$

where

$$F_S = \mu_q\left(E_0 - \gamma V_t\right) + \frac{d_l\left[1+\gamma L - \exp\left(\gamma L\right)\right]}{\varepsilon_0\,\varepsilon_s\,\gamma^2\,W\,X_S}\left(g_{dso} + j\omega C_{ds}\right) \tag{4.79}$$

υ_{gs}-configuration: $\upsilon_{gs} \neq 0$ and $\upsilon_{ds} = \upsilon_{bs} = 0$

This way of controlling the transistor is illustrated in Fig. 4.3. Under these conditions, excess carriers are injected from the source into the channel, and their rate of injection depends on the voltage υ_{gs}, quasi-static gate transconductance g_m, and angular frequency ω.

Let i_{d-QS}^{nc-g} stand for the quasi-static drain-terminal frequency-domain non-capacitive current of the transistor operating in the circumstances shown in Fig. 4.3, i.e., $\upsilon_{gs} \neq 0$, $\upsilon_{ds} = \upsilon_{bs} = 0$, and $\omega \to 0$.

Based on the definition of the quasi-static gate transconductance g_m, we obtain the following boundary condition, valid only for quasi-static operation of the transistor:

$$i_{d-QS}^{nc-g} = g_m\,\upsilon_{gs} \tag{4.80}$$

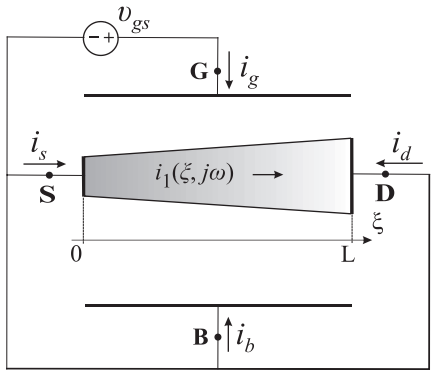

Fig. 4.3. An MOSFET excited only by the voltage υ_{gs}—the transistor works in the υ_{gs}-configuration.

Equation (4.80) allows us to determine the constant K of (4.39), which in this case is denoted by K_{gL}. Therefore, setting $\omega = 0$, $\upsilon_{ds} = 0$, and $K \equiv K_{gL}$ in (4.76) and (4.77), taking definition of γ into account (see Sec. 4.3.2), and finally solving (4.80) for K_{gL}, we get (omitting a lengthy algebra):

$$K_{gL} = \frac{-g_m\,\upsilon_{gs}\exp\left(-\gamma_0 L\right)}{qWSX_S F_{D0}} \tag{4.81}$$

where

$$\gamma_0 = \frac{1}{2}\left(\frac{E_0}{V_t} - \sqrt{a}\right) \tag{4.82}$$

$$F_{D0} = \mu_q \left(E_0 - \gamma_0 V_t\right) + \frac{d_l\, g_{dso}\left[\exp\left(-\gamma_0 L\right) + \gamma_0 L - 1\right]}{\varepsilon_0 \varepsilon_s\, \gamma_0^{\,2}\, W S X_S} \tag{4.83}$$

Substituting K by K_{gL} and setting $\upsilon_{ds} = 0$ in (4.76), we obtain a formula for the drain-terminal frequency-domain non-capacitive small-signal current of the transistor operating in the υ_{gs}-configuration, denoted by $i_d^{\,ncg}$:

$$i_d^{\,nc-g} = g_m\, \upsilon_{gs}\, \frac{F_D}{F_{D0}} \exp\left[\left(\gamma - \gamma_0\right) L\right] \tag{4.84}$$

The source-terminal frequency-domain non-capacitive small-signal current of the transistor operating in the υ_{gs}-configuration, denoted by $i_s^{\,ncg}$, is found in a similar way as the one presented above for $i_d^{\,ncg}$.

Let $i_{s-QS}^{\,nc-g}$ denote the quasi-static source-terminal frequency-domain non-capacitive current of the transistor operating in the circumstances shown in Fig. 4.3, i.e., $\upsilon_{gs} \neq 0$, $\upsilon_{ds} = \upsilon_{bs} = 0$, and $\omega \to 0$.

Based on the definition of the quasi-static gate transconductance g_m, we get the following boundary condition:

$$i_{s-QS}^{\,nc-g} = -g_m\, \upsilon_{gs} \tag{4.85}$$

Equation (4.85) allows us to determine the constant K of (4.39), which in this case is denoted by K_{g0}. Namely, setting $\omega = 0$, $\upsilon_{ds} = 0$, and $K \equiv K_{g0}$ in (4.78) and (4.79), taking definition of γ into account (see Sec. 4.3.2), and finally solving (4.85) for K_{g0}, we get (omitting a lengthy algebra):

$$K_{g0} = \frac{-g_m\, \upsilon_{gs}}{q W X_S F_{S0}} \tag{4.86}$$

where

$$F_{S0} = \mu_q \left(E_0 - \gamma_0 V_t\right) + \frac{d_l\, g_{dso}\left[1 + \gamma_0 L - \exp\left(\gamma_0 L\right)\right]}{\varepsilon_0 \varepsilon_s\, \gamma_0^{\,2}\, W X_S} \tag{4.87}$$

and γ_0 is defined by (4.82).

Substituting K by K_{g0} and setting $\upsilon_{ds} = 0$ in (4.78), we obtain a formula for the source-terminal frequency-domain non-capacitive small-signal current of the transistor operating in the υ_{gs}-configuration:

$$i_s^{nc-g} = - g_m \upsilon_{gs} \frac{F_S}{F_{S0}} \tag{4.88}$$

Coupling currents induced on the gate and in the body—denoted for the υ_{gs}-configuration, respectively, by i_g^{ind-g} and i_b^{ind-g}—are calculated from Kirchhoff's current law for non-capacitive currents [see (3.85)]:

$$i_g^{ind-g} + i_d^{nc-g} + i_b^{ind-g} + i_s^{nc-g} = 0 \tag{4.89}$$

and from the non-quasi-static channel charge partition rule (NQSCCPR) established in Sec. 3.8, whose mathematical form [see (3.146)] is:

$$\frac{i_b^{ind-g}}{i_g^{ind-g}} = \eta \tag{4.90}$$

where η is defined as follows:

$$\eta = \frac{g_{mb}}{g_m} \tag{4.91}$$

Taking (4.84) and (4.88) into account and solving (4.89) and (4.90) with respect to i_g^{ind-g} and i_b^{ind-g}, we have:

$$i_g^{ind-g} = \frac{g_m \upsilon_{gs}}{1+\eta} \left[\frac{F_S}{F_{S0}} - \frac{F_D}{F_{D0}} \exp\left[(\gamma - \gamma_0) L\right] \right] \tag{4.92}$$

$$i_b^{ind-g} = \frac{\eta g_m \upsilon_{gs}}{1+\eta} \left[\frac{F_S}{F_{S0}} - \frac{F_D}{F_{D0}} \exp\left[(\gamma - \gamma_0) L\right] \right] \tag{4.93}$$

A four-terminal equivalent circuit for the non-capacitive currents of the transistor working in the υ_{gs}-configuration ($\upsilon_{gs} \neq 0$ and $\upsilon_{ds} = \upsilon_{bs} = 0$) is given in Fig. 4.4.

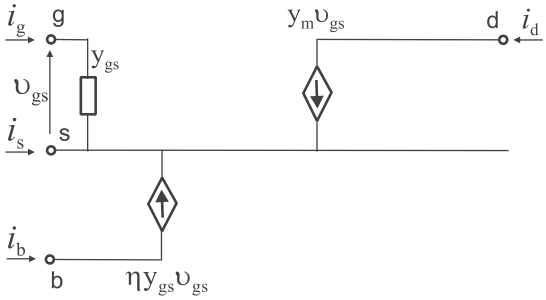

Fig. 4.4. A four-terminal equivalent circuit for the transistor working in the υ_{gs}-configuration ($\upsilon_{gs} \neq 0$ and $\upsilon_{ds} = \upsilon_{bs} = 0$).

We can infer from (4.84) that the transadmittance y_m of Fig. 4.4 is defined by

$$y_m = g_m \frac{F_D}{F_{D0}} \exp\left[(\gamma - \gamma_0) L\right] \tag{4.94}$$

Taking account of (4.92), we can define the admittance y_{gs} connected between the gate and source in Fig. 4.4, viz.:

$$y_{gs} = \frac{g_m}{1+\eta}\left[\frac{F_S}{F_{S0}} - \frac{F_D}{F_{D0}} \exp\left[(\gamma - \gamma_0) L\right]\right] \tag{4.95}$$

A voltage-controlled current source connected between the body and the source in Fig. 4.4 represents the coupling current $i_b^{ind\text{-}g}$ determined by (4.93). The value of the source current $(\eta y_{gs} \cdot v_{gs})$ results from taking account of (4.95) in (4.93).

v_{bs}-configuration: $v_{bs} \neq 0$ and $v_{ds} = v_{gs} = 0$

In this configuration, the transistor is excited only by the small voltage v_{bs}; see Fig. 4.5.

We find non-capacitive currents of the transistor in a similar way as the one presented above for the v_{gs}-configuration.

In this configuration, excess carriers are injected from the source into the channel, and their rate of injection depends on the voltage v_{bs}, quasi-static body transconductance g_{mb}, and angular frequency ω.

Let i_{d-QS}^{nc-b} stand for the quasi-static drain-terminal frequency-domain non-capacitive current of the transistor operating in the circumstances shown in Fig. 4.5, i.e., $v_{bs} \neq 0$, $v_{ds} = v_{gs} = 0$, and $\omega \to 0$.

Based on the definition of the quasi-static body transconductance g_{mb}, we get the following boundary condition valid only at quasi-static operation of the transistor:

$$i_{d-QS}^{nc-b} = g_m \, v_{bs} \tag{4.96}$$

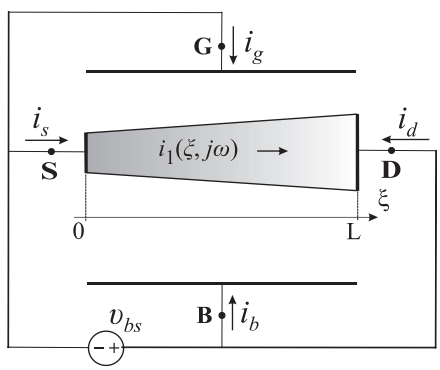

Fig. 4.5. An MOSFET excited only by the voltage v_{bs}—the transistor works in the v_{bs}-configuration.

Equation (4.96) allows us to determine the constant K of (4.39), which in this case is denoted by K_{bL}. Accordingly, setting $\omega = 0$, $\upsilon_{ds} = 0$, and $K \equiv K_{bL}$ in (4.76) and (4.77), taking definition of γ into account (see Sec. 4.3.2), and finally solving (4.96) for K_{bL}, we get (omitting a lengthy algebra):

$$K_{bL} = \frac{-g_{mb}\,\upsilon_{bs}\exp(-\gamma_0 L)}{qWSX_S F_{D0}} \tag{4.97}$$

where γ_0 is defined by (4.82), and F_{D0} by (4.83).

Substituting K by K_{bL} and setting $\upsilon_{ds} = 0$ in (4.76), we obtain a formula for the drain-terminal frequency-domain non-capacitive small-signal current of the transistor operating in the υ_{bs}-configuration, denoted by $i_d^{\,ncb}$,

$$i_d^{\,nc-b} = g_{mb}\,\upsilon_{bs}\,\frac{F_D}{F_{D0}}\exp\left[(\gamma-\gamma_0)L\right] \tag{4.98}$$

The source-terminal frequency-domain non-capacitive small-signal current of the transistor operating in the υ_{bs}-configuration, denoted by $i_s^{\,ncb}$, is found in a similar way as the one presented above for $i_d^{\,ncb}$.

Let $i_{s-QS}^{\,nc-b}$ denote the quasi-static source-terminal frequency-domain non-capacitive current of the transistor operating in the circumstances shown in Fig. 4.5, i.e., $\upsilon_{bs} \neq 0$, $\upsilon_{ds} = \upsilon_{gs} = 0$, and $\omega \to 0$.

Based on the definition of the quasi-static body transconductance g_{mb}, we get the following boundary condition:

$$i_{s-QS}^{\,nc-b} = -\,g_{mb}\,\upsilon_{bs} \tag{4.99}$$

Equation (4.99) enables us to determine a constant K of (4.39), which in this case is denoted by K_{b0}. Consequently, setting $\omega = 0$, $\upsilon_{ds} = 0$, and $K \equiv K_{b0}$ in (4.78) and (4.79), taking the definition of γ into account (see Sec. 4.3.2), and finally solving (4.99) for K_{b0}, we get (omitting a lengthy algebra):

$$K_{b0} = \frac{-g_{mb}\,\upsilon_{bs}}{qWX_S F_{S0}} \tag{4.100}$$

where F_{S0} is defined by (4.87).

Substituting K_{b0} for K and setting $\upsilon_{ds} = 0$ in (4.78), we obtain a formula for the source-terminal frequency-domain non-capacitive small-signal current of the transistor operating in the υ_{bs}-configuration:

$$i_s^{\,nc-b} = -\,g_{mb}\,\upsilon_{bs}\,\frac{F_S}{F_{S0}} \tag{4.101}$$

Coupling currents induced on the gate and in the body—denoted for the υ_{bs}-configuration, respectively, by $i_g^{\,ind-b}$ and $i_b^{\,ind-b}$—are calculated from Kirchhoff's current law for non-capacitive currents [see (3.85)],

$$i_g^{\,ind-b} + i_d^{\,nc-b} + i_b^{\,ind-b} + i_s^{\,nc-b} = 0 \tag{4.102}$$

and from the non-quasi-static channel charge partition rule (NQSCCPR) established in Sec. 3.8, whose mathematical form [see (3.146)] is:

$$\frac{i_b^{\,ind-b}}{i_g^{\,ind-b}} = \eta \tag{4.103}$$

where η is defined by (4.91).

Taking (4.98) and (4.101) into account and solving (4.102) and (4.103) with respect to $i_g^{\,ind-b}$ and $i_b^{\,ind-b}$, we have:

$$i_g^{\,ind-b} = \frac{g_{mb}\,\upsilon_{bs}}{1+\eta}\left[\frac{F_S}{F_{S0}} - \frac{F_D}{F_{D0}}\exp\left[(\gamma-\gamma_0)L\right]\right] \tag{4.104}$$

$$i_b^{\,ind-b} = \frac{\eta\, g_{mb}\,\upsilon_{bs}}{1+\eta}\left[\frac{F_S}{F_{S0}} - \frac{F_D}{F_{D0}}\exp\left[(\gamma-\gamma_0)L\right]\right] \tag{4.105}$$

A four-terminal equivalent circuit for the non-capacitive currents of the transistor working in the υ_{bs}-configuration ($\upsilon_{bs} \neq 0$ and $\upsilon_{ds} = \upsilon_{gs} = 0$) is given in Fig. 4.6.

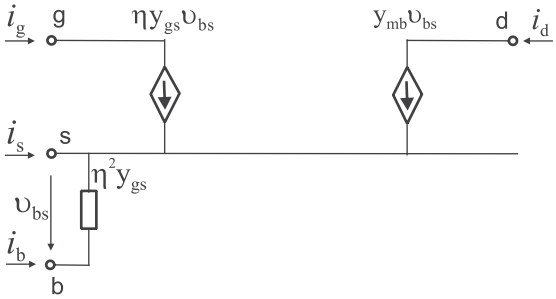

Fig. 4.6. A four-terminal equivalent circuit for the transistor working in the υ_{bs}-configuration ($\upsilon_{bs} \neq 0$ and $\upsilon_{ds} = \upsilon_{gs} = 0$).

Setting $g_{mb} = \eta \cdot g_m$ in (4.98) and taking (4.94) into account, one can obtain the following formula for the body transadmittance y_{mb} of Fig. 4.6:

$$y_{mb} = \eta\, y_m \tag{4.106}$$

A voltage-controlled current source connected between the gate and the source in Fig. 4.6 represents the coupling current $i_g^{\,ind-b}$ determined by (4.104). The value of the source current ($\eta y_{gs} \cdot \upsilon_{bs}$) results from noting that $g_{mb} = \eta \cdot g_m$ and taking account of (4.95) in (4.104).

Denoted by y_{bs}, the admittance connected between the body and the source in Fig. 4.6 results from the coupling current $i_b^{ind\text{-}b}$ determined by (4.105). Its value ($\eta^2 \cdot y_{gs}$) is obtained by setting $g_{mb} = \eta \cdot g_m$ in (4.105) and taking (4.95) into account. Hence,

$$y_{bs} = \eta^2 \, y_{gs} \tag{4.107}$$

v_{ds}-configuration: $v_{ds} \neq 0$ and $v_{gs} = v_{bs} = 0$

In this configuration, the transistor is excited only by the small voltage v_{ds}; see Fig. 4.7.

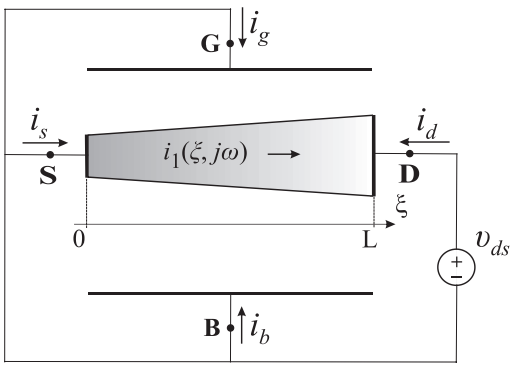

Fig. 4.7. An MOSFET excited only by the voltage v_{ds}—the transistor works in the v_{ds}-configuration.

Due to the DIBL effect, excess carriers are injected from the source into the channel, and their rate of injection depends on the voltage v_{ds}, quasi-static drain-to-source conductance g_{ds}, and angular frequency ω.

As shown in Appendix C, the quasi-static conductance g_{ds} splits into two parts [see (A.42)]:

$$g_{ds} = g_{dso} + g_{dsD} \tag{4.108}$$

where g_{dso} and g_{dsD} are, respectively, an ohmic part and DIBL part of g_{ds}.

Equation (4.108) can be written in a more convenient form, i.e.:

$$g_{ds} = g_{dso} + k_D \, g_{ds} \tag{4.109}$$

where k_D is a dimensionless factor defined as follows:

$$k_D = \frac{g_{dsD}}{g_{ds}}, \qquad (0 \leq k_D < 1) \tag{4.110}$$

Let i_{d-QS}^{nc-d} stand for the quasi-static drain-terminal frequency-domain non-capacitive current of the transistor operating in the circumstances shown in Fig. 4.7, i.e., $v_{ds} \neq 0$, $v_{gs} = v_{bs} = 0$, and $\omega \to 0$.

Based on the definition of the quasi-static conductance g_{ds} and taking account of (4.109), we get the following boundary condition, valid only at quasi-static operation of the transistor:

$$i_{d-QS}^{nc-d} = g_{dso}\,\upsilon_{ds} + k_D\,g_{ds}\,\upsilon_{ds} \tag{4.111}$$

Equation (4.111) allows us to determine the constant K of (4.39), which in this case is denoted by K_{dL}. Thus, setting $\omega = 0$ and $K \equiv K_{dL}$ in (4.76) and (4.77), taking definition of γ into account (see Sec. 4.3.2), and finally solving (4.111) for K_{dL}, we get (omitting a lengthy algebra):

$$K_{dL} = \frac{-k_D\,g_{ds}\,\upsilon_{ds}\exp(-\gamma_0 L)}{qWSX_S F_{D0}} \tag{4.112}$$

where γ_0 is defined by (4.82), and F_{D0} by (4.83).

Substituting K by K_{dL} in (4.76) and taking account of (4.109), we obtain a formula for the drain-terminal frequency-domain non-capacitive small-signal current of the transistor operating in the υ_{ds}-configuration, denoted by i_d^{ncd},

$$i_d^{nc-d} = g_{ds}\,\upsilon_{ds} + k_D\,g_{ds}\,\upsilon_{ds}\left\{\frac{F_D}{F_{D0}}\exp\left[(\gamma-\gamma_0)L\right]-1\right\} \tag{4.113}$$

The source-terminal frequency-domain non-capacitive small-signal current of the transistor operating in the υ_{ds}-configuration, denoted by i_s^{ncd}, is found in a similar way as the one presented above for i_d^{ncd}:

Let i_{s-QS}^{nc-d} denote the quasi-static source-terminal frequency-domain non-capacitive current of the transistor operating in the circumstances shown in Fig. 4.7, i.e., $\upsilon_{ds} \neq 0$, $\upsilon_{gs} = \upsilon_{bs} = 0$, and $\omega \to 0$.

Based on the definition of the quasi-static conductance g_{ds}, we get the following boundary condition:

$$i_{s-QS}^{nc-d} = -g_{dso}\,\upsilon_{ds} - k_D\,g_{ds}\,\upsilon_{ds} \tag{4.114}$$

Equation (4.114) allows us to determine the constant K of (4.39), which in this case is denoted by K_{d0}. Consequently, setting $\omega = 0$ and $K \equiv K_{d0}$ in (4.78) and (4.79), taking definition of γ into account (see Sec. 4.3.2), and finally solving (4.114) for K_{d0}, we get (omitting a lengthy algebra):

$$K_{d0} = \frac{-k_D\,g_{ds}\,\upsilon_{ds}}{qWX_S F_{S0}} \tag{4.115}$$

where F_{S0} is defined by (3.87).

Substituting K by K_{d0} in (4.78) and taking account of (4.109), we obtain a formula for the source-terminal frequency-domain non-capacitive small-signal current of the transistor operating in the υ_{ds}-configuration:

$$i_s^{nc-d} = -g_{ds}\upsilon_{ds} - k_D\, g_{ds}\,\upsilon_{ds}\left[\frac{F_S}{F_{S0}} - 1\right] \tag{4.116}$$

Coupling currents induced on the gate and in the body—denoted for the υ_{ds}-configuration, respectively, by i_g^{ind-d} and i_b^{ind-d}—are calculated from Kirchhoff's current law for non-capacitive currents [see (3.85)],

$$i_g^{ind-d} + i_d^{nc-d} + i_b^{ind-d} + i_s^{nc-d} = 0 \tag{4.117}$$

and from the non-quasi-static channel charge partition rule (NQSCCPR) established in Sec. 3.8, whose mathematical form [see (3.143)] is:

$$\frac{i_b^{ind-d}}{i_g^{ind-d}} = \eta \tag{4.118}$$

where η is defined by (4.91).

Taking (4.113) and (4.116) into account and solving (4.117) and (4.118) with respect to i_g^{ind-d} and i_b^{ind-d}, we have:

$$i_g^{ind-d} = \frac{k_D\, g_{ds}\upsilon_{ds}}{1+\eta}\left[\frac{F_S}{F_{S0}} - \frac{F_D}{F_{D0}}\exp\left[(\gamma-\gamma_0)L\right]\right] \tag{4.119}$$

$$i_b^{ind-d} = \frac{\eta\, k_D\, g_{ds}\upsilon_{ds}}{1+\eta}\left[\frac{F_S}{F_{S0}} - \frac{F_D}{F_{D0}}\exp\left[(\gamma-\gamma_0)L\right]\right] \tag{4.120}$$

A four-terminal equivalent circuit for the non-capacitive currents of the transistor working in the υ_{ds}-configuration ($\upsilon_{ds} \neq 0$ and $\upsilon_{gs} = \upsilon_{bs} = 0$) is given in Fig. 4.8.

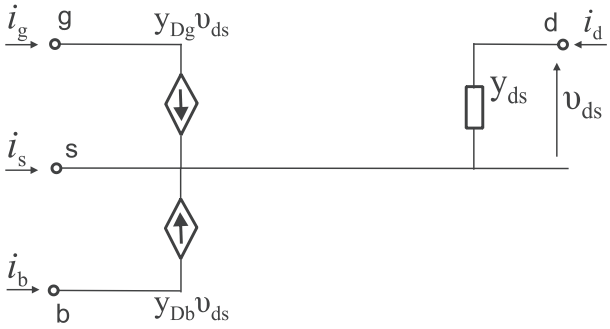

Fig. 4.8. A four-terminal equivalent circuit for the transistor working in the υ_{ds}-configuration ($\upsilon_{ds} \neq 0$ and $\upsilon_{bs} = \upsilon_{gs} = 0$).

Based on (4.113), we define the admittance y_{ds} connected between the drain and the source in Fig. 4.8 as follows:

$$y_{ds} = g_{ds} + k_D\, g_{ds} \left\{ \frac{F_D}{F_{D0}} \exp\left[(\gamma - \gamma_0) L\right] - 1 \right\} \tag{4.121}$$

A voltage-controlled current source ($y_{Dg} \cdot v_{ds}$) connected between the gate and the source in Fig. 4.8 represents the coupling current $i_g^{ind\text{-}d}$ determined by (4.119). As seen from (4.119), the transadmittance y_{Dg} of the source current is:

$$y_{Dg} = \frac{k_D\, g_{ds}}{1+\eta} \left[\frac{F_S}{F_{S0}} - \frac{F_D}{F_{D0}} \exp\left[(\gamma - \gamma_0) L\right] \right] \tag{4.122}$$

A voltage-controlled current source ($y_{Db} \cdot v_{ds}$) connected between the body and source in Fig. 4.8 represents the coupling current $i_b^{ind\text{-}d}$ determined by (4.120). As seen from (4.120), the transadmittance y_{Db} of the source current is:

$$y_{Db} = \frac{\eta\, k_D\, g_{ds}}{1+\eta} \left[\frac{F_S}{F_{S0}} - \frac{F_D}{F_{D0}} \exp\left[(\gamma - \gamma_0) L\right] \right] \tag{4.123}$$

Comparing (4.122) and (4.123), we have:

$$y_{Dg} = \frac{y_{Db}}{\eta} \tag{4.124}$$

Equivalent circuit for non-capacitive terminal currents

By virtue of the principle of superposition, we add the results obtained for each of the three configurations—see Figs. 4.4, 4.6, 4.8—and obtain a small-signal equivalent circuit for the non-capacitive terminal currents, which is shown in Fig. 4.9.

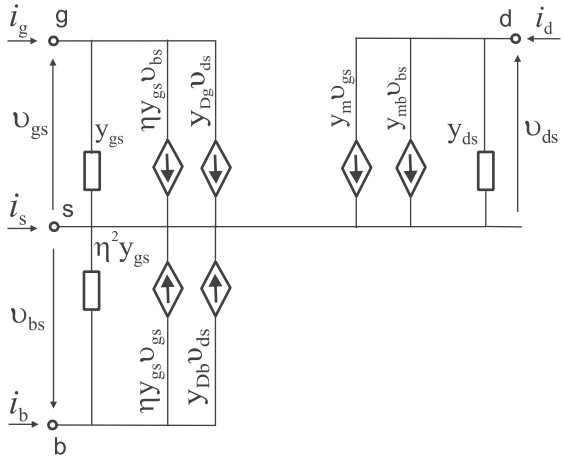

Fig. 4.9. A DIBL-included four-terminal equivalent circuit for the non-capacitive small-signal currents in the MOSFET.

The transadmittances y_m, y_{mb}, y_{Dg}, y_{Db} and the admittance y_{gs} are determined by (4.94), (4.106), (4.122), (4.123) and (4.95), respectively.

We wish to emphasize that y_m, y_{mb}, y_{Dg}, y_{Db}, y_{gs}, and the voltage-controlled current sources connected between the gate and the source as well as the body and the source in Fig. 4.9 define the electrical coupling between the channel and the transistor structure.

4.4.2. Four-terminal equivalent circuit for an idealized MOSFET

If we assume that the regions of the gate, source, drain, and body, as well as connection paths are perfect conductors, then an equivalent circuit for the quasi-2D four-terminal small-signal MOSFET model is as shown in Fig. 4.10.

By virtue of the principle of superposition, the equivalent circuit is composed of the circuit of Fig. 4.9 and reciprocal capacitances of Fig. 3.4.

The capacitance C_{gb} is given by [see (3.133)]:

$$C_{gb} = \frac{g_m \eta \tau_{tr}}{1+\eta} \tag{4.125}$$

where τ_{tr} is the transit time of carriers across the channel; see (3.99).

Alternatively, noting that $\tau_{tr} = L / (\mu_q \cdot E_0)$ for the model presented here, we obtain:

$$C_{gb} = \frac{g_m \eta L}{(1+\eta)\mu_q E_0} \tag{4.126}$$

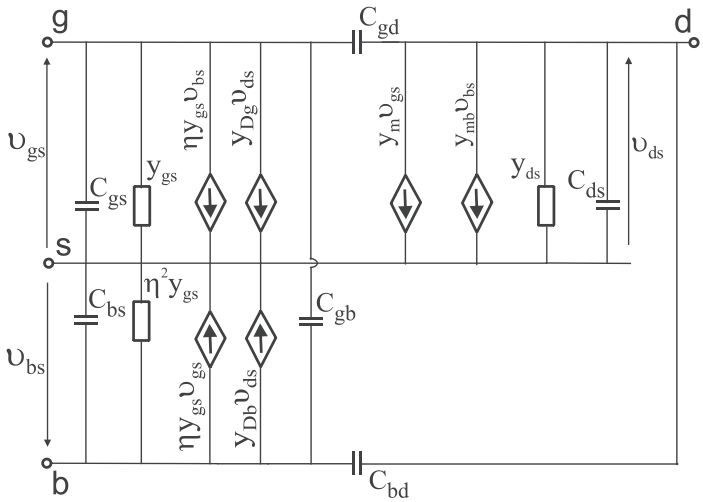

Fig. 4.10. A DIBL-included four-terminal equivalent circuit for an idealized MOS transistor.

4.4.3. Four-terminal equivalent circuit for the real MOSFET

An equivalent circuit of the quasi-2D four-terminal small-signal model for the real MOSFET without connecting paths which takes into account a finite conductivity of the gate, source, drain, and body is presented in Fig. 4.11.

The body-source and body-drain p-n junctions are modeled here in a very simple way, viz., by the series connections of the junction capacitances and respective parasitic resistances: see combinations $C_{bs}R_{bs}$ and $C_{ds}R_{ds}$ in the figure. We are aware that a more adequate model of the p-n junctions is needed for very high frequencies, however, it is beyond the scope of this work.

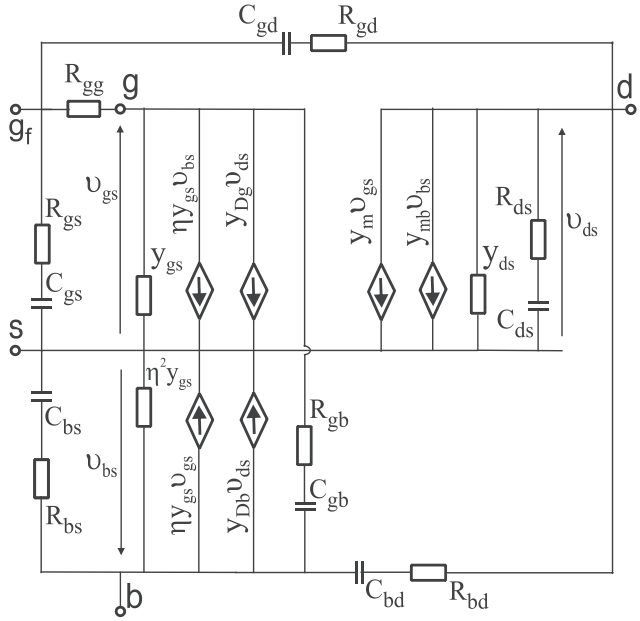

Fig. 4.11. A DIBL-included four-terminal small-signal equivalent circuit for the real MOSFET without connecting paths.

Modeling a three-dimensional nature of the current flow in the gate region is a difficult issue and can lead to a very complex circuit representation. To model this phenomenon in a simple way, we introduce a concept of an internal gate. The concept is illustrated in Fig. 4.12, where a sector of multi-finger structure of the transistor is shown. The internal gate (point *g* in Fig. 4.12) is connected with a so-called front wall (face) of the gate by a resistor representing a spreading resistance (R_{gg} in Fig. 4.11). In Fig. 4.12, the symbols g_f, *s*, and *d* refer to the front walls (faces) of the gate, source, and drain, respectively.

It is important to realize that although we have developed the four-terminal small-signal model based on the source-referenced analysis, the model can be used in an analysis based on any reference node via a straightforward transformation of the voltage phasors.

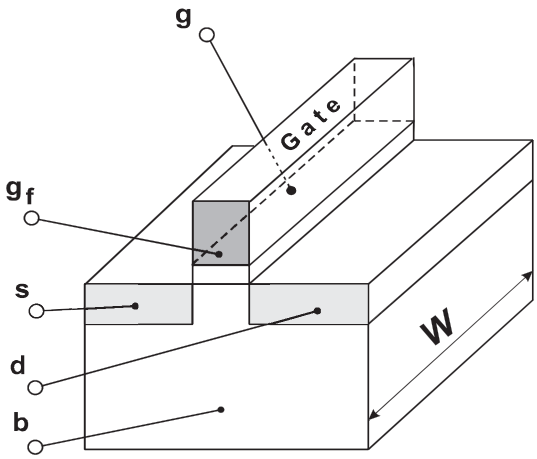

Fig. 4.12. A scheme illustrating the concept of an internal gate represented by point *g*.

4.5. Long-channel MOSFET model

The model presented in the previous section can be simplified if the MOSFET channel is long enough to have the DIBL effect ignored. In this case, setting $k_D = 0$ in (4.121)–(4.123), the model of Fig. 4.11 reduces to the one shown in Fig. 4.13.

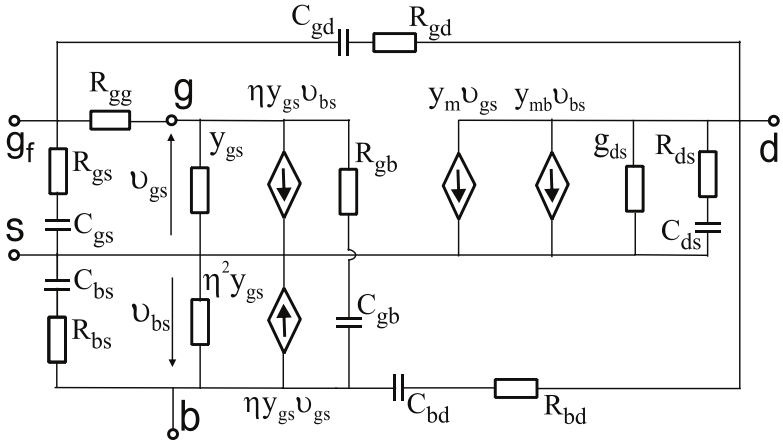

Fig. 4.13. A four-terminal small-signal equivalent circuit for the real long-channel MOSFET without connecting paths.

4.6. Conclusion

A novel DIBL-included quasi-2D NQS four-terminal frequency-domain small-signal MOSFET model is proposed in this chapter. The model takes into account: the velocity saturation effect of carriers in the channel, the dependence of the mobility on the electric field, the elec-

trical coupling between the perturbed charge in the channel and the gate and the body, local variations in the channel thickness, and the drain-induced barrier lowering (DIBL) effect. Unlike other models, this one is composed only of reciprocal capacitances.

A closed set of partial differential equations defining the model in the frequency domain is formulated and solved. The solution indicates that two types of waves can propagate from the source to the drain, viz., a longitudinal wave of a disturbance in the carrier density and a transverse wave of a disturbance in the channel thickness.

A closed set of equations for frequency-domain non-capacitive terminal currents in the MOSFET under dynamic operation is derived.

The four-terminal model can be used in analyzing any circuit topology, and can be implemented in commercially available circuit simulators. The model we propose is believed to enable us to gain a deeper insight into the principle of operation of the MOS transistor.

The results of experimental verification of the model derived in this chapter and discussion are presented in the next chapter.

References

[1] Kordalski W. and Stefanski T., "A non-quasi-static small-signal MOSFET model for radio and microwave frequencies including spreading gate resistances and capacitances", in *Proc. IEEE Radio Frequency Integrated Circuits* (*RFIC*) *Symposium*, pp. 365–368, June 8–10, 2003, Philadelphia, Pennsylvania, USA.

[2] Kordalski W., "A quasi-2D small-signal MOSFET model – main results", *Electronics*, No. 9/2014, pp. 48–51, [in Polish]. DOI: 10.15199/ELE-2014-131.

[3] Sze C. M. and Ng K. K., *Physics of semiconductor devices*, 3rd ed., Wiley and Sons, 2007.

[4] Tsividis Y. P. and McAndrew C., *The MOS transistor*, Int. 3rd ed., Oxford University Press, New York, Oxford, 2012.

[5] Sallese J. M., and Porret A.–S., "A novel approach to charge-based non-quasi-static model of the MOS transistor valid in all modes of operation", *Solid-State Electronics*, vol. 44, pp. 887–894, 2000.

[6] Aarts A. C. T., Smit G. D. J., Scholten A. J., and Klaassen D. B. M., "A PSP-based small-signal MOSFET model for both quasi-static and nonquasi-static operations", *IEEE Trans. on Electron Devices*, vol. ED-55, no. 6, pp. 1424–1432, June 2008.

Chapter 5

VALIDATION OF THE FREQUENCY-DOMAIN MODEL

Wiesław Kordalski, Tomasz Stefański, Damian Trofimowicz

5.1. Introduction

In this chapter, the results of an experimental verification of the new, physically consistent, DIBL-included quasi-2D four-terminal non-quasi-static frequency-domain small-signal MOSFET model, derived from the first principles in Chapter 4, are presented.

In Section 5.2, the layout of pads and interconnects in the measured transistors are shown. A small-signal model of the measured MOSFETs is presented in Section 5.3. The de-embedding procedure is briefly described in Section 5.4. In Section 5.5, the results of our experimental verification of the model in the range of up to the characteristic frequency f_T are reported. In Section 5.6, the new small-signal model for long-channel MOSFET (without DIBL effect) is experimentally verified up to 30 GHz. Section 5.7 contains a summary.

A general note: the symbols for physical quantities occurring in this chapter are consistent with those applied in Chapter 4.

5.2. Layout of the measured MOSFETs

5-finger enhancement-mode NMOS transistors with the channel length of 0.35 μm, and 1.4 μm and the width of 50 μm were used to validate the NQS small-signal model up to 30 GHz. The test structures were optimized for measurements of scattering parameters of the transistor in the common-source configuration with the use of air coplanar probes (ACPs).

The layout of pads and interconnects in the measured transistors is shown in Fig. 5.1. The bulk and source of the transistor were shorted by grounding the probes during RF measurements.

For the purpose of our verification of the NQS model, dummy structures (OPEN, SHORT, THRU) of the measured transistors were designed; see Fig. 5.2.

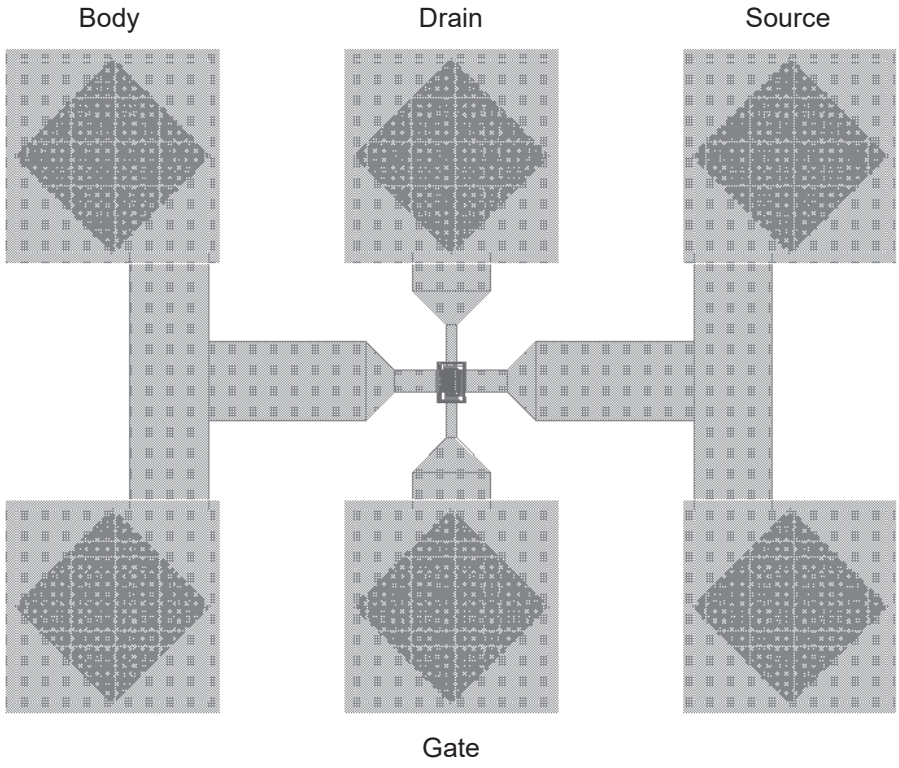

Fig. 5.1. The layout of pads and interconnects in the device under test (DUT).

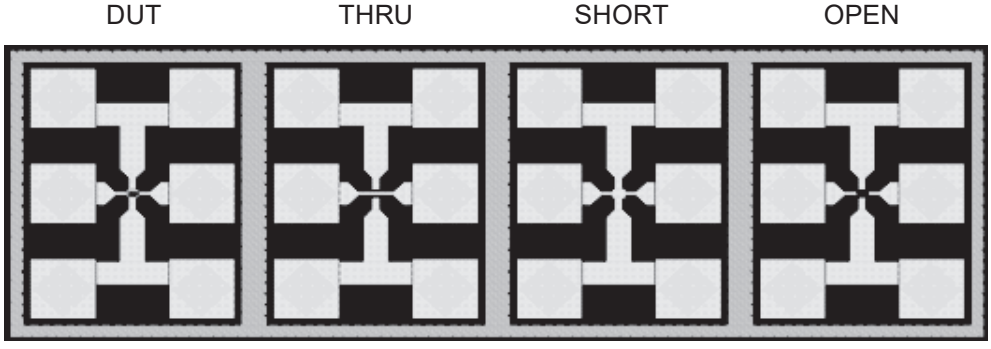

Fig. 5.2. The layouts of the devices under test (DUT) and dummy structures (OPEN, SHORT, THRU) for the de-embedding of RF characteristics.

5.3. Small-signal model of the measured MOSFETs

A new DIBL-included quasi-2D NQS four-terminal frequency-domain small-signal model of the real MOSFET (without connecting paths and pads) is developed in Sec. 4.4.3 and depicted in Fig. 4.11.

To simulate the theoretical frequency characteristics of the device under test (DUT), the model of Fig. 4.11 is adapted. This model is supplemented by some resistive and inductive elements corresponding to the transistor structure as measured by the ACPs.

In Fig. 5.3, we present a complete small-signal model of the DUT. Resistors R_b, R_d, R_g, and R_s as well as inductances L_b, L_d, L_g, and L_s represent, respectively, the resistances and inductances of the connection paths connecting the gate, source, drain and substrate of the transistor; see [1–3].

Admittances y_{gs} and y_{ds}, and transadmittances y_m, y_{mb}, $y_{Db,}$ and y_{Dg}, and a parameter η are defined in Sec. 4.4. The gate-to-body capacitance C_{gb} is calculated from (4.126).

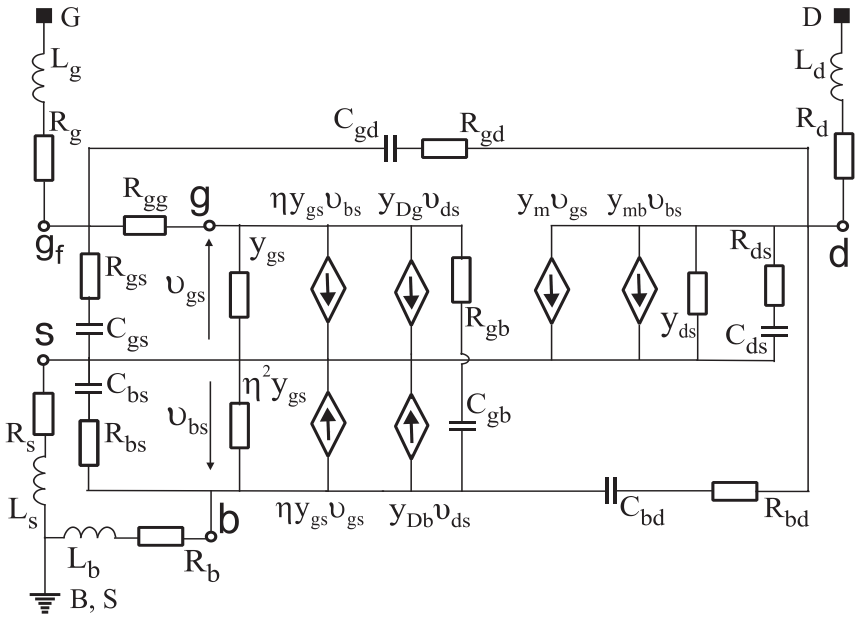

Fig. 5.3. A DIBL-included quasi-2D NQS four-terminal small-signal model for the DUT of Fig. 5.1.

5.4. De-embedding procedure

To obtain reliable and repeatable measurement results, four transistor structures were measured based on two different calibration techniques of a vector network analyzer (VNA). Two structures were measured with the use of the SOLT calibration method [4] in the 65MHz-to-25GHz frequency range, whereas the other structures were measured with the use of the LRM method [5] in the 65MHz-to-30GHz frequency range. The impedance substrate standard (ISS) was used to calibrate the VNA. Transmission lines on ISS were used to verify the quality of the VNA calibration. The procedure of de-embedding was based on the widely used open-short method [4]. The S-parameters were measured for the DUT, OPEN, SHORT, and THRU structures. Then, parallel parasitic elements were removed from DUT, SHORT and THRU by subtracting the Y-parameters of OPEN. Next, series parasitic elements were

removed from DUT and THRU by subtracting the Z-parameters of SHORT. Finally, the quality of the de-embedding procedure was positively verified with the use of the THRU structure. Almost the same results were obtained for the other tested transistors, thus the risk of a one-time wrong measurement was eliminated.

5.5. Results of the verification up to f_T

Some representative results of experimental verification of the new small-signal MOSFET model for transistors (denoted by DEVICE-1 and DEVICE-2) of two different channel lengths are shown in Figs. 5.4–5.7 and Table 5.1.

Biasing voltages, widths and lengths of channels of the tested transistors are presented in Table 5.1. There are also presented the values of quasi-static small-signal gate transconductance g_m, quasi-static small-signal body transconductance g_{mb}, and quasi-static small-signal drain-source conductance g_{ds} at the Q-point. The values of the other model parameters obtained by curve-fitting of the theoretical admittance frequency characteristics to the experimental ones are also given in Table 5.1; the capacitance C_{gb} is calculated from (4.126).

Table 5.1

Model parameter values for the devices under test.

Model parameter	DEVICE-1	DEVICE-2
V_{DS} [V]	2.1	3.3
V_{GS} [V]	1.0	0.9
L [μm]	1.42	0.37
W [μm]	50	50
μ_q [cm^2/ V s]	360	220
g_m [mS]	2.3	8.3
g_{mb} [mS]	1	2
g_{ds} [μS]	30	350
k_D [-]	0.1	0.4
D_C [-]	0.8	2
d_l [-]	0.08	0.29
S [-]	1.25	2.2
X_S [nm]	105	125
C_{bd} [fF]	35	20
C_{bs} [fF]	50	50
C_{ds} [fF]	8	18

continued tab. 5.1

C_{gb} [fF], calculated	41	5
C_{gd} [fF]	8.3	9.8
C_{gs} [fF]	170	40
R_b [Ω]	1.4	1.4
R_d [Ω]	1	1
R_g [Ω]	1	1
R_s [Ω]	1.4	1.4
L_b [pH]	29	29
L_d [pH]	1.5	1.5
L_g [pH]	1.5	1.5
L_s [pH]	29	29
R_{bd} [Ω]	400	400
R_{bs} [Ω]	350	350
R_{ds} [Ω	20	20
R_{gb} [Ω	2	2
R_{gd} [Ω]	2	2.3
R_{gg} [Ω	1.9	2.2
R_{gs} [Ω]	58	63
f_T [GHz], measured	1.55	21.5
f_T [GHz], calculated	1.6	21.4

In Figs. 5.6 and 5.7, two different representations of the measured and theoretical characteristics of H_{21}–parameters vs. frequency are displayed for DEVICE-1 and DEVICE-2, respectively.

One can see in the above-mentioned figures that close accuracy is attained in theoretical description of the measured data in the frequency range of up to the characteristic frequency f_T. It is worth noticing that the model parameters have realistic values.

Magnitude, real and imaginary parts of the calculated transadmittances y_m, y_{ds}, y_{gs} vs. frequency for DEVICE-1 are shown in Figs. 5.8, 5.10, and 5.12, whereas analogous frequency characteristics for DEVICE-2 are presented in Figs. 5.9, 5.11, and 5.13. One can observe in these figures that magnitude, real and imaginary parts of the calculated transadmittances y_m, y_{ds}, y_{gs} are monotonic functions of frequency from zero Hz to f_T.

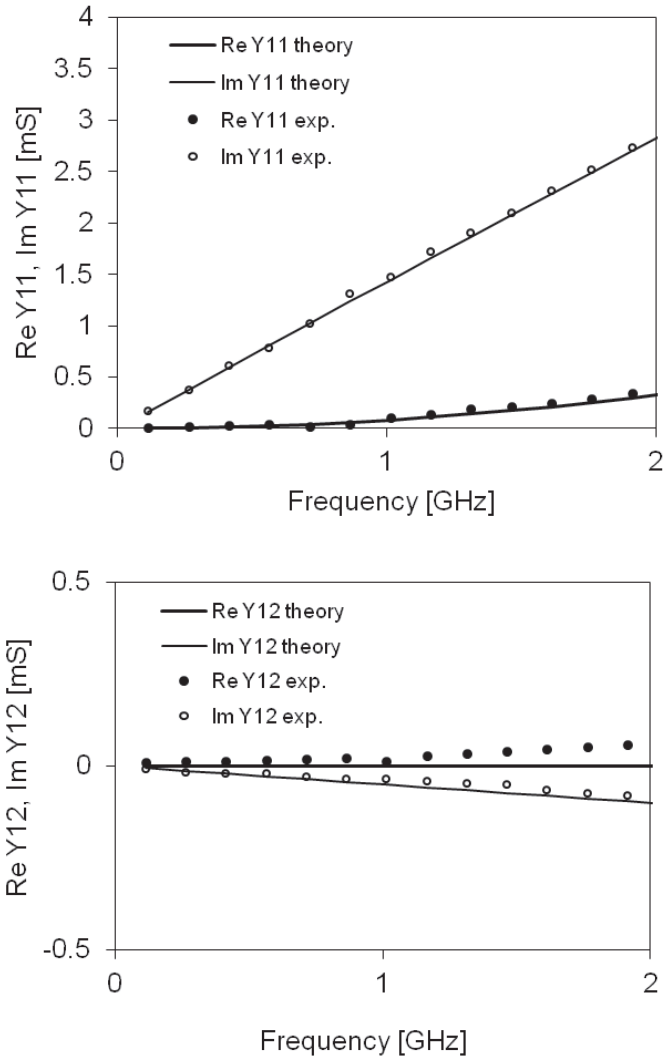

Fig. 5.4. Real and imaginary parts of the Y_{kl}–parameters vs. frequency: comparison between the measured (exp.) and theoretical (theory) data for DEVICE-1; f_T = 1.55 GHz.

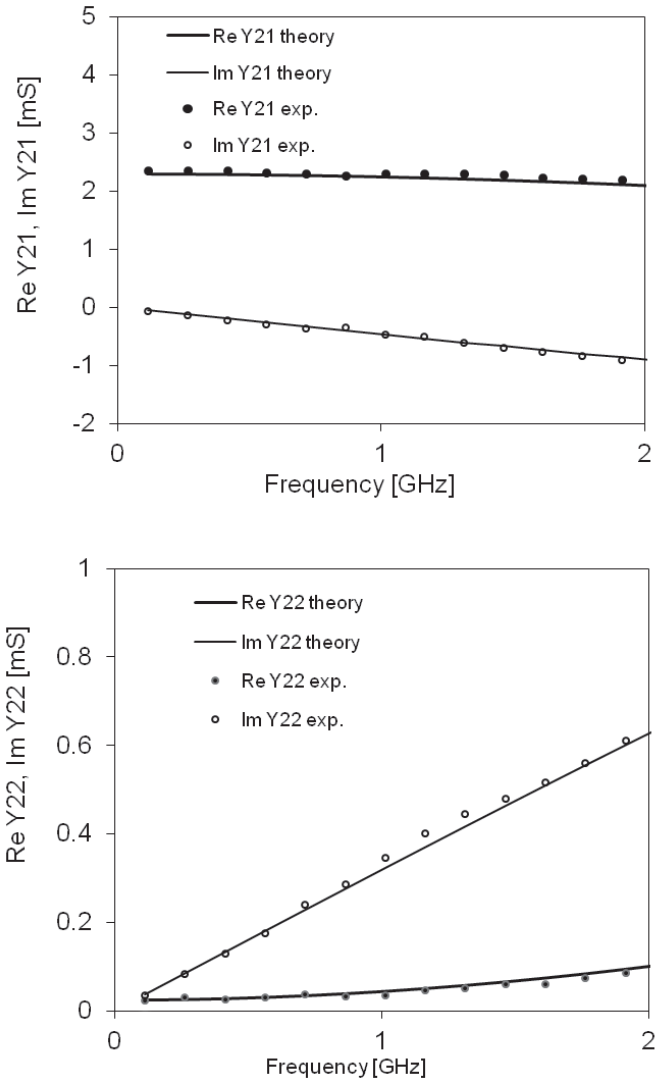

Fig. 5.4. (continued).

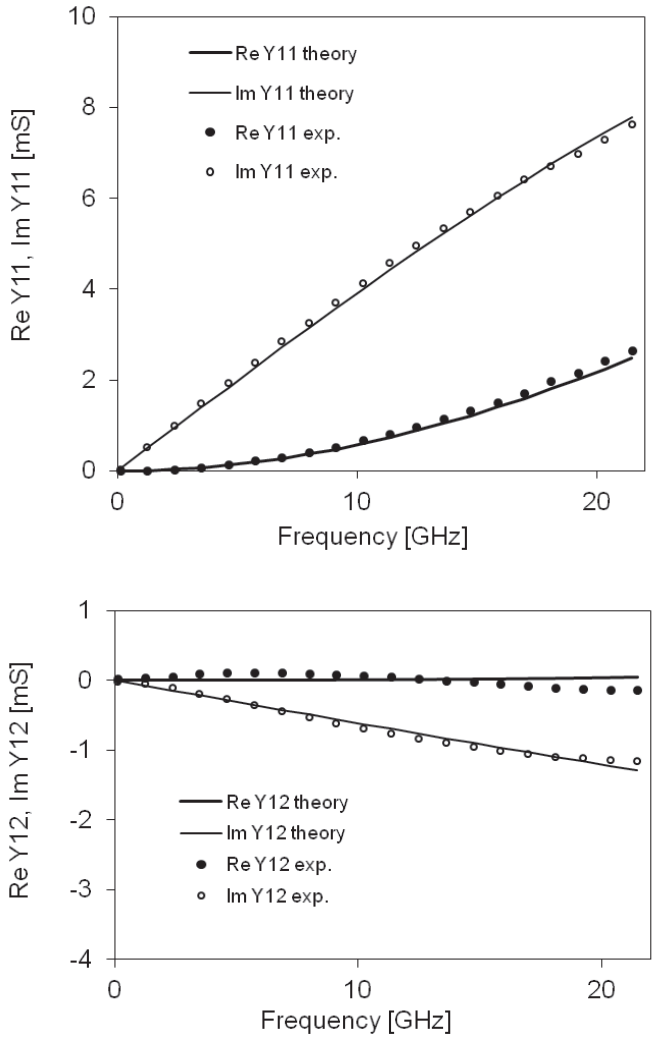

Fig. 5.5. Real and imaginary parts of the Y_{kl}–parameters vs. frequency: comparison between the measured (exp.) and theoretical (theory) data for DEVICE-2; f_T = 21.5 GHz.

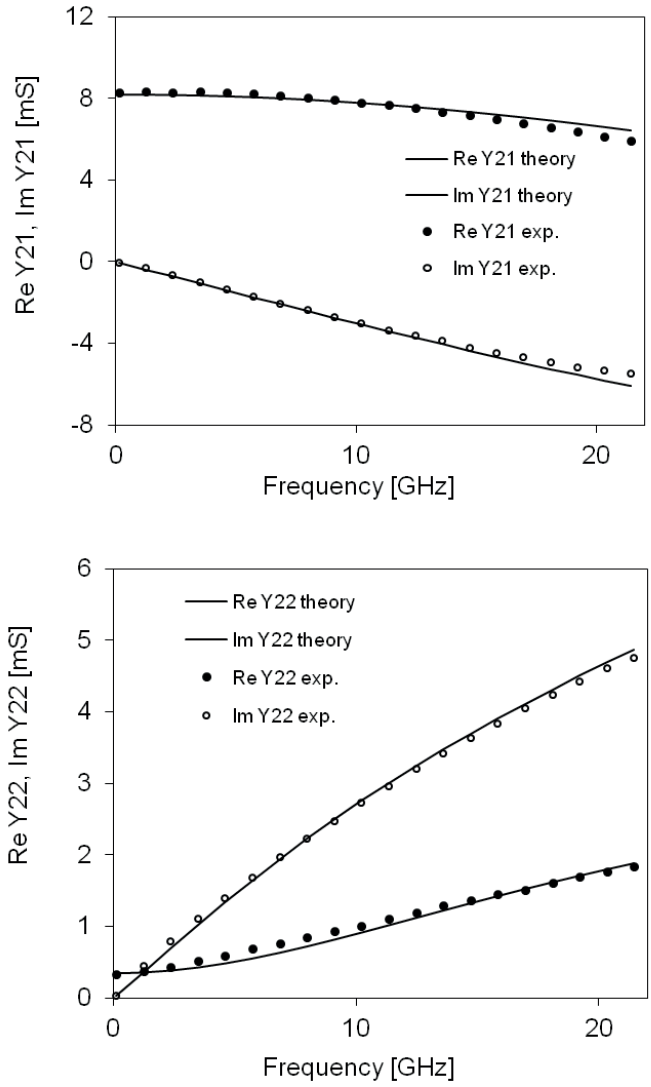

Fig. 5.5. (continued).

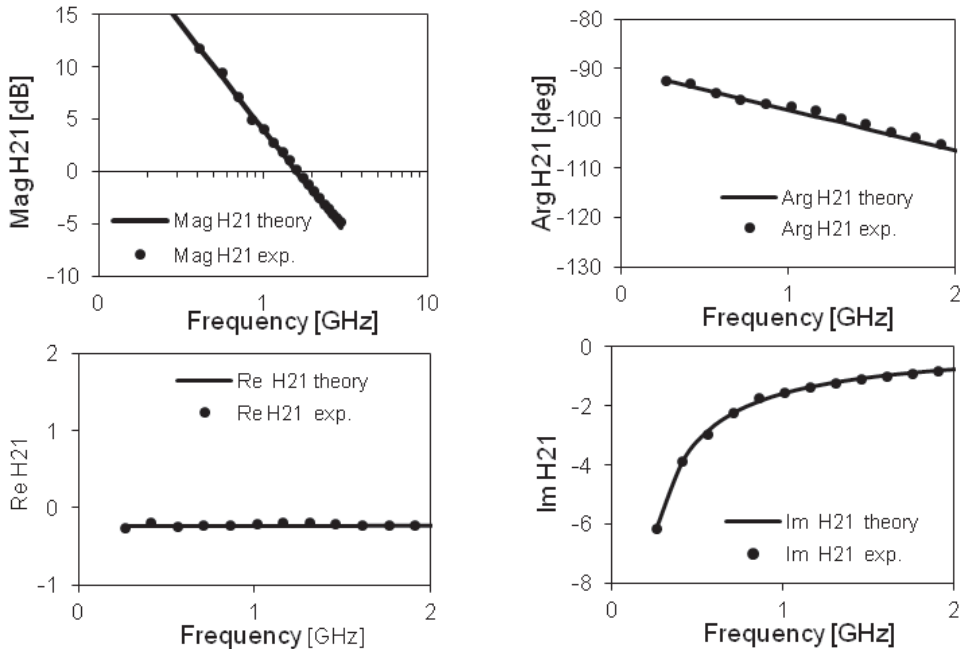

Fig. 5.6. Magnitude, argument, real and imaginary parts of the H_{21}–parameters vs. frequency: comparison between the measured (exp.) and theoretical (theory) data for DEVICE-1; f_T = 1.55 GHz.

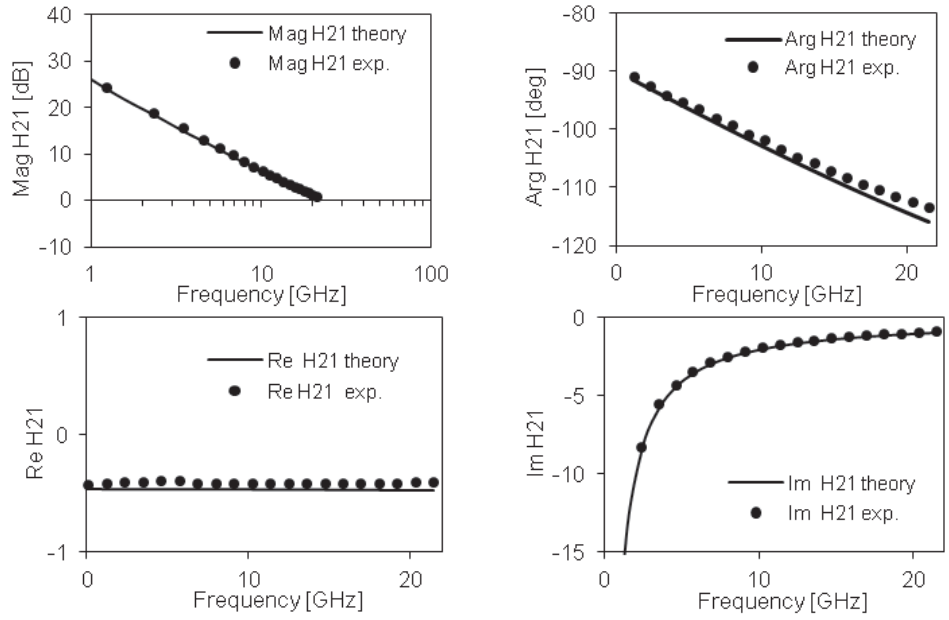

Fig. 5.7. Magnitude, argument, real and imaginary parts of the H_{21}–parameters vs. frequency: comparison between the measured (exp.) and theoretical (theory) data for DEVICE-2; f_T = 21.5 GHz.

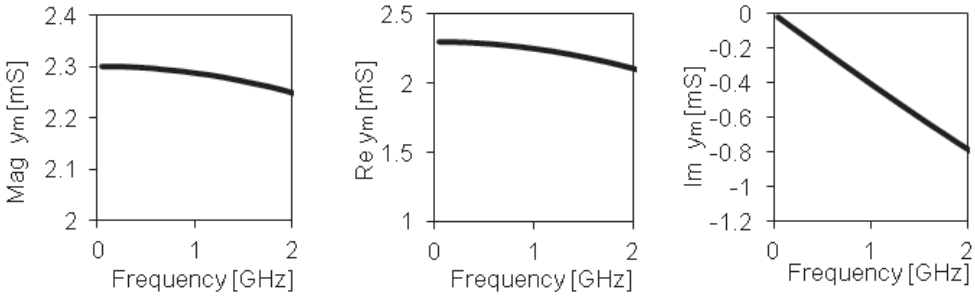

Fig. 5.8. Magnitude, real and imaginary parts of the transadmittance y_m vs. frequency for DEVICE-1; f_T = 1.55 GHz.

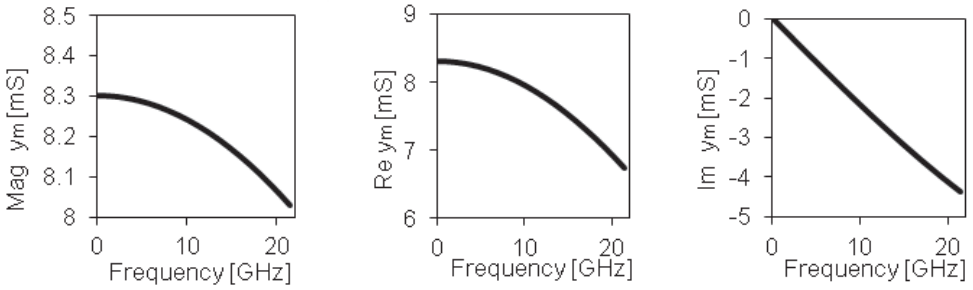

Fig. 5.9. Magnitude, real and imaginary parts of the transadmittance y_m vs. frequency for DEVICE-2; f_T = 21.5 GHz.

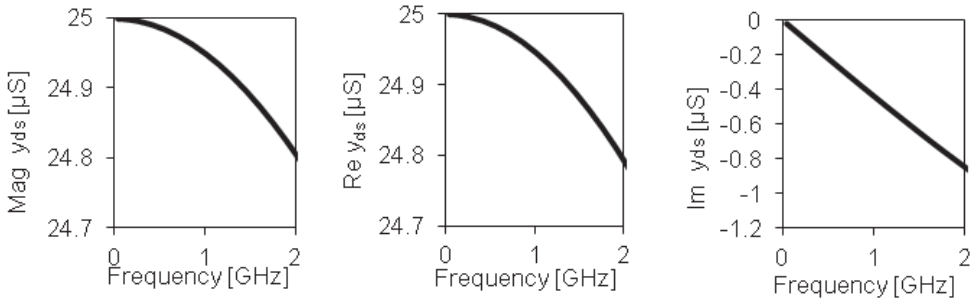

Fig. 5.10. Magnitude, real and imaginary parts of the transadmittance y_{ds} vs. frequency for DEVICE-1; f_T = 1.55 GHz.

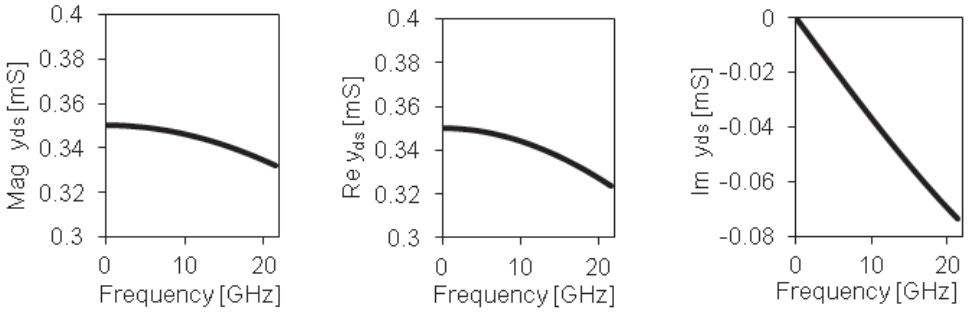

Fig. 5.11. Magnitude, real and imaginary parts of the transadmittance y_{ds} vs. frequency for DEVICE-2; f_T = 21.5 GHz.

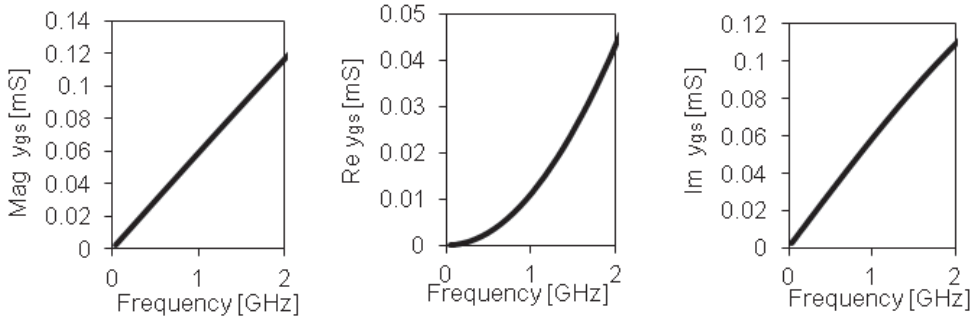

Fig. 5.12. Magnitude, real and imaginary parts of the transadmittance y_{gs} vs. frequency for DEVICE-1; f_T = 1.55 GHz.

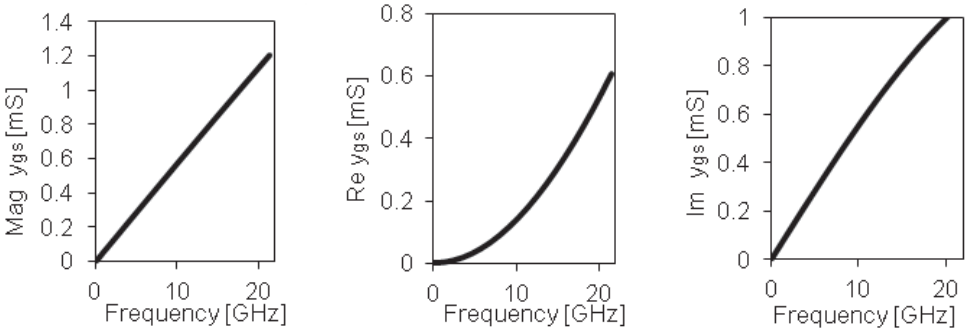

Fig. 5.13. Magnitude, real and imaginary parts of the transadmittance y_{gs} vs. frequency for DEVICE-2; f_T = 21.5 GHz.

5.6. Results of the verification in the range of up to thirteen times f_T

Some final results dealing with a simplified version (without the DIBL effect) of the new model of long-channel transistors are presnted in this section. The results refer to DEVICE-1 (L = 1.4 μm) biased with the dc drain-to-source voltage V_{DS} = 2.1 V and the gate-to-source voltage V_{GS} = 1.2 V *(*the measured f_T = 2.21 GHz at the Q-point). The results are obtained

under assumption $k_D = 0$, and—as in the previous section—the capacitance C_{gb} is calculated from (4.126).

Real and imaginary parts of the measured (exp. in figures) and theoretical (theory in figures) Y_{kl}–parameters for the transistor under test vs. frequency are shown in Fig. 5.14. In Fig. 5.15, two different representations of the measured and theoretical H_{21}–parameters vs. frequency are displayed. One can see from Figs. 5.14 and 5.15 that the theoretical and empirical characteristics are in good agreement even in the frequency range well above the characteristic frequency f_T (about 2.2 GHz).

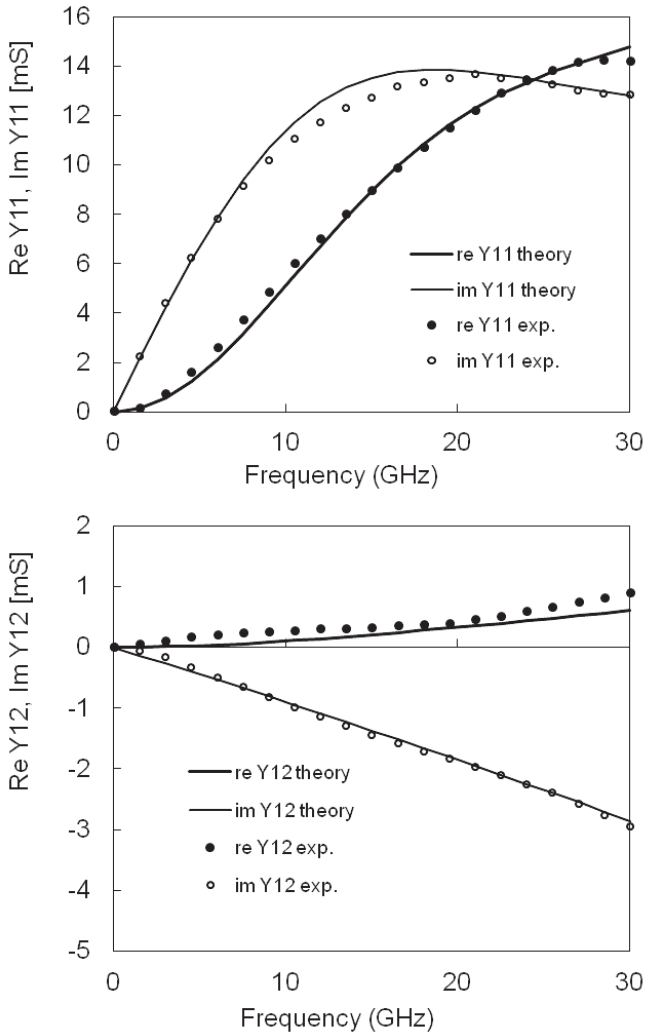

Fig. 5.14. Real and imaginary parts of the Y_{kl}–parameters vs. frequency: comparison between the measured (exp.) and theoretical (theory) data for DEVICE-1 ($V_{DS} = 2.1$ V, $V_{GS} = 1.2$ V, $f_T = 2.21$ GHz).

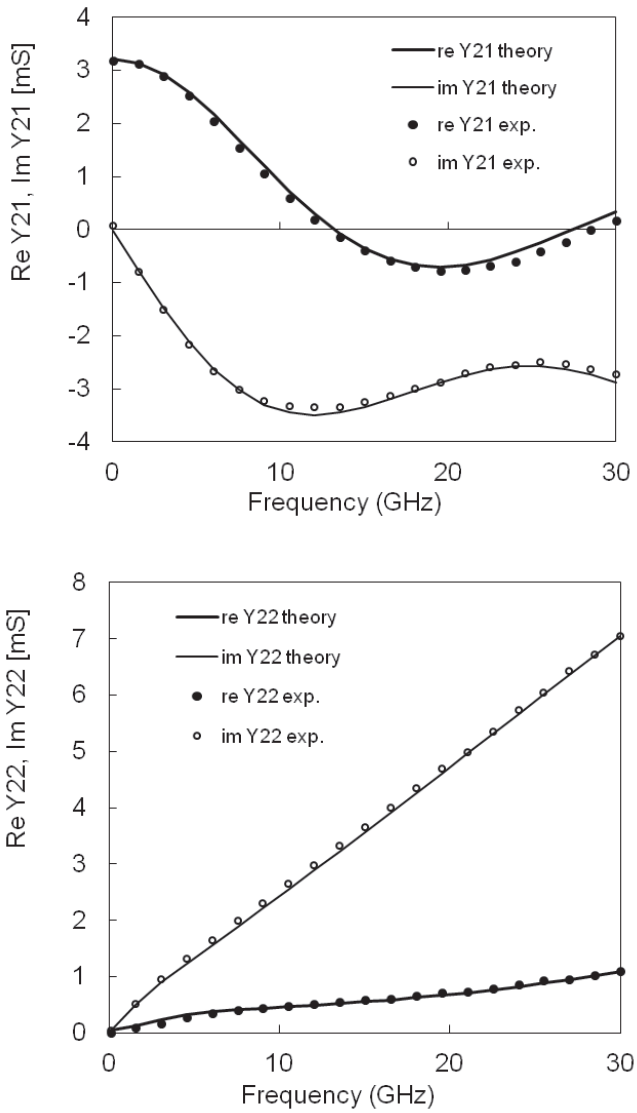

Fig. 5.14. (continued).

An interesting issue is to estimate the frequency f_T for an idealized MOS transistor in the common-source configuration ($f_{T,ideal}$); such a transistor has no capacitances, resistances, and inductances, as shown in Fig. 4.9. It is intuitively obvious that the idealized transistor should have a finite value of $f_{T,ideal}$ if we take into account the fact that the velocity of propagation of the charge carriers in the channel of the transistor is finite. Using the new model, one can calculate $f_{T,ideal}$. Calculations give $f_{T,ideal}$ = 10 GHz, so the value is over four times greater than that of the real device.

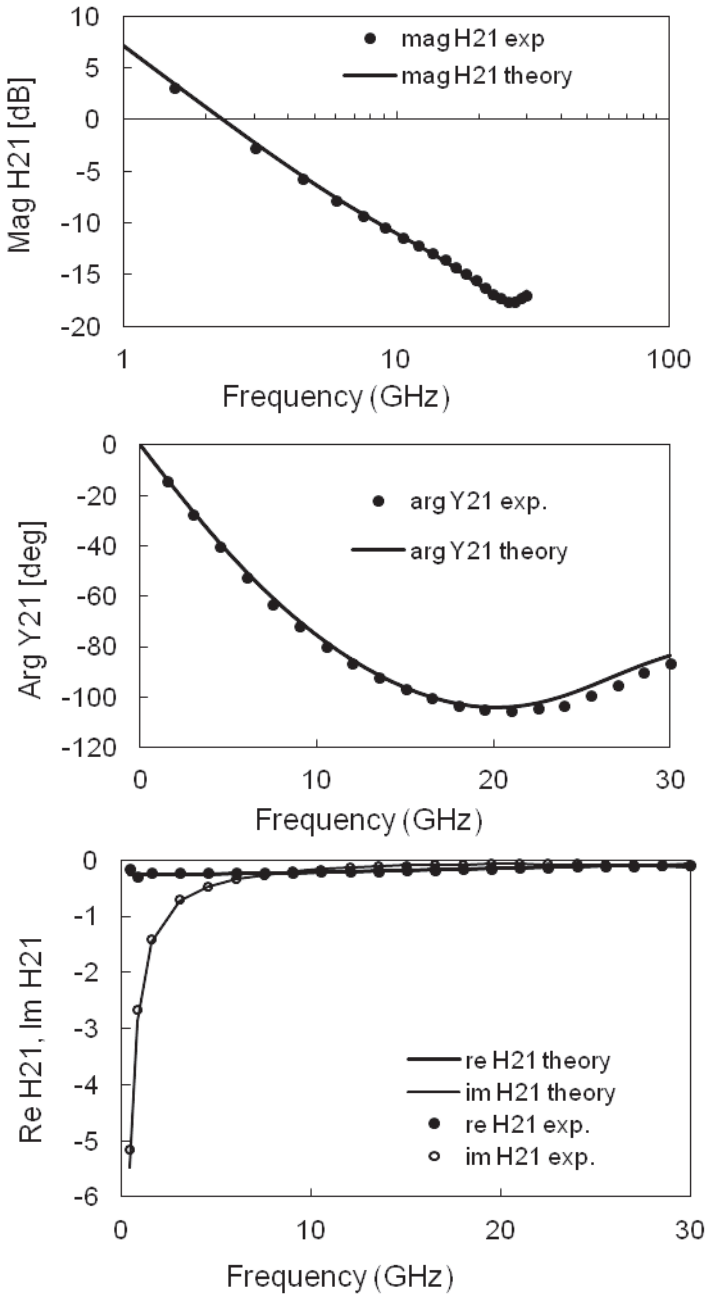

Fig. 5.15. Magnitude, argument, real and imaginary parts of the H_{21}–parameters vs. frequency: comparison of the measured (exp.) and theoretical (theory) data for DEVICE-1 (V_{DS} = 2.1 V, V_{GS} = 1.2 V, f_T = 2.21 GHz).

5.7 Conclusion

A new DIBL-included physics-based quasi-2D non-quasi-static four-terminal small-signal model of the MOSFET has been successfully verified experimentally up to 30 GHz. The model parameters have realistic values. The model can be implemented in commercially available circuit simulators.

References

[1] Lin Y.-S., "An analysis of small-signal source-body resistance effect on RF MOSFETs for low-cost system on chip (SoC) applications," *IEEE Trans. on Electron Devices,* vol. 52, no. 7, pp. 1442–1451, 2005.

[2] Sung R., Bendix P., and Das M. B., "Extraction of high-frequency equivalent circuit parameters of submicron gate-length MOSFET's," *IEEE Trans. on Electron Devices,* vol. 45, no. 8, pp. 1769–1775, 1998.

[3] Cho H. and Burk D. E., "A three-step method for the de-embedding of high-frequency s-parameter measurements," *IEEE Trans. on Electron Devices,* vol. 38, no. 6, pp. 1371–1375, 1991.

[4] Sischka F., Agilent technologies, "IC-CAP characterization & modeling handbook". available: http://eesof.tm.agilent.com/docs/iccap2002/iccap_mdl_handbook.html.

[5] Lautzenhiser S., Davidson A., and Jones K., "Improve accuracy of on-wafer tests via LRM calibration," *Microwaves & RF*, January 1990.

TIME- AND FREQUENCY-DOMAIN QUASI-2D SMALL-SIGNAL MOSFET MODELS

A novel approach to small-signal MOSFET modeling is presented in this monograph. As a result, time- and frequency-domain physics-based quasi-2D NQS four-terminal small-signal MOSFET models are proposed. The time-domain model provides the background to a novel DIBL-included quasi-2D NQS four-terminal frequency-domain small-signal MOSFET model. Parameters and electrical quantities of the frequency-domain model are described by explicit functions.

The models take into account: the velocity saturation effect of carriers in the channel, the dependence of the mobility on the electric field, the electrical coupling between the perturbed charge in the channel and the gate and the body, local variations in the channel thickness, and the DIBL effect.

Derivation of the models is based on an analysis of a current density vector field and the following newly introduced phenomena: gradual channel detachment effect (GCDE), channel thickness modulation effect CTME), and channel-lengthening effect (CLE).

A set of partial differential equations for the new physics-based small-signal MOSFET models is derived. The set consists of a quasi-2D small-signal continuity equation, a quasi-2D small-signal Poisson's equation, and a quasi-2D small-signal transport equation. All the equations give a mathematical description of the behavior of the carriers in the channel and charges in the gate and the body. A set of supplementary equations for coupling and non-capacitive displacement currents in the MOSFET under dynamic operation is also derived.

Based on the quasi-2D dc MOSFET representation, a useful formula for the gate-to-body capacitance C_{gb} is derived, and some rules dealing with channel-to-gate and channel-to-body coupling currents are established. Only reciprocal capacitances are present in these models.

The quasi-2D approach to the MOSFET modeling shows that two types of waves can propagate from the source to the drain, i.e., a longitudinal wave of disturbance in the carrier density and a transverse wave of disturbance in the channel thickness.

It is shown that the magnitudes of both gate and body transadmittances are decreasing functions of frequency.

The new frequency-domain small-signal MOSFET model has been successfully verified experimentally up to 30 GHz. The model parameters have realistic values.

The new model is valid from zero Hz to well above the cut-off frequency f_T.

Each model parameter describes some physical phenomenon.

The time- and frequency-domain four-terminal small-signal models can be used in an analysis of any circuit topology, and can be implemented in commercially available circuit simulators. The models are believed to enable us to gain a deeper insight into the principle of operation of the MOS transistor.

QUASI-DWUWYMIAROWE MODELE MAŁOSYGNAŁOWE TRANZYSTORA MOS W DZIEDZINIE CZASU I CZĘSTOTLIWOŚCI

W książce przedstawiono nowe podejście do modelowania małosygnałowej pracy tranzystora MOS. Jego rezultatem są opracowania dwóch quasi-dwuwymiarowych, nie-quasi-statycznych, czterokońcówkowych modeli małosygnałowych MOSFET-a w dziedzinie czasu i częstotliwości. Opracowany quasi-dwuwymiarowy model w dziedzinie czasu stanowi podstawę matematyczno-fizyczną do wyprowadzenia quasi-dwuwymiarowego, nie-quasi-statycznego, czterokońcówkowego modelu małosygnałowego MOSFET-a w dziedzinie częstotliwości, uwzględniającego efekt DIBL (ang. *Drain-Induced Barrier Lowering*). Parametry charakteryzujące model częstotliwościowy opisane są funkcjami jawnymi częstotliwości i wielkości elektro-fizycznych tranzystora.

W odróżnieniu od znanych modeli, w modelach nowoopracowanych uwzględniono następujące zjawiska: efekt nasycenia prędkości nośników w kanale tranzystora, zależność ruchliwości nośników od natężenia pola elektrycznego, zjawisko sprzężenia elektrycznego pomiędzy zaburzoną koncentracją nośników w kanale a bramką i podłożem, lokalną zmianę grubości kanału oraz efekt DIBL.

Wyprowadzenie tych modeli małosygnałowych oparte jest na analizie pola wektorowego gęstości prądu i nieuwzględnianych dotychczas takich zjawisk jak: zjawisko łagodnego (stopniowego) odrywania się kanału, zjawisko modulacji grubości kanału (statyczne i dynamiczne) oraz zjawisko wydłużania kanału.

Biorąc pod uwagę najbardziej podstawowe (rudymentarne) prawa fizyki, wyprowadzono układ równań różniczkowych cząstkowych opisujących model małosygnałowy tranzystora MOS w dziedzinie czasu. Układ ten składa się z quasi-dwuwymiarowego równania ciągłości, quasi-dwuwymiarowego równania Poisson'a i quasi-dwuwymiarowego równania transportu. Równania te stanowią matematyczną podstawę kinetyki nośników w kanale i pozwalają obliczyć ładunki indukowane w bramce i podłożu. Wyprowadzono również równania opisujące prądy sprzężenia kanał-bramka i kanał-podłoże oraz zdefiniowano niepojemnościowe prądy przesunięcia.

Opierając się na opracowanej quasi-dwuwymiarowej reprezentacji stałoprądowej tranzystora MOS wyprowadzono wzór na pojemność bramka-podłoże C_{gb} oraz sformułowano reguły ustalające relację pomiędzy prądami sprzężenia kanał-bramka i kanał-podłoże. Nowoopracowane modele zawierają tylko pojemności wzajemne.

Z przeprowadzonej analizy wynika, że dwa typy fal mogą propagować się w kanale tranzystora MOS: podłużna fala zaburzeń koncentracji nośników i poprzeczna fala zaburzeń grubości kanału.

Wykazano, że moduły zespolonych transadmitancji bramki i podłoża są malejącymi funkcjami częstotliwości.

Nowy małosygnałowy model MOSFET-a w dziedzinie częstotliwości został pozytywnie zweryfikowany eksperymentalnie aż do częstotliwości 30 GHz. Parametry modelu przyjmują realistyczne wartości.

Małosygnałowy model częstotliwościowy może być stosowany od zera Hz do częstotliwości kilkakrotnie większej od f_T.

Każdy parametr modelu opisuje jakieś zjawisko fizyczne.

Obydwa nowe modele małosygnałowe mogą być użyte do analizy scalonych układów mikroelektronicznych o dowolnej topologii, a także mogą być zaimplementowane w komercyjnych symulatorach układów elektronicznych.

Jesteśmy przekonani, że zaproponowane nowe modele pozwalają głębiej wniknąć w zasadę działania tranzystora MOS.

Appendix A

DERIVATION OF QUASI-2D CONTINUITY EQUATION

Wiesław Kordalski

Let $L^*(\xi, t)$ be the limit of the left-hand side of (3.25) as $\Delta\xi \to 0$, i.e.:

$$L^*(\xi,t) = \lim_{\Delta\xi\to 0} q\,\frac{1}{\Delta\xi}\int_{\xi}^{\xi+\Delta\xi}\frac{\partial}{\partial t}\left[\,p(\xi,t)\,X(\xi,t)\right]d\xi \tag{A1}$$

The quotient of the integral of the right-hand side of (A1) by $\Delta\xi$ has the limit:

$$\lim_{\Delta\xi\to 0}\frac{1}{\Delta\xi}\int_{\xi}^{\xi+\Delta\xi}\frac{\partial}{\partial t}\left[\,p(\xi,t)\,X(\xi,t)\right]d\xi = \frac{\partial}{\partial t}\left[\,p(\xi,t)\,X(\xi,t)\right] \tag{A2}$$

Indeed, noting that $p(\xi, t)$ and $X(\xi, t)$ are nonnegative functions and applying the mean value theorem to the integral, we can write:

$$\begin{aligned}\frac{1}{\Delta\xi}\int_{\xi}^{\xi+\Delta\xi}\frac{\partial}{\partial t}\left[\,p(\xi,t)\,X(\xi,t)\right]d\xi &= \frac{\partial}{\partial t}\left[\,p(\xi+\alpha\cdot\Delta\xi,t)\right.\\ \left.\times\;X(\xi+\alpha\cdot\Delta\xi,t)\right] &\xrightarrow[\Delta\xi\to 0]{} \frac{\partial}{\partial t}\left[\,p(\xi,t)\,X(\xi,t)\right]\end{aligned} \tag{A3}$$

since $\alpha = \alpha(\xi, \Delta\xi) \in (0, 1)$.

Thus, combining (A1) with (A2), we obtain:

$$L^*(\xi,t) = q\,\frac{\partial}{\partial t}\left[\,X(\xi,t)\,p(\xi,t)\right] \tag{A4}$$

Differentiating (A4) with respect to t and employing (3.14) and (3.15) leads to:

$$L^*(\xi,t) = q\left[\,p_0(\xi)\frac{\partial X_1(\xi,t)}{\partial t} + X_0(\xi)\frac{\partial p_1(\xi,t)}{\partial t} + p_1(\xi,t)\frac{\partial X_1(\xi,t)}{\partial t} + X_1(\xi,t)\frac{\partial p_1(\xi,t)}{\partial t}\right] \tag{A5}$$

Confining considerations to linear analysis (ignoring the two mixed terms in the preceding equation) and using (3.21) yields:

$$L^*(\xi,t) = q\, X_0(\xi)\left[1+D_C(\xi,t)\right]\frac{\partial p_1(\xi,t)}{\partial t} \tag{A6}$$

Denoting the right-hand side of (3.25) by $R(\xi, t)$ and inserting the following formulas:

$$J(\xi+\Delta\xi,t) = J(\xi,t)+\frac{\partial J(\xi,t)}{\partial \xi}\Delta\xi + o_1(\Delta\xi) \tag{A7}$$

$$X(\xi+\Delta\xi,t) = X(\xi,t)+\frac{\partial X(\xi,t)}{\partial \xi}\Delta\xi + o_2(\Delta\xi) \tag{A8}$$

into (3.25), we obtain:

$$\begin{aligned} R(\xi,t) = \frac{-1}{\Delta\xi}\Bigg[& X(\xi,t)\frac{\partial J(\xi,t)}{\partial \xi}\Delta\xi + J(\xi,t)\frac{\partial X(\xi,t)}{\partial \xi}\Delta\xi + X(\xi,t)\cdot o_1(\Delta\xi) + J(\xi,t)\cdot o_2(\Delta\xi) \\ & + \frac{\partial J(\xi,t)}{\partial \xi}\Delta\xi\cdot o_2(\Delta\xi) + \frac{\partial X(\xi,t)}{\partial \xi}\frac{\partial J(\xi,t)}{\partial \xi}\left(\Delta\xi\right)^2 + o_1(\Delta\xi)\cdot o_2(\Delta\xi) + \frac{\partial X(\xi,t)}{\partial \xi}\Delta\xi\cdot o_1(\Delta\xi)\Bigg] \end{aligned} \tag{A9}$$

where $o_1(\Delta\xi)$ and $o_2(\Delta\xi)$ are some infinitesimals of higher order than $\Delta\xi$ as $\Delta\xi \to 0$.

Denoting the limit of (A9) as $\Delta\xi \to 0$ by $R^*(\xi, t)$, i.e.:

$$R^*(\xi,t) = \lim_{\Delta\xi\to 0} R(\xi,t) \tag{A10}$$

and taking account of (3.15) and (3.16), we obtain:

$$\begin{aligned} R^*(\xi,t) = & -X_0(\xi)\frac{dJ_0(\xi)}{d\xi} - J_0(\xi)\frac{dX_0(\xi)}{d\xi} - X_0(\xi)\frac{\partial J_1(\xi,t)}{\partial \xi} - J_1(\xi,t)\frac{dX_0(\xi)}{d\xi} \\ & - X_1(\xi,t)\frac{dJ_0(\xi)}{d\xi} - J_0(\xi)\frac{\partial X_1(\xi,t)}{\partial \xi} - J_1(\xi,t)\frac{\partial X_1(\xi,t)}{\partial \xi} - X_1(\xi,t)\frac{\partial J_1(\xi,t)}{\partial \xi} \end{aligned} \tag{A11}$$

The first two terms in (A11) represent the continuity equation in differential form for dc conditions, and their sum is equal to zero. Indeed, differentiation of (2.18) with respect to ξ leads to:

$$X_0(\xi)\frac{dJ_0(\xi)}{d\xi} + J_0(\xi)\frac{dX_0(\xi)}{d\xi} = 0 \tag{A12}$$

which is what we wanted to prove.

Thus, taking (A12) into consideration and combining (A6) with (A11), we have:

$$q\,X_0(\xi)\left[1+D_C(\xi,t)\right]\frac{\partial p_1(\xi,t)}{\partial t} = -X_0(\xi)\frac{\partial J_1(\xi,t)}{\partial \xi} - J_1(\xi,t)\frac{d\,X_0(\xi)}{d\xi}$$
$$-X_1(\xi,t)\frac{d\,J_0(\xi)}{d\xi} - J_0(\xi)\frac{\partial X_1(\xi,t)}{\partial \xi} - J_1(\xi,t)\frac{\partial X_1(\xi,t)}{\partial \xi} - X_1(\xi,t)\frac{\partial J_1(\xi,t)}{\partial \xi} \tag{A13}$$

Appendix B

DERIVATION OF QUASI-2D POISSON'S EQUATION

Wiesław Kordalski

Let $L^*(\xi, t)$ be the limit of the left-hand side of (3.50) as $\Delta\xi \to 0$, i.e.:

$$L^*(\xi,t) = \lim_{\Delta\xi\to 0} \frac{q}{\Delta\xi} \int_{\xi}^{\xi+\Delta\xi} X(\xi,t)\big[N(\xi) + p(\xi,t)\big]\, d\xi \tag{A14}$$

By analogy with (A2), the quotient of the integral of the right-hand side of (A14) by $\Delta\xi$ has the limit:

$$\lim_{\Delta\xi\to 0} \frac{1}{\Delta\xi} \int_{\xi}^{\xi+\Delta\xi} X(\xi,t)\big[N(\xi) + p(\xi,t)\big]\, d\xi = X(\xi,t)\big[N(\xi) + p(\xi,t)\big] \tag{A15}$$

Thus, inserting (A15) into (A14) and taking account of (3.14) and (3.15), we obtain:

$$\begin{aligned} L^*(\xi,t) = q\, \big[& X_0(\xi)\, N(\xi) + X_0(\xi)\, p_0(\xi) + X_0(\xi)\, p_1(\xi,t) \\ & + N(\xi)\, X_1(\xi,t) + p_0(\xi)\, X_1(\xi,t) + p_1(\xi)\, X_1(\xi,t)\big] \end{aligned} \tag{A16}$$

Now, we proceed to calculate the limit of the right-hand side of (3.50) as $\Delta\xi \to 0$. We denote the limit by $R^*(\xi, t)$.

By analogy with (A15), we note:

$$\lim_{\Delta\xi\to 0} \frac{1}{\Delta\xi} \int_{\xi}^{\xi+\Delta\xi} E_{CB}(\xi,t)\, d\xi = E_{CB}(\xi,t) \tag{A17}$$

$$\lim_{\Delta\xi\to 0} \frac{1}{\Delta\xi} \int_{\xi}^{\xi+\Delta\xi} E_{CG}(\xi,t)\, d\xi = E_{CG}(\xi,t) \tag{A18}$$

To compute $R^*(\xi, t)$, we need to know the limit of $B(\xi, t)$ as $\Delta\xi \to 0$, where

$$B(\xi,t) = \frac{1}{\Delta\xi}\big[X(\xi+\Delta\xi,t)\, E(\xi+\Delta\xi,t) - X(\xi,t)\, E(\xi,t)\big] \tag{A19}$$

Inserting the following formulas:

$$E(\xi+\Delta\xi,t)=E(\xi,t)+\frac{\partial E(\xi,t)}{\partial\xi}\Delta\xi+o_1(\Delta\xi) \tag{A20}$$

$$X(\xi+\Delta\xi,t)=X(\xi,t)+\frac{\partial X(\xi,t)}{\partial\xi}\Delta\xi+o_2(\Delta\xi) \tag{A21}$$

into (A19), we obtain:

$$\begin{aligned}B(\xi,t)=\frac{1}{\Delta\xi}\Bigg[&X(\xi,t)\frac{\partial E(\xi,t)}{\partial\xi}\Delta\xi+X(\xi,t)\cdot o_1(\Delta\xi)+E(\xi,t)\frac{\partial X(\xi,t)}{\partial\xi}\Delta\xi\\&+E(\xi,t)\cdot o_2(\Delta\xi)+\frac{\partial E(\xi,t)}{\partial\xi}\Delta\xi\cdot o_2(\Delta\xi)+\frac{\partial X(\xi,t)}{\partial\xi}\Delta\xi\cdot o_1(\Delta\xi)\\&+\frac{\partial X(\xi,t)}{\partial\xi}\frac{\partial E(\xi,t)}{\partial\xi}(\Delta\xi)^2+o_1(\Delta\xi)\cdot o_2(\Delta\xi)\Bigg]\end{aligned} \tag{A22}$$

where $o_1(\Delta\xi)$ and $o_2(\Delta\xi)$ are some infinitesimals of higher order than $\Delta\xi$ as $\Delta\xi\to 0$.

The limit of (A22) as $\Delta\xi\to 0$ is:

$$\lim_{\Delta\xi\to 0}B(\xi,t)=X(\xi,t)\frac{\partial E(\xi,t)}{\partial\xi}+E(\xi,t)\frac{\partial X(\xi,t)}{\partial\xi} \tag{A23}$$

Taking account of (3.6), (3.7), (A23), and noting that

$$\frac{\partial X(\xi,t)}{\partial\xi}=\frac{dX_0(\xi)}{d\xi}+\frac{\partial X_1(\xi,t)}{\partial\xi} \tag{A24}$$

$$\frac{\partial E(\xi,t)}{\partial\xi}=\frac{dE_0(\xi)}{d\xi}+\frac{\partial E_1(\xi,t)}{\partial\xi} \tag{A25}$$

we can write:

$$\begin{aligned}\lim_{\Delta\xi\to 0}B(\xi,t)=&X_0(\xi)\frac{dE_0(\xi)}{d\xi}+E_0(\xi)\frac{dX_0(\xi)}{d\xi}+X_0(\xi)\frac{\partial E_1(\xi,t)}{\partial\xi}+E_1(\xi,t)\frac{dX_0(\xi)}{d\xi}\\&+X_1(\xi,t)\frac{dE_0(\xi)}{d\xi}+E_0(\xi)\frac{\partial X_1(\xi,t)}{\partial\xi}+E_1(\xi,t)\frac{\partial X_1(\xi,t)}{\partial\xi}+X_1(\xi,t)\frac{\partial E_1(\xi,t)}{\partial\xi}\end{aligned} \tag{A26}$$

Utilizing (A17), (A18), (A26) and taking account of (3.8) and (3.9), we can write the limit $R^*(\xi, t)$ of the right-hand side of (3.50) as $\Delta\xi\to 0$ as follows:

$$R^*(\xi,t) = \varepsilon_0\varepsilon_s\left[E_{CG0}(\xi)+E_{cg}(\xi,t)+X_0(\xi)\frac{dE_0(\xi)}{d\xi}+E_0(\xi)\frac{dX_0(\xi)}{d\xi}\right.$$
$$+X_0(\xi)\frac{\partial E_1(\xi,t)}{\partial\xi}+E_1(\xi,t)\frac{dX_0(\xi)}{d\xi}+E_0(\xi)\frac{\partial X_1(\xi,t)}{\partial\xi}+X_1(\xi,t)\frac{dE_0(\xi)}{d\xi} \quad \text{(A27)}$$
$$\left.+E_{CB0}(\xi)+E_{cb}(\xi,t)+E_1(\xi,t)\frac{\partial X_1(\xi,t)}{\partial\xi}+X_1(\xi,t)\frac{\partial E_1(\xi,t)}{\partial\xi}\right]$$

Equating (A16) with (A27), $L^*(\xi, t) = R^*(\xi, t)$ and confining considerations to linear analysis, i.e., ignoring mixed terms in (A16) and (A27), we obtain:

$$q\ [X_0(\xi)\,N(\xi)+X_0(\xi)\,p_0(\xi)+X_0(\xi)\,p_1(\xi,t)+N(\xi)\,X_1(\xi,t)+p_0(\xi)\,X_1(\xi,t)]$$
$$=\ \varepsilon_0\varepsilon_s\,[E_{CG0}(\xi)+E_{cg}(\xi,t)]+\varepsilon_0\varepsilon_s\left[X_0(\xi)\frac{dE_0(\xi)}{d\xi}+E_0(\xi)\frac{dX_0(\xi)}{d\xi}+E_{CB0}(\xi)+E_{cb}(\xi,t)\right.$$
$$\left.+X_0(\xi)\frac{\partial E_1(\xi,t)}{\partial\xi}+E_1(\xi,t)\frac{dX_0(\xi)}{d\xi}+X_1(\xi,t)\frac{dE_0(\xi)}{d\xi}+E_0(\xi)\frac{\partial X_1(\xi,t)}{\partial\xi}\right] \quad \text{(A28)}$$

One can see that (A28) contains terms corresponding to both dc conditions and small-signal time-varying conditions. We can thus split (A28) into two equations: a quasi-2D Poisson's equation for dc conditions,

$$q\,[X_0(\xi)\,N(\xi)+X_0(\xi)\,p_0(\xi)]=\varepsilon_0\varepsilon_s\,[E_{CG0}(\xi)+E_{CB0}(\xi)]$$
$$+\varepsilon_0\varepsilon_s\left[X_0(\xi)\frac{dE_0(\xi)}{d\xi}+E_0(\xi)\frac{dX_0(\xi)}{d\xi}\right] \quad \text{(A29)}$$

and a quasi-2D Poisson's equation for small-signal time-varying conditions,

$$q\,[X_0(\xi)\,p_1(\xi,t)+N(\xi)\,X_1(\xi,t)+p_0(\xi)\,X_1(\xi,t)]=\varepsilon_0\varepsilon_s\,[E_{cg}(\xi,t)+E_{cb}(\xi,t)]$$
$$+\varepsilon_0\varepsilon_s\left[X_0(\xi)\frac{\partial E_1(\xi,t)}{\partial\xi}+E_1(\xi,t)\frac{dX_0(\xi)}{d\xi}+X_1(\xi,t)\frac{dE_0(\xi)}{d\xi}+E_0(\xi)\frac{\partial X_1(\xi,t)}{\partial\xi}\right] \quad \text{(A30)}$$

Appendix C

QUASI-STATIC SMALL-SIGNAL CONDUCTANCE g_{ds}

Wiesław Kordalski

Combining (2.16) and (2.17), an equation for the dc drain current I_D of a *p*-channel MOSFET (see Fig. A.1) at a given Q-point can be written as follows:

$$I_D = - W Q_{C0}(\xi) \upsilon_0(\xi) \tag{A.31}$$

where $Q_{C0}(\xi)$ is the channel charge per unit area [see (2.17)] and $\upsilon_0(\xi)$ is the velocity of carriers.

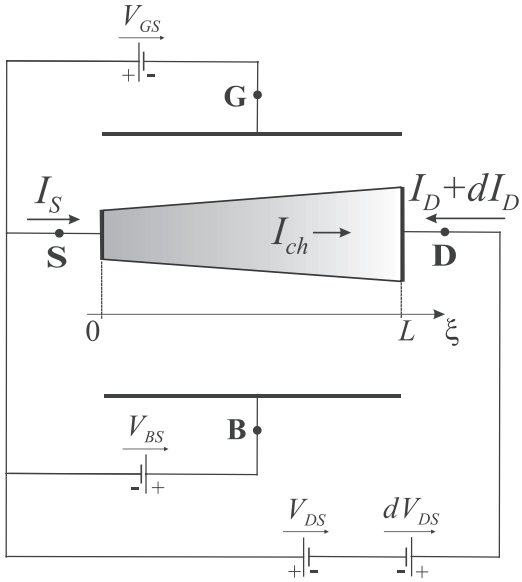

Fig. A.1. An MOSFET under a quasi-static small perturbation dV_{DS}.

In the circuit shown in Fig. A.1, the voltages V_{GS} and V_{BS} do not vary. Considering that, we may state that an infinitesimally small quasi-static increase in the drain-source voltage dV_{DS} causes an infinitesimally small quasi-static variations in the velocity υ_0 of carriers

[through an increase in longitudinal electric field $E_0(\xi)$] and in the charge Q_{C0} (through an injection of carriers into the channel due to the DIBL effect). Therefore, we may rewrite (A.31) in the form:

$$I_D = - W\, Q_{C0}(\xi, V_{DS})\, \upsilon_0\big(E_0(\xi)\big) \tag{A.32}$$

An infinitesimally small quasi-static increase in the drain current dI_D can be calculated by differentiation of (A.32) with respect to V_{DS} and $E_0(\xi)$, yielding:

$$dI_D = - W\, Q_{C0}(\xi, V_{DS}) \frac{d\upsilon_0\big(E_0(\xi)\big)}{dE_0(\xi)} dE_0(\xi) - W\, \upsilon_0\big(E_0(\xi)\big) \frac{\partial Q_{C0}(\xi, V_{DS})}{\partial V_{DS}} dV_{DS} \tag{A.33}$$

If we assume that, for small perturbation in the drain-source voltage dV_{DS}, the differential of the longitudinal electric field $dE_0(\xi)$ is independent of ξ, then, differentiating (4.7), we obtain:

$$dE_0(\xi) = - dV_{DS} / L \tag{A.34}$$

Taking account of (A.34) and noting that the derivative $d\upsilon_0(E_0(\xi))/dE_0(\xi)$ is equal to the differential mobility μ_d at the Q-point, see (4.10), we can rewrite (A.33) as follows:

$$dI_D = W \frac{\mu_d\, Q_{C0}(\xi, V_{DS})}{L} dV_{DS} - W\, \upsilon_0(\xi, E_0) \frac{\partial Q_{C0}(\xi, V_{DS})}{\partial V_{DS}} dV_{DS} \tag{A.35}$$

One can see that the first term of the right-hand side of (A.35) represents an ohmic current, whereas the second one is a current determined by DIBL effect. Therefore, we can introduce the following two notions: a quasi-static small-signal (differential) ohmic conductance, denoted by g_{dso}, and a quasi-static small-signal (differential) DIBL conductance, denoted by g_{dsD} and determined by DIBL effect. Hence, (A.35) can be written as

$$dI_D = (g_{dso} + g_{dsD})\, dV_{DS} \tag{A.36}$$

where

$$g_{dso} = W \frac{\mu_d\, Q_{C0}(\xi, V_{DS})}{L} \tag{A.37}$$

and

$$g_{dsD} = - W\, \upsilon_0(\xi, E_0) \frac{\partial Q_{C0}(\xi, V_{DS})}{\partial V_{DS}} \tag{A.38}$$

Using (2.17), we have an alternative form of (A.37):

$$g_{dso} = q \frac{W}{L} \mu_d\, p_0(\xi)\, X_0(\xi) \tag{A.39}$$

On the other hand, taking into account the definition of the quasi-static small-signal (differential) drain-source conductance g_{ds},

$$g_{ds} = \frac{\partial I_D(V_{DS}, V_{GS}, V_{BS})}{\partial V_{DS}} \tag{A.40}$$

we can write the following:

$$dI_D = g_{ds}\, dV_{DS} \tag{A.41}$$

Comparing (A.36) and (A.41), we obtain:

$$g_{ds} = g_{dso} + g_{dsD} \tag{A.42}$$

One can see from (A.42) that g_{ds} consists of two components, viz., g_{dso} and g_{dsD}. For simplicity, they can be called, respectively, an ohmic part of g_{ds} and a DIBL part of g_{ds}.

Appendix D

FINDING THE HOLE CONCENTRATION $p_1(\xi, j\omega)$

Wiesław Kordalski

A solution to (4.38) is sought in the following form:

$$p_1(\xi, j\omega) = K \exp(\gamma \xi) \tag{A.43}$$

Putting it into (4.38), we get a characteristic equation for γ:

$$0 = \gamma^2 - \frac{E_0}{V_t}\gamma - \left[\frac{d_l\, g_{dso}\, L}{\varepsilon_0 \varepsilon_s\, \mu_q V_t\, W\, X_{ch}} + \frac{j\omega(1+D_C)}{\mu_q V_t} \right] \tag{A.44}$$

Using standard procedure, we obtain two solutions for γ:

$$\gamma = \frac{E_0}{2V_t} - \frac{\sqrt{2}}{4}\sqrt{a+\sqrt{a^2+b^2}} - j\frac{\sqrt{2}}{4}\sqrt{-a+\sqrt{a^2+b^2}} \tag{A.45}$$

$$\gamma^* = \frac{E_0}{2V_t} + \frac{\sqrt{2}}{4}\sqrt{a+\sqrt{a^2+b^2}} + j\frac{\sqrt{2}}{4}\sqrt{-a+\sqrt{a^2+b^2}} \tag{A.46}$$

in which

$$a = \frac{E_0^2}{V_t^2} + \frac{4\, d_l\, g_{dso}\, L}{\varepsilon_0 \varepsilon_s\, \mu_q V_t\, W\, X_{ch}}, \quad b = \frac{4\,\omega\,(1+D_C)}{\mu_q V_t} \tag{A.47}$$

Appendix E

FINDING THE ELECTRIC FIELD $E_1(\xi, j\omega)$

Wiesław Kordalski

Substituting (4.39) into (4.35), one can obtain the following differential equation with separable variables:

$$dE_1 = \frac{q\, d_l\, K \exp(\gamma \xi)}{\varepsilon_0 \varepsilon_s} d\xi \tag{A.48}$$

Integrating (A.48) yields

$$\int_{E_1(0,j\omega)}^{E_1(\xi,j\omega)} dE_1 = \frac{q\, d_l\, K}{\varepsilon_0 \varepsilon_s} \int_0^{\xi} \exp(\gamma \xi)\, d\xi \tag{A.49}$$

Solution to (A.49) is:

$$E_1(\xi, j\omega) = E_1(0, j\omega) + \frac{q\, d_l\, K\left[\exp(\gamma \xi) - 1\right]}{\varepsilon_0\, \varepsilon_s\, \gamma} \tag{A.50}$$

Electric field $E_1(\xi, j\omega)$ must satisfy the following boundary condition:

$$\upsilon_{ds} = -\int_0^L E_1(\xi, j\omega)\, d\xi \tag{A.51}$$

where υ_{ds} is the drain-source voltage phasor.

Inserting (A.50) in (A.51) and integrating the resultant equation, one can obtain a formula for $E_1(0, j\omega)$ as follows:

$$E_1(0, j\omega) = -\frac{\upsilon_{ds}}{L} - \frac{q\, d_l\, K\left[\exp(\gamma \xi) - \lambda L - 1\right]}{\varepsilon_0\, \varepsilon_s\, \gamma^2 L} \tag{A.52}$$

Gdańsk University of Technology Publishing House

Edition I. Publishing sheet 6,2, sheet printing 7,63, 205/1056

Printing and binding: Volumina.pl Daniel Krzanowski
ul. Księcia Witolda 7-9, 71-063 Szczecin, tel. 91 812 09 08